Thesis for the Degree of Doctor of Philosophy

Chemoresistance and metastatic potential of ovarian cancer cells governed by the tumor microenvironment

암 미세환경에 의해 조절되는 난소암세포의 항암제 저항성과 전이능 연구

2021 년 2 월

서울대학교 대학원

농생명공학부 바이오모듈레이션

Youngjin Han

암 미세환경에의해 조절되는 난소암세포의 항암제 저항성과 전이능 연구

지도교수 송 용 상

이 논문을 농학박사학위논문으로 제출함
2021 년 2 월

서울대학교 대학원
농생명공학부 바이오모듈레이션 전공
한 영 진

한영진의 농학박사 학위논문을 인준함
2021년 2월

위 원 장 _____ (인)
부위원장 _____ (인)
위 원 _____ (인)
위 원 _____ (인)
위 원 _____ (인)

Chemoresistance and metastatic potential of ovarian cancer cells governed by the tumor microenvironment

By

Youngjin Han

A thesis submitted to the Department of Agricultural Biotechnology in partial fulfillment of the requirements for the Degree of Doctor of Philosophy in Biomodulation at College of Agriculture and Life Sciences, Seoul National University

February 2021

Approved by Thesis Committee:

Professor Yoe Yong Han Chairman

Professor Yong Sang Song Vice chairman

Professor _____

Professor Junho Chung

Professor Jae-Hoon Kim

Abstract

Chemoresistance and metastatic potential of ovarian cancer cells governed by the tumor microenvironment

Youngjin Han
Biomodulation, Department of Agricultural Biotechnology,
College of Agriculture and Life Sciences,
Seoul National University

Ovarian cancer is the most lethal type of gynecologic malignancy with high rates of mortality. About 70% of patients diagnosed with the cancer show recurrence of cancer despite the cytoreductive surgery and platinum-based chemotherapy. This is mainly due to the highly metastatic capacity of ovarian cancer and extrinsic mechanisms of chemoresistance exerted by extrinsic factors known as the tumor microenvironment. In this series of studies on the ovarian cancer tumor microenvironment, the effects of the tumor microenvironmental factors (hypoxia, inflammation and malignant ascites) affecting chemoresistance and metastatic potential were investigated.

Mitochondria are often referred to as the power plants of a cell. They are vital organelles within a eukaryotic cell, constantly undergoing fission and fusion processes in response to the external stimuli in the surrounding cues. Dysregulation of mitochondrial fission and fusion processes has been shown to be linked to onsets and the progression of many serious diseases such as neurodegenerative diseases, cardiovascular diseases and cancer. Hypoxia is a critical feature of the tumor microenvironment affecting cancer progression through modulation of cancer hallmarks. Hypoxia stimulates the production of reactive oxygen species (ROS), inducing changes in mitochondrial function, metabolism and structures. In this study, we sought to investigate the effect of hypoxia on mitochondrial dynamics of ovarian cancer cells. We investigated alterations in mitochondrial networks under hypoxic conditions (< 1% O2) and

the subsequent effect of the mitochondrial alteration on drug response in ovarian cancer cells. Hypoxia-induced ROS caused an increase in mitochondrial fission, a response abolished by free radical scavenging with N-acetylcysteine (NAC) and Trolox. Also, the treatment of hydrogen peroxide (H2O2) decreased inhibitory p-Drp1 (Ser637) content and increased mitochondrial fission. Suppression of mitochondrial fission enhanced the CDDP sensitivity of hypoxic ovarian cancer cells. Lastly, in tumor spheroids from malignant ascites or tissues of patients with advanced-stage ovarian cancer, pre-treatment with Mdivi-1 increased the CDDP sensitivity. Taken together, our results implicate that hypoxia-induced ROS triggers mitochondrial fission and CDDP resistance in ovarian cancer cells. Mitochondrial dynamics of cancer cells adapting to the hypoxic tumor microenvironment could be a promising target for ovarian cancer treatment.

Next, a growing body of evidence suggests that inflammation is closely associated with the development and progression of ovarian cancer. Herein, we postulated that TNF-mediated activation of the alternative NFκB pathway promotes invasiveness and resistance to cell death induced by TNF. Among the inflammation-related cytokines, we found that TNF is highly expressed in ovarian cancer tissues, compared to that in the other types of solid tumors. Ovarian cancer cells exposed to TNF for 48 hours showed increased colony-forming capacity and cell cycle progression. Additionally, the gene expression levels of TNF and it receptors (TNFRSF1A and TNFRSF1B) were elevated in the metastatic ovarian cancer tissues than the primary tissues from the same patient. Also, the results from the Matrigel-coated transwell insert assay showed that TNF promotes invasiveness of ovarian cancer cells. To investigate the mechanisms involved in this process, we examined the protein expression of classical (p50:p65) and alternative (RelB:P52) NFκB pathway regulators. higher expression of the alternative NFKB transcription factor, RelB was associated with poor survival rates. Using 307 ovarian tumor samples from The Cancer Genome Atlas (TCGA), we found a significant positive correlation between the alternative NFKB pathway genes (RelB and P52) and cancer invasion-related protease (MMP9, PLAU). Protease array revealed that PLAU

was upregulated by TNF but this response was absent in the RelB knockdown ovarian cancer cell. Collectively, these findings highlight the involvement of the alternative NFκB pathway-mediated by RelB expression in metastatic processes in ovarian cancer cells.

Lastly, to understand cellular interactions, present within the metastatic niche of the ovarian cancer tumor microenvironment, malignant ascites, we utilized single-cell RNA sequencing data from 5 patients with ovarian cancer. We identified 7 distinct cell types based on the expression patterns of cell-type-specific signatures. Macrophages were the most heterogeneous cell type with eleven sub-clusters in the ascites tumor microenvironment. Annotation of macrophage subpopulations was done using MacSpectrum. Also, intra- and inter-tumoral heterogeneities of OC cells in the ascites were assessed. The communication between immune and OC cells was predicted through ligand-receptor interaction analysis with NicheNet. We uncovered that CCL5 is enriched in T cells and NK cells, modulating OC cell survival in the ascites presumably through SDC4. Average SDC4 expression positively correlates with OC cell proportion in each sample. Elevated SDC4 expression predicted poor overall survival of OC patients. Altogether, our study highlights the potential tumor-promoting role of T cells and NK cells in long-term survival outcomes, suggesting that SDC4 is a vital molecule for OC cell survival and a prognostic marker in OC patients.

……

Keywords: Ovarian cancer, chemoresistance, Tumor microenvironment, Hypoxia, Mitochondrial dynamics, Malignant ascites, Metastatic Potential, RelB

***Student number*: 2015-22697**

Table of contents

List of figures and table

Main figures

Table

Supplementary figures

List of abbreviations

2-DG: 2-deoxy-d-glucose

AMP: Adenosine monophosphate

AMPK: AMP-activated protein kinase

ANOVA: Analysis of variance

ASC: Adipose-derived stem cell

bFGF: Basic fibroblast growth factor

BMPR2: Bone morphogenic protein receptor 2

CAF: Cancer-associated fibroblast

CaMKIα: Calcium/calmodulin-dependent protein kinase I alpha

DCFH-DA: 2,7-dichloro-dihydrofluorescein diacetate

DEG: Differentially expressed gene

DHE: Dihydroethidium

Drp1: Dynamin related protein 1

EGF: Epidermal growth factor

EMT: Epithelial-to-mesenchymal transision

ER: Endoplasmic reticulum

Fis1: Mitochondrial fission 1

GEO: Gene expression omnibus

GSK3β: Glycogen synthase kinase 3β

HBSS: Hank's balanced salt solution

HF-LPLI: High-fluence low-power laser irradiation

Hif1α: Hypoxia-inducible fator-1 alpha

hMSC: Human mesenchymal stem cell

HUVEC: Human Umbilical Vein Endothelial Cells

IFN-γ: Interferon-γ

IL-6: Interleukin-6

INF2: Isoform of inverted formin-2

Lig3: Ligase III

LPS: Lipopolysaccharides

MAM: Mitochondrial-associated membrane

MAPL: Mitochondria-associated protein ligase

Mff: Mitochondrial fission factor

Mfn1/2: Mitofusins 1 and 2

MIEF1/2: Mitochondrial elongation factor 1/2

miR: MicroRNA

Miro1: Mitochondrial RhoGTPase-1

MMP: Metalloprotienase

mtDNA: Mitochondrial DNA

NOX: NADPH oxidases

OPA1: Optic atrophy1

PDGF: Platelet-derived growth factor

PDS: Patient-derived spheroids

Phb1: Prohibitin

Pim-1: Proviral integration site for Moloney murine leukemia virus-1

PKA: Protein kinase A

RAGE: Receptor called advanced glycation endproduct

Redox: Oxidation-reduction

ROCK1: Rho-associated protein kinase 1

ROS: Reactive oxygen species

scRNA-seq: Single-cell RNA sequencing

SERCA2a: AMPK/sarcoplasmic endoplasmic reticulum Ca2+ATPase 2a

SNARE: Secretory granule-associated vesicle-soluble N-ethylmaleimide-sensitive factor attachment protein receptor

STS: Staurosporine

SUMO: Small ubiquitin-like modifier

T-ALL: T-cell acute lymphoblastic leukemia

TNF-α: Tumor necrosis factor-α

TNT: Tunneling nanotube

TRAIL: Tumor necrosis factor-related apoptosis-inducing ligand

VSMC: Vascular smooth muscle cell

1. Chapter I: Literature review

1.1 Introduction

Mitochondria, originally prokaryotic cells, are essential power plants of eukaryotic cells playing vital roles in regulating cellular bioenergetics, calcium signaling, oxidation-reduction (redox) status and apoptotic pathway (1). Numerous onsets and progressions of diseases are closely associated with mitochondrial dysfunctions. For instance, studies have reported changes in cellular regulation of mitochondrial dynamics in neurodegenerative diseases, endocrine dysfunction, cardiovascular diseases and cancer (2). Mitochondria are not static cellular compartments. Rather, they are dynamic organelles undergoing continuous processes of fission and fusion. Studies on microscopic analysis have shown that numbers, structures and sizes of mitochondria vary widely in various types of cells and even within the same cells. This morphological heterogeneity of mitochondria is closely related to fission and fusion processes in order to maintain their cellular homeostasis and mitochondrial DNA integrity at optimal levels (2, 3).

Cancer cells use a distinct cellular and molecular machinery from normal cells, resulting in acquisition of several phenotypes denoted by the list of cancer hallmarks (4). Cancer cells show increased ability to proliferate and to survive from apoptotic stimuli compared to normal cells. The activity of mitochondria in cancer cells is different from those in normal cells (5). In 1920s, German biochemist Otto Warburg demonstrated that cancer cells exhibit increased glycolysis under aerobic condition (6). Since then, the importance of mitochondrial metabolism has been undervalued in cancer.

The efficient functioning of cellular metabolism is necessary for cancer cells, developing unique strategy of metabolic regulation for survival and aberrant proliferation. Altered metabolism could have an impact on the regulation of mitochondrial dynamics. Expression of adenosine monophosphate (AMP)-activated protein kinase (AMPK) increases to preserve energy homeostasis under the low concentration of ATP. Dysfunction of mitochondria can activate AMPK, triggering the activation of mitochondrial fission factor (Mff), and increasing mitochondrial fission (7). This suggests that regulation of

mitochondria dynamics may be related to the metabolic stress as an adaptive mechanism of cells. Succinate stimulates migration of human mesenchymal stem cells (hMSCs), increasing capability of tissue regeneration by promoting migration of the cells through dynamin related protein 1 (Drp1)-mediated fission of mitochondria (8). Thus, to meet the bioenergetics requirement of cells in a certain microenvironment, fine-tuning of cellular metabolism by adjusting mitochondrial structure is necessary. Normal cells homeostatically maintain structural organization of mitochondria. Likewise, cancer cells retain homeostatic regulatory mechanisms of mitochondrial dynamics in response to various stress cues. The tumor microenvironment related to the cancer progression includes inflammation, hypoxia, nutrient deprivation and oxidative stress. However, how cancer cells respond to those stress conditions of tumor microenvironment and subsequent changes in metabolic regulation remains largely elusive.

Tumor microenvironment is extremely dynamic and unstable owing to various factors (9). A number of stress signals in the tumor microenvironment are associated with the mitochondrial dynamics. It would be worthwhile to delve into altered regulation of mitochondrial network for discovery of potential therapeutic targets in cancers. Recent findings on context-dependent regulation of mitochondrial dynamics and the subsequent impact of altered mitochondrial dynamics on drug sensitivity of cancer will be addressed in this review.

1.2 Molecular regulators of mitochondrial dynamics

Up till now, a number of molecules involved in regulation of fission and fusion that determines mitochondrial morphology have been reported (Figure 1). Changes in regulation of mitochondrial morphology by fission and fusion machineries could bring about altered mitochondrial function and metabolism (10). Mitochondria consist of outer and inner membranes. Unlike outer membrane of mitochondria, the inner membrane known as cristae is folded inwards to maximize the functionality by increasing the surface area (11).

Fission of mitochondria destabilizes complex structure of folded cristae by decreasing the number of folds, resulting in reduced mitochondrial function (12, 13). Fission and fusion processes of mitochondria are mediated by different sets of molecules. The key proteins involved in fission and fusion events are members of dynamin family and mitochondrial membrane-bound receptors (14).

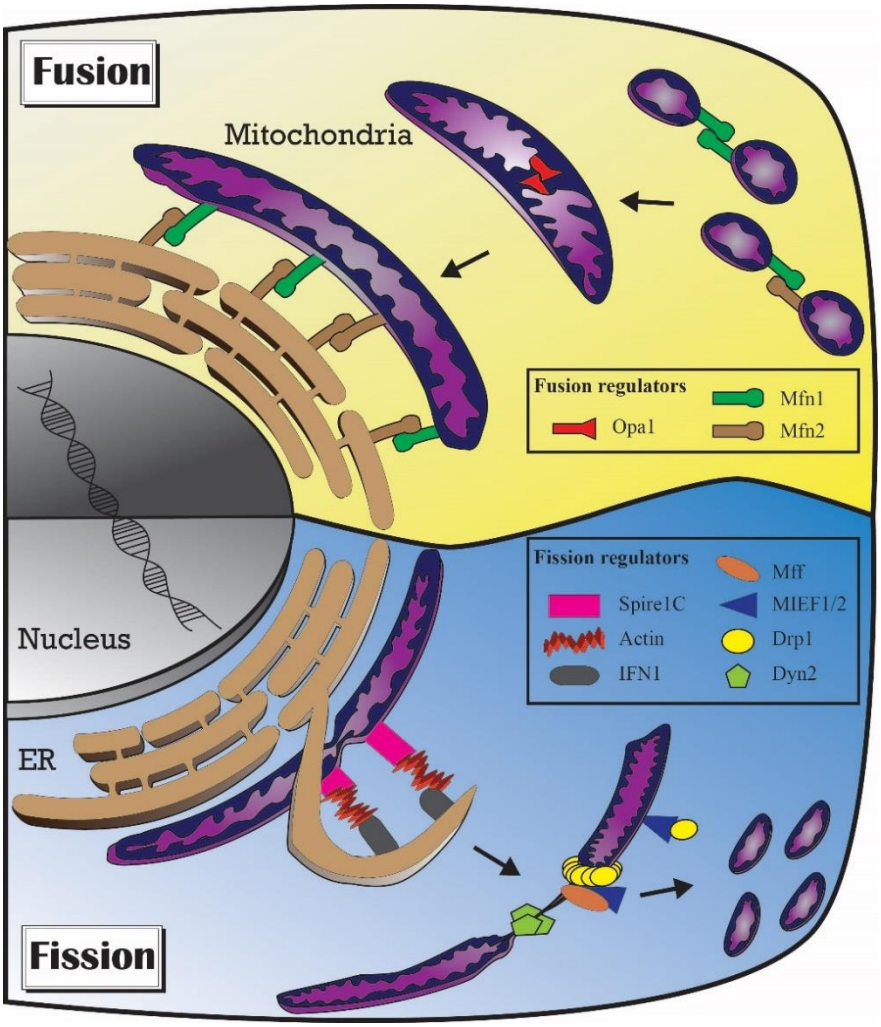
Fusion
Mitochondria
Fusion regulators
Opa1
Mfn1
Mfn2
Nucleus
ER
Fission regulators
Spire1C
Actin
IFN1
Mff
MIEF1/2
Drp1
Dyn2
Fission

Figure 1. A schematic diagram illustrating dynamic processes of mitochondria fusion (top) and fission (bottom).

The key regulators of those processes are displayed in the boxes. Mitochondrial inner membrane fusion is regulated by Opa1. Mfn1/2 are responsible for fusion of mitochondrial outer membrane and mitochondria-ER interaction through the formation of the homo-/hetero-dimeric complex. For mitochondrial fission, initial constriction of mitochondria at ER-mitochondria contact sites is mediated by Spire1C located at mitochondria and IFN1 located at ER through actin polymerization. Then further constriction of mitochondrial membranes is facilitated by Drp1. Drp1 interacts with Mff expressed at the mitochondrial outer membrane, forming a multimeric loop around mitochondria. Low to moderate expression of MIEF1/2 which is also expressed at the mitochondrial outer membrane enhances recruitment of Drp1 to the mitochondrial fission site. The final step of mitochondrial fission is driven by the action of Dyn2. Expressions and activities of those proteins are crucial for maintaining homeostasis of mitochondrial dynamics.

1.2.1 Mitochondrial fission

Recent studies have unraveled that actin polymerization at a endoplasmic reticulum (ER)-mitochondria contact site is involved in the initial step of mitochondrial fission (15). The ER-bound isoform of inverted formin-2 (INF2) which recruits and polymerizes actin subunits is located at the interaction site of ER and mitochondria (16) and Spire1C which induces actin assembly at the ER-mitochondria contact site initiate the fission process through the constriction of mitochondria (17). While, actin-depolymerizing protein called cofilin1 prevents Drp1 accumulation at mitochondria, counterbalancing mitochondrial fission by INF2 and Spire1C-mediated actin polymerization (18). Syntaxin17 (Syn17), the secretory granule-associated vesicle-soluble N-ethylmaleimide-sensitive factor attachment protein receptor (SNARE) protein, present at raft-like structures of ER-mitochondria contact sites increases translocation and subsequent binding of Drp1 to mitochondrial outer membrane. In response to nutrient deprivation, interaction between Syn17 and Drp1 is disrupted, resulting in hyperfusion of mitochondria (19).

Mitochondrial fission 1 (Fis1), a known mitochondrial membrane-bound receptor of Drp1 has no or minimal role in induction of mitochondrial fission in mammalian cells although it is critical for the fission process in budding yeasts (20, 21). In human cells, localization of Drp1 to mitochondria is mediated through binding of Drp1 to mitochondrial elongation factor 1/2 (MIEF1/2) and Mff at the mitochondrial outer membrane (21, 22). MIEFs and Mff are capable of binding Drp1 independently. MIEFs are able to interact with both Drp1 and Mff simultaneously, serving as an adaptor for Drp1. However, the expression ratio of Mff to MIEFs affects the fission/fusion status of mitochondrial structure. Excessive expression of MIEFs could impede interaction between Drp1 and Mff, resulting in highly elongated form of mitochondria, whereas low to moderate expression of MIEFs enhances interaction between Mff and Drp1 through the formation of trimeric complex (23-25). Results from yeast two-hybrid analysis for interaction of Mff with Drp1 revealed selective recruitment of Drp1 oligomers to Mff (26). These

results imply that binding of Drp1 to Mff is crucial for the fission process, and MIEFs interacting with Mff in mitochondrial outer membrane strengthen interaction of Mff with Drp1. Furthermore, cardiolipin, the mitochondria-specific lipid content is involved in recruitment of Drp1 to the site of fission by altering Drp1 structure and function (27). This type of lipid is normally located at the inner membrane of mitochondria. However, it becomes exposed to the mitochondrial outer membrane for fission of mitochondria. Seemingly, both cardiolipin and mitochondrial adaptor signaling act as important facilitators in the process of mitochondrial fission (28, 29). Once oligomerized Drp1 molecules are properly positioned around the outer membrane of mitochondria through the formation of spiral-like shape, GTP hydrolysis of Drp1 is driven to constrict mitochondrial membrane in the tiny loop created by Drp1 oligomers (30). Studies on mechanism of Drp1 assembly utilizing cryo-electron microscopy showed that in the presence of GTP, 13 to 18 monomeric Drp1 molecules constitute oligomeric rings through GTP hydrolysis (31). Constricted mitochondrial membrane is then subjected to further fission process by the action of dynamin 2 (Dyn2). Dyn2 has been appreciated to have a chief role in facilitating cytokinesis and endocytosis at the plasma membrane (32). An additional function of Dyn2 has recently been found to execute mitochondrial fission at the final step. Inhibiting Drp1 or Dyn2 disrupted mitochondrial fission/fusion equilibrium in cells resulting in hyperfusion of mitochondrial compartments (33).

Drp1 function and localization are tightly regulated by different types of PTMs, such as phosphorylation, SUMO (small ubiquitin-like modifier)-ylation, S-nitrosylation, O-GlcNAcylation and ubiquitination. Various enzymes responsible for phosphorylation of Drp1 have been identified, and the site at which Drp1 is phosphorylated determines its function and activity. Serine 616 (Ser616) and serine 637 (Ser637) residues are the two major phosphorylation sites of Drp1 protein (34). For human Drp1, phosphorylation at Ser616 is done by the action of PKCδ, CDK1 or ERK. Increased reactive oxygen species (ROS) production by hypertensive stress led to an increase of mitochondrial fission by phosphorylation of Drp1 by PKCδ (35). During mitosis, CDK1-mediated

phosphorylation of Drp1 at Ser616 triggered an increase in mitochondrial fission in order to maintain mitochondrial DNA integrity and evenly distribute mitochondrial compartments to daughter cells (36). Studies have reported expression of CDK1 is related to paclitaxel resistance in cancer (37). ERK which plays roles in oncogenic and anti-apoptotic signaling pathways has been shown to phosphorylate Drp1 at Ser616, promoting mitochondrial fission (38, 39). While majority of studies have shown phospho-Drp1 (Ser616) facilitates mitochondrial fission, other studies demonstrated suppression of mitochondrial fission through CDK5-mediated drp1 phosphorylation at Ser616 (40, 41). Phosphorylation of Drp1 at Ser637 could be exerted by several enzymes such as AMPK, glycogen synthase kinase 3β (GSK3β), calcium/calmodulin-dependent protein kinase I alpha (CaMKIα), proviral integration site for Moloney murine leukemia virus-1 (Pim-1), Rho-associated protein kinase 1 (ROCK1) and protein kinase A (PKA) (42-46). Phospho-Drp1 (Ser637) exhibited a decrease in GTPase activity and impaired translocation from cytosol to mitochondria, thereby preventing mitochondrial fission (47). Dephosphorylation of Drp1 at Ser637 is mediated by calcineurin (48).

SUMOylation of Drp1 is also involved in regulation of Drp1 activity. SUMO1 and SUMO2/3 are different forms of SUMO proteins and are responsible for adding SUMO group onto Drp1. As docking of Drp1 to Mff is the crucial mechanism in mitochondrial fission event, the removal of SUMO2/3 from Drp1 by SENP3 increased binding capacity of Drp1 to Mff, thereby stimulating mitochondrial fission (49, 50). Whereas, during apoptosis, mitochondria-associated protein ligase (MAPL) stabilized Drp1 recruited at the ER-mitochondria contacts through SUMOylation (51). S-nitrosylation of Drp1 has also been reported to increase GTPase activity of Drp1, inducing Drp1-mediated mitochondrial fission and this has been shown to be related to development of Alzheimer's disease (52). Moreover, O-GlcNAcylation of Drp1 mediated by O-GlcNAc transferase induces mitochondrial translocation of Drp1 (53). Therefore, many types of PTMs on Drp1 are determining factors of Drp1 activation status. Overall, mitochondrial fission process is modulated by the concerted actions of dynamin family molecules, specific lipid contents and

adaptor molecules embedded in the mitochondrial outer membrane.

1.2.2 Mitochondrial fusion

Fusion of mitochondria is merge of mitochondrial compartments, producing elongated form of mitochondria. Fusion of mitochondria is also facilitated by molecules of dynamin superfamily. Mitofusins 1 and 2 (Mfn1/2) embedded in mitochondrial outer membrane act to fuse two separate mitochondrial membranes together, initiating the fusion process of mitochondria (54). Depletion of Mfn1/2 causes the imbalance in the mitochondrial dynamics, resulting in mitochondrial fission. For outer membrane fusion of mitochondria, conformational changes of Mfn1 induced by GTPase activity facilitate dimerization of Mfn1, physically bringing two separate mitochondrial compartments in close proximity (55, 56). After fusion of mitochondrial outer membranes, optic atrophy1 (OPA1) located at the mitochondrial inner membrane drives mitochondrial inner membrane fusion (57). Mitochondrial-associated membrane (MAM) of ER is also involved in fusion of mitochondria. Mfn2 mostly found in MAM has been shown to function in tethering of mitochondria to ER (58, 59). A mitochondrial ubiquitin ligase, MITOL (also known as MARCH5) is located at the mitochondrial outer membrane. MITOL specifically regulates activity of mitochondrial Mfn2 through ubiquitination. Knockdown of MITOL increased Drp1-mediated mitochondrial fission in HeLa cells (60).

Post-transcriptional regulation of Mfn1 by microRNAs (miRs) has been reported to affect the control of mitochondrial dynamics. Translation of Mfn1 was suppressed by miR-140 which targets 3' untranslated region (3' UTR) of Mfn1. An increase of miR-140 expression shifted the balance towards fission of mitochondria and subsequently induced apoptosis in cardiomyocytes (61). While, apoptosis was inhibited when miR-19b that suppresses mfn1 expression was upregulated (62).

A dynamin-like GTPase Opa1 is bound to the inner membrane of mitochondria through N-terminal transmembrane domain. Other protein

domains including GTPase domain face intermembrane space of mitochondria (63). Opa1 which has two cleavage sites, S1 and S2 is cleaved by the mitochondrial protease OMA1 and the inner membrane-embedded AAA protease YME1L respectively. Once cleaved by the activity of the proteases, L-Opa1 anchored to mitochondrial inner membrane forms soluble S-Opa1, being released into intermembrane space. Balance of L-OPA1 and soluble S-Opa1 is critical for determining the fission/fusion status of mitochondria (64). Remodeling of the mitochondrial cristae is another major function of OPA1 in the adaptation of mitochondrial metabolism, monitoring responses to tissues damages by apoptosis, atrophy and ischemia (13, 65).

While cardiolipin composition at the mitochondrial outer membrane is involved in the fission by enhancing interaction of Drp1 with mitochondrial outer membrane, a member of the phospholipase D family called mitoPLD bound to the outer membrane of mitochondria promotes fusion process by acting on phospholipids of mitochondrial outer membrane (66). The C-terminal domain of mitoPLD is anchored to mitochondrial outer membrane. The N-terminal catalytic domain is positioned at the cytosol. The conversion of cardiolipin into phosphatidic acid is done by mitoPLD, and the increased activity of mitoPLD results in the suppression of mitochondrial fission processes (67).

1.2.3 Motility and distribution

Mitochondrial compartments could be transported, employing cytoskeletal motor system. Daughter cells from budding yeasts inherit mitochondria using cytoskeletal trafficking system driven by Myo2 (68). Along the track of cytoskeletal system like actin and microtubule, mitochondria are conveyed within a single cell or even between two different cells. Several context-dependent signaling pathways linked to intracellular trafficking of mitochondria have been identified. In neurons, transport of mitochondria to synaptic region is activated to maintain calcium concentration and energy supply at subcellular regions (14).

For anterograde transport of mitochondria, the kinesin Kif5 is involved, whereas the retrograde transport of mitochondria is controlled by dynein. In order to load the mitochondrial compartments onto the cytoskeletal motor system, adaptor proteins that bridge between mitochondria and motor proteins are required. Mitochondrial RhoGTPase-1 (Miro1) tethered at the mitochondrial outer membrane forms a complex with Milton/TRAK, mediating the interaction between mitochondria and actin cytoskeleton. Although trafficking of mitochondria in cancer cells is largely unexplored, accumulative evidence suggests that the mitochondrial trafficking is important in metastasizing cancer cells (69). Syntaphilin acts as a brake halting the mitochondrial trafficking by interfering the interaction between Kif5 and Milton/TRAK (70).

In addition to intracellular trafficking of mitochondria, a growing body of evidence suggests mitochondria could be transferred from one cell to adjacent cells via the mode of cell-to-cell interaction termed tunneling nanotube (TNT) (71). This type of intercellular communication allows cells to exchange copious cellular components including mitochondria through the tubular structure created by the extension of plasma membrane (72). The diameter of TNTs formed between two cells ranges from 50 nm to 380 nm, which is enough space for a fragment of mitochondria to traverse (73). With the assistance of Miro1, mitochondria are transferred uni-directionally from one cell to another along the cytoskeleton through TNTs created between two cells (74). Although the exact role of intercellular transfer of mitochondrial compartment in cancer remains largely elusive to date, several studies have reported the establishment of TNTs are involved in drug resistance and metastasis (75, 76).

1.3 Tumor microenvironment and mitochondrial dynamics

Mitochondrial dynamics is critical for normal cell homeostasis. Thus, defects in mitochondrial dynamics could lead to development of diseases including cancer. In cancer, stress signals could alter regulation of mitochondrial dynamics. Stress-induced signaling pathways interact with the molecular

machinery of mitochondrial dynamics, determining the resultant morphology and structure of mitochondria as a process of adaptive mechanism. It has been documented that the cellular stress in tumor microenvironment contributes to aberrant regulation of mitochondrial dynamics. The process of mitochondrial dynamics can be altered by many factors such as cytokines, metabolites and oxygen availability in tumor microenvironment (Figure 2).

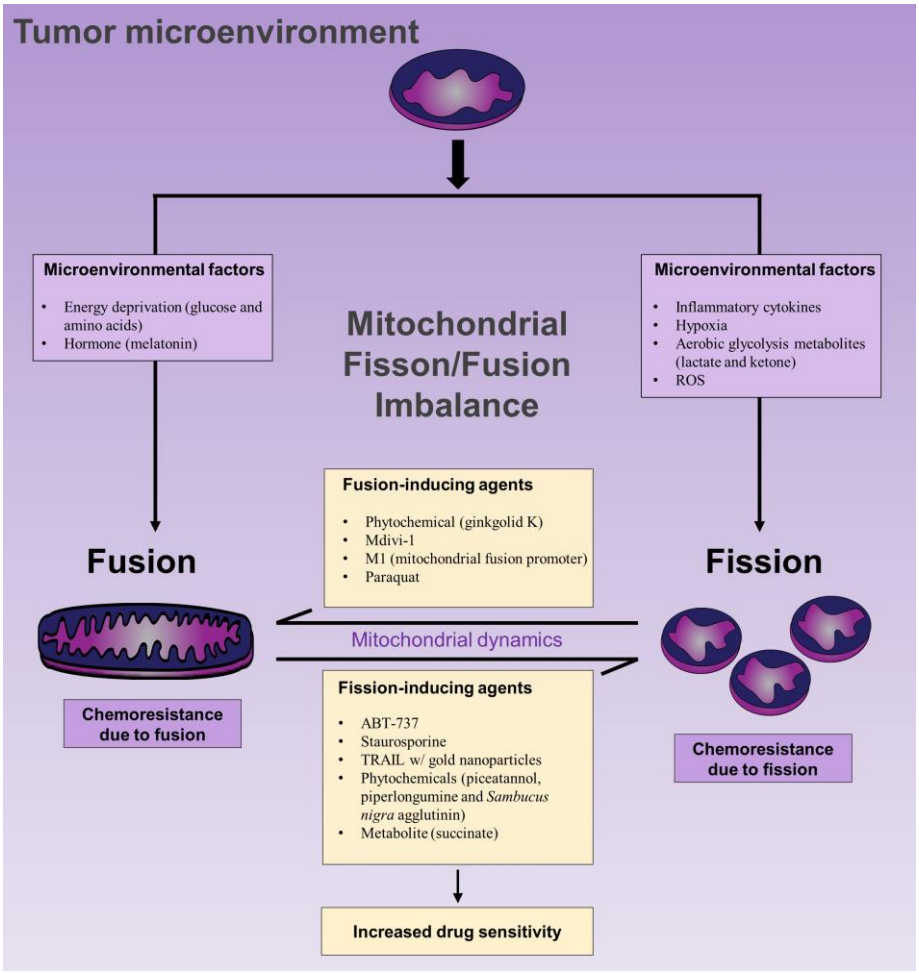

Figure 2. Context-dependent regulation of mitochondrial dynamics in the tumor microenvironment and chemical modulators affecting mitochondrial fission/fusion.

Stress signals involved in regulation of mitochondrial fission and fusion processes are summarized. Chemical agents affecting mitochondrial fission/fusion status are listed, possibly enhancing drug-sensitivity of cancer.

1.3.1 ROS and mitochondrial dynamics

Metabolic byproducts from mitochondria are utilized for biosynthesis of macromolecules like nucleotides. In cancer, energy metabolism involved in glucose consumption is altered to a great extent (77). Although cancer cells exhibit enhanced aerobic glycolysis, mitochondrial metabolism remains highly functional in cancer cells. Moreover, compared to primary tumor, metastatic cancer cells, which are generally resistant to anti-cancer drugs, were more dependent on the mitochondrial oxidative phosphorylation (OXPHOS) system (78). Mitochondria are thought to be a major source of ROS which are byproducts of mitochondrial metabolism. Other main contributors of intracellular ROS production include ER, peroxisome and NADPH oxidases (NOX) family of enzymes located in the cytosol and the plasma membrane (79). Genetic alterations like oncogenic mutations drive cancer cells to elevate the production of ROS (80). Due to the fact that proliferative capacity is greater in most cancer cells, they require more ATPs than normal cells, causing excessive generation of ROS through aberrant metabolic regulation (81).

Studies have suggested that mutation and copy number alterations of mitochondrial DNA (mtDNA) may be associated with metabolic capacity of cancer. An individual cell contains multiple copies of mitochondrial DNA. Low copy number of mtDNA in cancer is associated with decreased antioxidant activity, displaying increased sensitivity to chemotherapeutic agents (82). Whereas, one meta-analysis showed that elevated copy number of mtDNA in tumor tissue is associated with better prognosis (83). Although mitochondrial DNA encodes only a small fraction of cellular proteins, largely involved in the electron transport chain, in cells and majority of mitochondrial proteins are from nuclear DNA, mutations in mitochondrial DNA could confer malignant phenotypes of cancer like drug resistance (84). Moreover, intracellular level of ROS could affect mtDNA mutation and copy number (85). The damage in mtDNA by ROS is often repaired through the base excision repair pathway (86). APE1 is the base excision repair enzyme which is an endonuclease. Under oxidative stress conditions, APE, which is normally expressed in cytosol,

translocates into the nucleus, and N-terminal truncated form of APE1 translocates to the mitochondria to prevent mtDNA from being permanently damaged by oxidative stress. In transgenic mouse model of colorectal cancer, haplo-insufficiency of the gene coding for APE1 impairs the abundance and the integrity of mtDNA (87). Additionally, mammalian cells have 3 distinct types of DNA ligases and among those, ligase III (Lig3) has been shown to function specifically in DNA repairing process of mitochondria, critical for maintaining the mtDNA integrity (88). Mitochondria-localized topoisomerase I (Top1mt) which plays a role in regulating mtDNA replication and mitochondrial homeostasis is indispensable for maintaining mitochondrial integrity and activity of cellular energy metabolism. Knockout of Top1mt promoted generation of ROS and DNA damage in murine embryonic fibroblasts with decreased production of ATP (89).

To survive from the situation where intracellular ROS level is persistently high, cancer cells develop their own way of detoxification mechanism (90). Accumulating evidence suggests that ROS contributes to various oncogenic signaling pathways in cancer (91). ROS derived from mitochondrial metabolism is essential for cell proliferation and tumorigenesis in an oncogenic Kras-driven mouse model of lung cancer (92). Interestingly, several studies have suggested that dynamics of mitochondria are modulated by ROS. Stem-like cancer cells showing resistance to conventional anti-cancer agents increase mitochondrial biogenesis through ROS-mediated up-regulation of PGC1α which plays critical roles in both mitochondrial biogenesis and anti-oxidative mechanism of cells (93). Treatment of anti-oxidative ascorbic acid attenuated mitochondrial fission induced by a herbicide, paraquat, in mouse alveolar type II cells (94). Increased production of ROS triggered by high-fluence low-power laser irradiation (HF-LPLI) caused mitochondrial dysregulation and dysfunction in human lung adenocarcinoma cells and African green monkey SV40-transformed kidney fibroblast cells, favoring mitochondrial fission over fusion owing to imbalanced expression of mitochondrial fission/fusion molecules (95).

1.3.2 Inflammatory microenvironment and mitochondrial dynamics

Inflammation is a common feature of tumor microenvironment and the pro-inflammatory cytokines not only modulate mitochondrial metabolism but also affect the mitochondrial dynamics. Inflammatory cytokines such as interferon-γ (IFN-γ), interleukin-6 (IL-6) and tumor necrosis factor-α (TNF-α) are present at high levels within a malignant tumor (96, 97). Prolonged inflammation stimulates fission of mitochondria. A member of the large superfamily of GTPases, guanylate-binding protein 2 (GBP2) has been shown to regulate mitochondrial dynamics through the direct interaction with Drp1. IFN-γ, a soluble cytokine, induced expression of GBP2 in breast cancer cells. Binding of GBP2 to Drp1 blocked translocation of Drp1 to mitochondria, inhibiting mitochondrial fission and invasion of breast cancer cells (98). Additionally, cancer cachexia-induced inflammation has been revealed to cause mitochondrial dysfunction. Proper maintenance of mitochondrial quality is necessary for the skeletal muscle function. Elevated levels of circulatory pro-inflammatory cytokines in cancer cachexia induced mitochondrial fission, promoting excessive production of ROS and reducing efficiency for the ATP synthesis in skeletal muscle cells (99, 100). Excessive mitochondrial fission activated AMPK signaling, which can disrupt protein synthesis causing decreased muscle mass (101).

Development of malignant ascites is a common feature for abdominal cavity cancers such as stomach and ovarian cancer (102). Ascitic fluid is very common in ovarian cancer and rich in inflammatory cytokines (103). Ovarian cancer cells treated with malignant ascitic fluid showed increased invasiveness through the activation of IL-6 signaling pathway (104). Mitochondrial fission has been shown to be one of the features of metastatic cancer cells. Thus, it could be presumed that increased invasiveness in cancer could be explained, at least in part, by increased mitochondrial fission due to pro-inflammatory cytokines.

1.3.3 Reduced blood supply and mitochondrial dynamics

Normal cells lack the ability to survive under harsh conditions such as oxygen- and nutrient-deprived environment, whereas cancer cells are better equipped to survive and proliferate in such conditions (105, 106). Loss of regional blood supply is a common characteristic of malignant tumor. In solid tumors, the rate of angiogenesis is slower than the proliferation rate of cancer cells, creating hypoxic and nutrient-depleted areas (107). In oxygen- and nutrient-deprived environment, the balance between mitochondrial fission and fusion dynamics are disrupted and the subsequent fragmentation of mitochondria promotes apoptosis in normal cells (108). In contrast, cancer cells are equipped with adaptive mechanisms.

As a consequence of reduced blood supply, sub-regions of cancer cells are exposed to hypoxic and nutritional stress. Hypoxic tumor environment induces stabilization and activation of hypoxia-inducible fator-1 alpha (Hif1α) in cells (109). Hif1α is a transcription factor that regulates expression of numerous genes. Under hypoxic condition, stabilized Hif1α induces upregulation of various growth factors including basic fibroblast growth factor (bFGF), platelet-derived growth factor (PDGF) and epidermal growth factor (EGF). Among the several factors upregulated by Hif1α, PDGF could affect the regulation of mitochondrial dynamics (110). In vascular smooth muscle cells (VSMCs), PDGF treatment induces mitochondrial fission, enhancing proliferative capacity of VSMCs (111). Hypoxia elicits accumulation of the outer mitochondrial membrane protein FUNDC1 at MAM. This, in turn, causes recruitment of Drp1 to mitochondria and subsequent mitochondrial fission. Knockdown of FUNDC1 prevents hypoxia-induced mitochondrial fission in HeLa cells (112). In metastatic breast cancer cells (MDA-MB-231), hypoxia promoted Drp1-mediated mitochondrial fission, increasing migration of the cancer cells (113).

Aside from mtDNA repairing enzymes, studies have suggested mitochondrial fusion process is required for cells to maintain the integrity of mtDNA. Hence, dysregulation of mitochondrial dynamics may have an impact

on the maintenance of mtDNA integrity. Bone morphogenic protein receptor 2 (BMPR2) regulates sets of molecules related to the mitochondrial function and mtDNA integrity under hypoxia followed by reoxygenation conditions in pulmonary arterial endothelial cells. Silencing BMPR2 results in mitochondrial fission. In the hypoxia followed by reoxygenation model, knockdown of BMPR2 resulted in the deletion of mtDNA (114). Presumably, BMPR2 could act, at least in part, as an upstream regulator of mitochondrial dynamics under hypoxic conditions.

Cancer cells are characterized by the enhanced glycolysis and reduced OXPHOS for ATP production. The activity of OXPHOS is identified to be associated with mitochondrial fusion (115). Recent studies have shown that when cells undergo energy deprivation, mitochondrial fusion increases. Specific amino acid depletion elicited downregulation of mitochondrial fission protein, Drp1 (116). Furthermore, physical exercise and caloric restriction induced mitochondrial fusion together with upregulation of the fusion proteins, Opa1 and Mfn1 (117). When cells undergo energy depletion, mitochondrial fusion is promoted to maximize efficiency for ATP generation (118). Treatment of inhibitors of glucose metabolism such as Hank's balanced salt solution (HBSS) or 2-deoxy-d-glucose (2-DG) induced mitochondrial elongation in cancer cells by suppressing mitochondrial translocation of Drp1. Mitochondrial fusion by metabolic stress promoted an increase of OXPHOS, suppressing glycolysis through NAD+-dependent SIRT1 activation (119). Low expression of Mfn2 is linked to the poor prognosis in breast cancer. Limited availability of nutrients in breast cancer cells caused suppression of MFN2-mediated mitochondrial fusion, leading to reduced OXPHOS and ROS production. This phenotypic change of mitochondria allows breast cancer cells to survive in response to metabolic stress which is common in solid tumors (120).

1.3.4 Intercellular communication and mitochondrial dynamics

Cross-talk between cancer cells and the cellular components of tumor

microenvironment has been highlighted. Recent evidence has shown that mitochondrial dynamics of cell types other than cancer are aberrantly regulated. Cancer cells educate adjacent fibroblasts to promote aerobic glycolysis, driving increased secretion of metabolites such as lactate and ketone. Excess lactate in tumor microenvironment is taken up by cancer cells, being used as a fuel for mitochondrial metabolism (121). This process of cancer cells mining and utilizing energy-rich metabolites from cancer-associated fibroblasts (CAFs) is termed reverse Warburg effect. CAFs exhibit overexpression of Mff. Mff-overexpressed fibroblast displayed fragmented structure of mitochondria, weakening mitochondrial function. Through aerobic glycolysis of fibroblast, fuel metabolites such as lactate, ketone and glutamine are generated and deposited into extracellular regions of tumor microenvironment (122). Cancer cells uptake and consume these metabolites for growth as well as metastasis. In breast cancer xenograft model, administration of 3-hydroxy-butyrate (ketone body) and L-lactate increased proliferation and lung metastases (121).

Melatonin suppressed mitochondrial fission preventing apoptosis induced by lipopolysaccharides (LPS) in Human Umbilical Vein Endothelial Cells (HUVEC) through activation of AMPK/sarcoplasmic endoplasmic reticulum Ca2+ATPase 2a (SERCA2a) pathway (123). High-mobility group box 1 (HMGB1) released from necrotic tumor cells promoted cancer growth (124). HMGB1 binds to receptor called advanced glycation endproduct (RAGE) which is overexpressed in cancer. Activation of RAGE upon binding of HMGB1 enhanced phosphorylation of ERK1/2, consequently causing an increase in mitochondrial ATP generation. This process is vital for the growth of cancer cells to fulfill the increased bioenergetic demand (125).

Immune cells such as T cells and macrophages are the major cellular constituents of tumor microenvironment (126). Immune suppression in tumor microenvironment is one of the cancer hallmarks (4). T cells lose their mitochondrial function and numbers in tumor microenvironment because PGC1α-mediated mitochondrial biogenesis is blocked. In cancer-specific effector T cells, the expression of PGC1α was decreased by activation of Akt signaling, leading to loss of anti-tumor activity (127). Changed regulation of

mitochondrial dynamics in T cell elicits metabolic reprogramming of the cells. Activated effector T cells with high glycolytic activity, showed fragmented structure of mitochondria. While, memory T cells with the increased mitochondrial metabolism, are present with highly fused mitochondrial structure. Promoting mitochondrial fusion in effector T cells by treating M1 (fusion promotor) and Mdivi-1 gave memory T cell properties. The process of mitochondrial fusion was required for efficient functioning of mitochondrial metabolism through the formation of highly organized cristae. During this process, Opa1 dictates mitochondrial fission/fusion balance and crista remodeling, eliciting metabolic shift of T cells, and thereby changing cellular fate of T cell (128).

1.4 Drug resistance and mitochondrial dynamics in cancer

Cancer cells exhibit characteristics of rapid proliferation and resistance to cell death (4). Fission of mitochondria plays a significant role in various cellular functions such as cellular proliferation and intrinsic apoptosis. Thus, both cell cycle regulation and apoptotic stimuli can affect the mitochondrial dynamics (129, 130). Aberrant proliferation of cells could result in disrupted regulation of mitochondrial dynamics. Increased production of mitochondrial ROS has been shown to be promoted by mitochondrial fission (113). A number of studies have suggested mitochondrial fission enhances susceptibility of cancer cells to conventional anti-cancer agents (129). However, mitochondrial dynamics is regulated in response to the external stimuli, possibly adaptive mechanism of cancer cells to cellular stresses (131). Cancer sphere cells forming in vivo-like structure of cancer displayed elevated ROS production and hypoxic gradient and exhibited fission of mitochondria, implicating cancer cells favor mitochondria fission over fusion under in-vivo like culture conditions. The formation of cancer spheres induced chemoresistance of the ovarian cancer cells to cisplatin (93). Inhibition of mitochondrial fission by Mdivi-1 or Mfn2 gene therapy suppressed tumor growth in the mice xenograft model of human lung cancer cells (132). Hence, enhancement of mitochondrial fission might not

always make cancer cells susceptible to apoptotic stimuli. Phytochemicals targeting mitochondrial dynamics of cancer cells might enhance efficacy of conventional anti-cancer agents in context-dependent manner. Many molecules regulating mitochondrial dynamics have been reported to be critical for drug resistance in cancer (Table 1).

Table 1. Proteins involved in mitochondrial fission/fusion processes and their roles in drug resistance of cancer

Protein	Function	Site of action	Relationship between expression and drug/apoptotic resistance	Associated cellular event/stress	References
Direct and indirect regulators of mitochondrial fission					
Spire1C	Actin nucleation; regulation of actin assembly at mitochondria-ER contacts	ER-mitochondria contact zones	Upregulation of Spire1/2 in HeLa and HEK293T cells → Induction of DNA repair	DNA damage	(17, 133)
INF2	Actin polymerization	ER-mitochondria contact zones	Downregulation in ovarian cancer cells (A2780) → Increased resistance to cisplatin	Decreased expression of vimentin	(16, 134)
Drp1	GTP hydrolysis; constriction of mitochondria	Mitochondrial outer membrane	Downregulation of phosphorylated Drp1 (Ser637) in ovarian cancer cells → Increased sensitivity to cisplatin	ROS	(135)
ROCK1	Formation of stress fiber; ROS production; apoptotic cell death; phosphorylation of Drp1 at Ser637	Cytosol	Inhibition by Y-27632 in neuroblastoma → Development of chemoresistance	Small Rho GTPases activity	(44, 136)
Dyn2	Regulation of endocytosis at the plasma membrane; constriction of mitochondria	Mitochondrial surface	Downregulation in ovarian cancer cells by hypoxia → Suppression of endocytosis which is an energy-requiring process	Hypoxia	(33, 137)
Mff	Recruitment of Drp1 to mitochondrial outer membrane	Mitochondrial surface	Upregulation in tongue squamous carcinoma cells → Increased sensitivity to cisplatin	BRCA1 activation	(21, 24)
MIEF1/2	Recruitment of Drp1 to mitochondrial outer membrane	Mitochondrial surface	Upregulation in 293T and HeLa cells → Associated with sensitivity to apoptotic stimuli	Autophagy	(23, 25)
Oma1	Mitochondrial metalloprotease responsible for proteolytic cleavage of OPA1	Intermembrane space of mitochondria	Upregulated upon cisplatin treatment in chemosensitive ovarian and cervical cancer cells but not in the chemoresistant	p53 mutation	(138)

			cancer cells → Increased sensitivity to cisplatin		
CDK1	Drp1 phosphorylation at serine 616	Cytosol	Upregulation in pancreatic adenocarcinoma → Increased resistance to gemcitabine and hyperproliferation	p53 mutation	(37, 139)
Erk	Drp1 phosphorylation at serine 616	Cytosol	Upregulation in non-small cell lung cancer (NSCLC) cells → Increased resistance to cisplatin	Inflammatory signals (galectin-1, COX-2 and TGF-β1)	(38, 39, 140)
CaMK1a	Drp1 phosphorylation at serine 637	Cytosol	Upregulation in chemoresistant ovarian cancer cells → Increased sensitivity to cisplatin through Drp1-mediated mitochondrial fragmentation	Intracellular calcium concentration	(43, 141)
Calcineurin	Dephosphorylation of Drp1 at serine 637	Cytosol	Inhibition in cervical cancer cells (HeLa) → Induction of anti-apoptotic pathway	Interaction with FKBP38	(48, 142)
MAPL	Drp1 SUMOylation at multiple residues; stabilization of ER-mitochondria contact sites via Drp1 signaling	ER-mitochondria contact zones	Upregulation in cervical cancer cells (HeLa) → Enhancement of Drp1-dependent apoptosis	ER/mitochondrial contact stabilization	(51)
PKCδ	Regulation of Drp1 phosphorylation at Ser616	Cytosol	Upregulated in human uterus sarcoma drug-resistant cells (MES-SA/Dx5) → Increased resistance to doxorubicin	Frizzled1 (FZD1) overexpression	(143, 144)
SENP3	DeSUMOylation of Drp1; enhancement of Drp1 recruitment to Mff	Cytosol	Upregulation in head and neck cancer when exposed to tobacco extract → Increased cell proliferation, angiogenesis and epithelial-mesenchymal transition	ROS	(49, 50)
O-GlcNAc transferase	Addition of O-linked N-acetylglucosamine at Thr585 and Thr586 of Drp1; enhancement of	Cytosol	Upregulated in breast cancer → Increased resistance to apoptosis	ER stress	(53, 145)

	Drp1 translocation to mitochondrial surface				
Direct and indirect regulators of mitochondrial fusion					
Mfn1	GTP hydrolysis; fusion of mitochondrial outer membrane	Mitochondrial outer membrane	Upregulation in colon cancer cells (LS174) → Protection from apoptotic stimuli	Hypoxia	(56)
Mfn2	GTP hydrolysis; fusion of mitochondrial outer membrane; tethering of mitochondria to ER	ER-mitochondria contact zones	Upregulation in hepatocellular carcinoma → Induction of apoptosis via mitochondrial apoptotic pathway	p53 activation	(59)
Opa1	GTP hydrolysis; fusion of mitochondrial inner membrane	Mitochondrial inner membrane	Upregulation of L-Opa1 in ovarian cancer cells (OV2008) → Induction of apoptosis	p53 activation induced by cisplatin	(138, 146)
YME1L	Proteolytic processing of OPA1	Intermembrane space of mitochondria	Knockdown in human embryonic kidney cells (HEK293) → Induction of apoptosis	Apoptotic stimuli (staurosporine and H_2O_2)	(147)
Cofilin1	Depolymerization of actin	Mitochondrial surface	Upregulation of phosphorylated cofilin1 in taxol-resistant ovarian cancer cells (SKOV3/TR2500, SKOV3/TR30 and A2780/TR) and primary ovarian cancer tissues from chemoresistant cases → Increased resistance to taxol	Persistent exposure to taxol	(18, 148)
Pim-1	Serine/threonine kinase; inhibition of Drp1 translocation to mitochondria	Cytosol	Upregulated in hypoxic pancreatic ductal (PCI-10, PCI-35, PCI-43, KMP-4), cervical (HeLa) and colorectal (HCT-116) cancer cells → Stabilization of mitochondrial membrane potential and resistance to cisplatin	Hypoxia	(46, 149)
CDK5	Drp1 phosphorylation at Ser616	Cytosol	Inhibition in tumor spheres of urinary cancer cells and mammary gland	Tumor sphere formation	(40, 41)

			adenocarcinoma cells (T24 and MCF7) → Stabilization of Foxo1 and induction of apoptosis via Bim-mediated apoptosis		
PKA	Drp1 phosphorylation at Ser637	Cytosol	Upregulation in doxorubicin-resistant sarcoma (MES-SA/Dx5) and mammary gland adenocarcinoma cells (MCF7/ADR2) → Increased resistance to doxorubicin	Persistent exposure to doxorubicin; Wnt5a activation	(42, 150)

1.4.1 Mitochondrial fusion and chemoresistance

Several plant-derived compounds elicit disrupted regulation of mitochondria, showing anti-cancer effect. Treatment of cryptolepine, an active plant alkaloid from the roots of the shrub Cryptolepis sanguinolenta suppressed the expression of proteins regulating mitochondrial dynamics, resulting in inhibition of melanoma cell growth (151). Also, apoptosis of ovarian cancer cells was augmented by piceatannol, human bioactive metabolite of resveratrol, in combination with conventional anti-cancer agent, cisplatin, through enhancement of Drp1-dependent mitochondrial fission (152). Piperlongumine induced apoptosis in cisplatin resistant ovarian cancer cells through down-regulation of inhibitory phospho-Drp1 (Ser637) (135). Treatment of the lectin, Sambucus nigra agglutinin on ovarian cancer cells elicited overexpression of sialic acids on the cell surface leading to activation of AKT/ERK pathways and inducing mitochondrial fission-mediated apoptosis by stimulating Drp1 translocation to mitochondria (153). Whereas, in neuroblastoma cells, ginkgolid K isolated from Ginkgo biloba leaves has been shown to prevent apoptosis induced by ischemic reperfusion injury through inhibition of mitochondrial fission (154).

Several studies have suggested that induction of mitochondrial fission sensitizes cancer cells to cell death induced by chemotherapeutic agents. Inhibition of BCL-2/Xl by ABT-737 enhances sensitivity to cisplatin by triggering mitochondrial fission and mitophagy formation in cisplatin-insensitive cholangiocarcinoma cells (155) and metastatic melanoma cells (156). Prohibitin (Phb1) overexpressed in ovarian cancer has been shown to promote stabilization of mitochondrial structure. Knockdown of Phb1 disrupts mitochondrial connectivity by enhancing fission process of mitochondria, and this, in turn, sensitizes ovarian cancer cells to cell death induced by staurosporine (STS) (157). Resistance to tumor necrosis factor-related apoptosis-inducing ligand (TRAIL) has been reported in many types of cancer (158). Compared to treatment with TRAIL alone, co-treatment of TRAIL and gold nanoparticles sensitized non-small-cell lung cancer cells to TRAIL

through Drp1-mediated mitochondrial fission (159). Knockdown or inhibition of Drp1 suppressed cisplatin-induced generation of ROS, desensitizing breast cancer cells to cisplatin (113).

About one-half of cancer from melanoma patients harbor BRAFV600 mutation, displaying highly activated MAPK signaling. Therapy specifically targeting MAPK pathway for melanoma patients with BRAF mutation has been incorporated, while a large proportion of patients treated with MAPK inhibitor showed intrinsic resistance to the therapy. Targeting mitochondrial biogenesis processes enhanced efficacy of MAPK inhibitor in melanoma cells (160). Moreover, hyper-fusion state of mitochondria has been found to be associated with chemoresistant properties of gynecologic cancer cells (161). Thus, disrupting regulation of mitochondrial fusion and biogenesis might be an effective therapeutic strategy through sensitization of cancer cells to anti-cancer agents.

1.4.2 Mitochondrial fission and chemoresistance

Recent studies have suggested that fission of mitochondria are involved in cytoprotective effect as an adaptive mechanism against cellular stress. Decreased mitochondrial ROS generation through suppression of mitochondrial metabolism in cancer cells has been shown to be associated with chemoresistance. Soluble factors secreted by bone marrow-derived mesenchymal stem cells trigger mitochondrial fission by activating Erk/Drp1 pathway, giving rise to chemoresistant phenotype in T-cell acute lymphoblastic leukemia (T-ALL) cells (38). Mitochondrial fission mediated by ROS led to increased survival of hepatocellular carcinoma cells (162). Downregulation of Six1 by miR-488 inhibited Drp1-mediated mitochondrial fission, resulting in sensitization of ovarian cancer cells to cisplatin (163). Collectively, fission-state of mitochondria may be an important adaptive mechanism of cancer cells under the circumstances of high level of ROS and could be a therapeutic target against cancer.

1.4.3 Mitochondrial trafficking and chemoresistance

TNT-mediated intercellular trafficking of mitochondria has been shown to be linked to malignant phenotypes of cancer such as survival from apoptotic signals and invasiveness. Intercellular transfer of mitochondria from healthy pheochromocytoma (PC) 12 cells to apoptotic cells rescued the apoptotic cells from cell death (164). Similarly, apoptotic H9c2 cardiomyocytes experiencing ischemic stress was rescued by receiving mitochondrial compartment from bone-marrow derived mesenchymal stem cells through TNTs (165). Formation of TNTs between two different bladder cancer cell lines increased metastatic potential of cancer cells in vivo and in vitro (75). Pasquier et al. have shown the presence of TNTs in tumor spheroids and cancer explant cultures. Trafficking of mitochondria between endothelial cells and cancer cells was associated with an increase of chemoresistant phenotype in cancer (76). In addition, hypoxia increased formation of TNTs in chemoresistant ovarian cancer cell lines (SKOV3 and C200) (166).

The results from above studies investigated relationship between mitochondrial dynamics and chemoresistance in different cancer types may imply that mitochondrial dynamics is regulated in a context-dependent manner. The shape of mitochondria is prone to be altered by external stimuli. Various factors present in tumor microenvironment including hypoxia, ROS and inflammatory signals have been shown to modulate mitochondrial dynamics, conferring cellular heterogeneity and chemoresistance. Therefore, profound understanding of mitochondrial dynamics in relation to the type of cancer and acellular factors in tumor microenvironment may increase the opportunity of developing a novel druggable target of drug-resistant cancer.

1.5 Study summary

Tumor microenvironment has been recognized as an important regulator of malignant phenotypes of cancer cells, giving rise to intra-tumoral heterogeneity in many types of cancer.

Cells from different tissues or even the same type of cells from the same tissue could have different numbers and morphology of mitochondria depending on external cues present in tissue microenvironment. In **chapter 2**, Our study showed the impact of hypoxic tumor microenvironment on regulation of mitochondrial dynamics as well as its association with cisplatin resistance in ovarian cancer.

We found a chemoresistance mechanism of ovarian cancer cells under hypoxia, acquired through mitochondrial fission. We showed that inhibition of mitochondrial fission significantly increased sensitivity of hypoxic ovarian cancer cells to cisplatin, whereas normoxic (20% oxygen) cancer cells did not show the same effect when mitochondrial fission was inhibited. For further confirmation in clinical samples from patients with advanced ovarian cancer, we treated mitochondrial fission inhibitor and cisplatin on primary tissue and ascites-derived spheroids. Taken together, our results indicate that mitochondrial fission-induced chemoresistance is specific to hypoxic cancer cells and it could be a druggable target of ovarian cancer to increase the efficacy of cisplatin.

In **chapter 3**, to understand a critical cytokine regulator cancer metastasis, publicly-available data was analyzed and TNF is uncovered to be important modulator of ovarian cancer microenvironment. We revealed that TNF singnaling is modulated by RELB. Subsequently, upregulation of RELB promoted invasive capacity of ovarian cancer cells by regulating PLAU (uPA) expression.

Ovarian cancer spreads to various organs through fluid accumulated in the peritoneal cavity termed malignant ascites, aggravating cancer progression. So **in chapter 4**, Our study shows the landscape of molecular and cellular heterogeneity in the malignant ascites with a specific focus on the anoikis-

resistant phenotype of cancer cells by interrogating ligand-receptor interactions between immune and cancer cells enriched in the malignant ascites. We incorporated a single-cell RNA sequencing data from five malignant ascites samples to delve into cellular composition, cell-to-cell communication and vital signaling pathways of cancer cells in the malignant ascites. We identified seven distinct cell types based on the expression patterns of cell-type-specific signatures. Macrophages were the most heterogeneous cell type with eleven sub-clusters. We analyzed signaling pathways enriched in the different clusters and subtypes of cells. We have implemented a recently published method called 'NicheNet' to predict the communication between immune and ovarian cancer cells. We revealed that CCL5 is enriched in T cells and NK cells, potentially governing ovarian cancer cell survival in the ascites through SDC4. We showed that SDC4 is globally expressed receptor in the cancer cells from the five ascites samples. This finding was further corroborated by analyzing the recently published. We found that average SDC4 expression strongly correlates with ovarian cancer cell proportion in each sample, further supporting the potential role of SDC4 in cancer cell survival under the ascites microenvironment. Moreover, elevated SDC4 expression predicted poor overall survival outcomes of ovarian cancer patients. Thus, we suggest interactions between immune cell-secreted CCL5 and cancer cell-expressed SDC4 as a novel druggable target of ovarian cancer which may curtail chances of cancer cell survival in the malignant ascites microenvironment.

2. Chapter II: Mitochondrial fission causes cisplatin resistance under hypoxic conditions via ROS in ovarian cancer cells

2.1 Introduction

Ovarian cancer is the most lethal gynecologic malignancy which is the leading cause of cancer-related deaths in women (167). The five-year survival rate of the advanced-stage cancer is below 40% worldwide (168). For past decades, ovarian cancer survival has not improved due largely to frequent relapses and the lack of effective screening tools detecting the cancer at an early stage (169). Although cytoreductive surgery followed by platinum-based chemotherapy (CDDP or carboplatin) in combination with taxanes (paclitaxel or docetaxel) is standard of care, the recurrence rate of the advanced-stage cancer is still around 70% (170). Therefore, a complete understanding of molecular mechanisms accounting for relapse and subsequent chemoresistance is critical for establishing the most effective treatment strategies.

The importance of tumor microenvironment in cancer progression has been increasingly emphasized in recent years. Rapid proliferation of cancer cells and slow rate of angiogenesis make a tumor hypoxic in most solid tumors. At the tissue level, the actual oxygen level ranges from 1 to 11%, deviating greatly from the 20% which is the atmospheric oxygen level. Hypoxia may refer to less than 1% oxygen tension (171). Cellular homeostasis is adjusted in response to the oxygen availability in cancer cells by altering intracellular signaling pathways. For example, the transcription factor, hypoxia-inducible factors 1 α subunit (HIF-1α) is stabilized by hypoxia and transactivates various target genes (172). Additionally, more recent studies on ovarian and breast cancer cells suggest chromatin remodeling is promoted by hypoxia to regulate expression of gene sets (173, 174). Solid tumors that are more hypoxic show more malignant behavior through fine-tuning of oncogenic signaling pathways. The degree of tumor hypoxia varies from patient to patient and is correlated with poor prognosis in epithelial ovarian cancer (175, 176).

The term ‘mitochondrial dynamics’ refers to changes in shapes and localization of mitochondria (177, 178). While previous studies have shown that the structure of mitochondria dynamically change through fission and fusion processes in response to various microenvironmental cues (179), the

factors in tumor microenvironment that regulate mitochondrial dynamics is not entirely understood. However, several key molecules involved in the fission and fusion of mitochondria have been revealed recently. Mitofusins 1 and 2 (Mfn1/2) are crucial molecules for mediating fusion of mitochondrial outer membranes and tethering the outer membrane to the endoplasmic reticulum (ER). Mitochondrial fission is driven by dynamin-related protein 1 (Drp1) which translocates from cytosol to mitochondrial outer membrane upon activation. Phosphorylation of Drp1 can dictate its activation status. Studies have shown Drp1 phosphorylation at Ser616 activates Drp1 and induces mitochondrial fission (36, 180). Whereas, Drp1 phosphorylation at Ser637 inactivates Drp1, thus inhibiting mitochondrial fission (181).

Our previous study has revealed that the formation of tumor sphere enhanced mitochondrial fission (93). Sphere-forming cancer cells are more resistant to anti-cancer agents and are exposed to decreasing oxygen gradient towards the center of the sphere, leading us to postulate that hypoxia could be a critical factor affecting the mitochondrial dynamics and chemoresistance. To date, the consequences of hypoxia-mediated changes in mitochondrial dynamics in relation to sensitivity to anti-cancer drugs have not been explored. In this study, we demonstrate that mitochondrial fission elicited by Drp1 under hypoxia is associated with CDDP resistance in ovarian cancer cells.

2.2 Materials and methods

2.2.1 Cell lines

Human ovarian cancer cell lines, SKOV3, OVCAR3 and PA1 were purchased from American Type Culture Collection (Rockville, MD). All three cancer cell lines were grown in RPMI1640 (WELGENE, Seoul, South Korea) containing 10% Fetal Bovine Serum (FBS; Gibco, Gaithersburg, MD), 100 U/mL penicillin and 100 μg/mL streptomycin (Invitrogen, Carlsbard, CA). IOSE385 were generously provided by Prof. Young Kee Shin and grown in Dulbecco's Modified Eagle Medium/Nutrient Mixture F-12 (DMEM/F12; Gibco) containing 10% FBS (Gibco), 100 U/mL penicillin and 100 μg/mL streptomycin (Invitrogen). All the cell lines used in this study were authenticated and tested for mycoplasma. Cells were maintained in 5% CO_2 humidified incubator at 37 ºC. For hypoxia, cells were grown in the anaerobic system model 1025 (Thermo Forma, Waltham, MA).

2.2.2 Chemical reagents

CDDP, NAC and Trolox were obtained from Sigma-Aldrich (St. Louis, MO). Mdivi-1 and M1 were purchased from Merck-Millipore (Burlington, MA, USA). H_2O_2 was purchased from Junsei (Tokyo, Japan).

2.2.3 Bioinformatics

The GEO dataset, GSE14407, was used to analyze mRNA levels of SLC2A1 (Probe ID: 201250_s_at), VEGFA (Probe ID: 212171_x_at), PDGFB (Probe ID: 216061_x_at), DNM1L (probe ID: 203105_s_at) and Mfn1(probe ID: 207098_s_at) in 12 normal ovarian surface epithelium tissues and 12 ovarian cancer tissues obtained through laser capture microdissection. For gene set enrichment analysis (GSEA), mRNA expression of ovarian cancer tissue samples (n=12) from GSE14407 was used, and a formatted GCT file was used as an input for the GSEA algorithm v3.0 (broadinstitute.org/gsea).

2.2.4 Immunoblotting analysis

Cells were lysed with 2X lysis buffer (10 mM Tris-HCl, 150 mM NaCl, 1 mM EDTA, 1 mM EGTA), 1% Triton X-100, 1 mg sodium deoxycholate, EDTA-free protease inhibitor cocktail, 1 mM phenylmethylsulfonyl fluoride and 1 mM Na3VO4 for 20 min. Protein concentration was measured using BCA Protein Assay Kit (Thermo Scientific, Waltham, MA). SDS-PAGE was conducted with the appropriate polyacrylamide gel concentration (6%, 7.5% and 9% gels). Separated protein samples were then transferred onto nitrocellulose membrane. Membranes were blocked with 5% dry skim milk (w/v) in TBS-T for 2 h and incubated overnight at 4°C with specific primary antibody. Membranes were then washed with TBS-T and incubated with a horseradish peroxidase-conjugated secondary antibody (1:5000) diluted in 5% dry skim milk for 2 h at room temperature. Primary antibodies used in this study are Mfn1 (1:1000; sc-50330, SantaCruz Biotechnology, Santa Cruz, CA), Drp1 (1:1000; #8570, Cell Signaling Technology, Beverly, MA), p-Drp1Ser616 (1:1000; #3455, Cell Signaling Technology), p-Drp1Ser637 (1:1000; #4867, Cell Signaling Technology), HIF-1α (1:500; MA1-16504, Invitrogen), PARP-1 (sc-7150, SantaCruz Biotechnology) and α-tubulin (1:5000; T5168, Sigma-Aldrich). Chemiluminescence detection kit (AbFrontier, Seoul, Korea) was used to detect signals. To obtain protein expression ratios, protein bands were quantified using Fiji (ImageJ ver. 1.52a).

2.2.5 MTT assay

Cell viability of ovarian cancer cell lines with different treatment groups was measured by MTT assay. Cells were plated onto 96-well plates and patient-derived spheroids embedded in Matrigel were seeded on to 24-well plates. For analysis, 2 mg/mL of MTT dissolved in phosphate-buffered saline (PBS) was added. After 3 h incubation with MTT, culture medium containing MTT solution was removed and DMSO was added to solubilize formazan generated. For patient-derived spheroids, Matrigel was mechanically dissociated by pipetting thoroughly after addition of DMSO. Optical density values were

measured at a wavelength of 540 nm using a spectrophotometer (LabSystem, Helsinki, Finland).

2.2.6 Apoptosis analysis

Apoptosis was measured by flow cytometric analysis using Annexin V-FITC apoptosis kit (BD Bioscience, San Jose, CA) according to the manufacturer's protocol. In brief, cells were trypsinized and centrifuged at 500 x g for 5 min at 4°C. Cell pellets were stained with Annexin V-FITC and propidium iodide (PI) in PBS. Apoptotic cells were analyzed by BD FACS Canto II flow cytometer (BD Bioscience).

2.2.7 Analysis of relative mitochondrial activity and mass

Cells were harvested and suspended in serum-free medium with either 200 nM MitoTracker™ Orange (M7510) or 200 nM MitoTracker™ Green FM (M7514) which were obtained from Molecular Probes, Inc. (Eugene, OR). Cells were stained by incubation (37ºC, 30 min) and washed with PBS to remove excessive dyes. Relative fluorescence intensity of cells was analyzed using BD FACS Canto II flow cytometer (BD Bioscience).

2.2.8 Immunocytochemistry and confocal microscopy

Cells and Matrigel-embeded PDS cultured on NuncTM Lab-TekTM II 4-well chamber slideTM w/ removable wells (Thermo Scientific) were stained with 250 nM MitoSpyTM Orange CMTM ROS dye (BioLegend, San Diego, CA) for 20 min at 37°C. Then cells were fixed with 4% paraformaldehyde (PFA) in PBS, permeabilized with 0.1% Triton X-100, blocked with 10% goat serum and incubated with the specific primary antibody (1:250) and the Alexa Fluor 488-conjugated secondary antibody (Abcam, Cambridge, United Kingdom). Cells were stained with 1 μg/mL DAPI (Thermo Scientific) before mounting the samples with ProLongTM Glass Antifade Mountant (Thermo Scientific). Prepared samples were visualized with a 63x oil immersion objective lens of an LSM800 (Carl Zeiss, Oberkochen, Germany) confocal microscope. To

quantify mitochondrial fission, mitochondrial length from three independent experiments was measured using ImageJ. Lengths of 123-163 mitochondria from 12-18 cells in different groups were measured.

2.2.9 Detection of relative ROS levels

Intracellular ROS levels were measured using 2,7-dichloro-dihydrofluorescein diacetate (DCFH-DA; Sigma-Aldrich) which was used to detect intracellular hydrogen peroxide level. Dihydroethidium (DHE; Sigma-Aldrich) oxidized by intracellular superoxide and emits fluorescent signal, was used to compare intracellular superoxide level in groups of cells with different oxygen status. Cultured cells were washed once and incubated with either DCFH-DA (20 μM, 30 min) or DHE (5 μM, 10 min). Relative DCF or DHE fluorescence of cells was analyzed using BD FACS Canto II flow cytometer (BD Bioscience).

2.2.10 TUNEL assay

To measure DNA damage levels, TUNEL assay was conducted using a Click-iT™ Plus TUNEL Assay kit (Invitrogen). Cells cultured on Nunc™ Lab-Tek™ II 4-well chamber slide™ w/ removable wells (Thermo Scientific) were washed once with PBS and fixed with 4% PFA for 15 min. For permeabilization, cells were incubated with 0.25% Triton X-100 in PBS for 20 min at room temperature. Then, TUNEL staining was done according to the manufacturer's protocol. Before mounting cover slips onto the slides, cells were stained with DAPI (1 μg/mL; Thermo Scientific) for 5 min. For quantification of TUNEL positive cells, 100-150 cells were analyzed from three independent cell counts.

2.2.11 Transfection of siRNA

For Drp1 silencing, SKOV3 and PA1 cells were transfected with 50 nM si-Drp (SantaCruz Biotechnology), using RNAiMax (Invitrogen). In a negative control group, 50 nM scramble siRNA (mBioTech, Korea) was transfected. At 24 h post-transfection, cells were harvested and reseeded for assays.

2.2.12 Isolation and culture of primary cells and patient-derived spheroids

This study was conducted after approval from the Institutional Review Board (IRB) of Seoul National University Hospital (IRB no.: 1409-154-616) and performed in compliance with the Declaration of Helsinki. To use patient samples for this study, informed consent was obtained from all subjects. PBMCs and adipose ASCs were isolated and cultured as previously described (182, 183). PBMCs were grown in RPMI1640 (WELGENE) containing 10% FBS (Gibco), 100 U/mL penicillin and 100 μg/mL streptomycin (Invitrogen). ASCs were cultured in MesenPRO RS medium (Gibco) containing 1% GlutaMAX (Gibco), 100 U/mL penicillin and 100 μg/mL streptomycin (Invitrogen).

Malignant ascites obtained from four ovarian cancer patients at the time of primary debulking surgery were used for isolation of primary tumor cells/spheroids. Malignant ascites was centrifuged at 1400 x g for 10 min. Ficoll density gradient centrifugation with Ficoll-PaqueTM (GE healthcare, Franklin Lakes, NJ) was used to remove erythrocytes. Primary tumor tissues were obtained during primary debulking surgery. Tissues were washed three times with PBS and mechanistically minced using a razor blade. Fragmented tissues were then incubated (37°C, 60 min) in 2.4 U/mL of dispase (Gibco) diluted in PBS. Thereafter, the undigested large tissue debris was removed by filtering through a 100-μm cell strainer. Isolated cells/spheroids were washed three times with PBS and the number of cells/spheroids was counted. The medium components required for estrogen receptor stimulation, stemness, ROCK inhibition, anti-oxidation and TGF-β receptor kinase inhibition were adapted from previous studies of organoid culture (184-187). Cells/spheroids embedded in phenol red-free Matrigel Growth Factor Reduced Basement Membrane Matrix (BD Bioscience) were cultured in Advanced DMEM/F12 (Gibco) supplemented with 10 mM HEPES (Gibco), 1x GlutaMax (Gibco), 1 μM β-Estradiol (Sigma-Aldrich), 1 mM nicotinamide (Sigma-Aldrich), 10 ng/mL

recombinant human Noggin (PeproTech, Rocky Hill, NJ, USA), 10 ng/mL recombinant R-Spondin1 (PeproTech), 1x N2 (Invitrogen), 1x B27 (Invitrogen), 10 ng/mL EGF (Invitrogen), 10 ng/mL FGF2 (PeproTech), 10 ng/mL FGF10 (PeproTech), 10 μM Y-27632 dihydrochloride (Sigma-Aldrich), 0.5 μM SB431542 (Sigma-Aldrich) and 1mM N-acetylcysteine (Sigma-Aldrich).

2.2.13 Statistical analysis

For statistical comparisons between two groups, two-sided independent samples t-test was conducted. For comparisons between more than two groups, one-way analysis of variance (ANOVA) with Bonferroni's PostHoc test was performed. These tests were performed using IBM SPSS statistics 25 (SPSS Inc., Chicago, IL). Correlation values were calculated by the Pearson correlation coefficient test using the GraphPad Prism 5 software. A P value < 0.05 was considered statistically significant.

2.3 Results

2.3.1 Hypoxia makes ovarian cancer cells resistant to CDDP irrespective of p53 status

Hypoxia has been shown to be related with the recurrence and chemoresistance of cancer cells. Using the publicly available dataset from the gene expression omnibus (GEO) database, GSE14407, which contains microarray data from normal and ovarian cancer tissue samples, transcript expressions of hypoxia markers in normal and ovarian cancer tissue samples were compared. Hypoxia markers (SLC2A1, VEGFA and PDGFB) were significantly upregulated in ovarian cancer tissues than the normal ovarian epithelial tissues (Fig. 3a). These data indicate that cancer tissues are more hypoxic than normal tissues.

Ovarian cancer exhibits a high mutation rate of TP53, the gene encoding p53, that over 90% of high-grade serous epithelial ovarian cancer tissues harbor the mutation at this gene (188). Previous studies have shown hypoxia induces activation of p53 and can induce cancer cell death (189, 190). We examined the effect of hypoxia on CDDP sensitivity, incorporating ovarian cancer cells with different p53 mutational status. SKOV3 (p53 null-type), OVCAR3 (p53 mutant-type) and PA1 (p53 wild-type) were cultured under 20% O_2 or hypoxia (< 1% O_2). To confirm hypoxic condition given to cancer cells, protein level of a hypoxia-induced transcription factor, HIF-1α, was determined using Western blotting. Protein content of HIF-1α was increased in the cancer cells cultured under hypoxic conditions as well as in the positive control group which is cobalt chloride ($CoCl_2$)-treated cells cultured under 20% O_2 (Supplementary Fig. 1). Cell viability of both 20% O_2 and hypoxia-cultured cancer cells after incubating with increasing concentrations of CDDP for 24 and 48 h was analyzed. The viability of hypoxic cancer cells was significantly higher than that of 20% O_2-cultured cancer cells when treated with the same concentration of CDDP (Fig. 3b). Also, the proportion of apoptotic cells (positive for either Annexin V-FITC or both Annexin V-FITC and PI staining) in hypoxia-cultured cancer cells were markedly lower than those in the 20% O_2-cultured cancer cells after incubation

with CDDP for 48 h (Fig. 3c). These results suggest that hypoxia induces CDDP resistance in ovarian cancer cells irrespective of their p53 status.

a

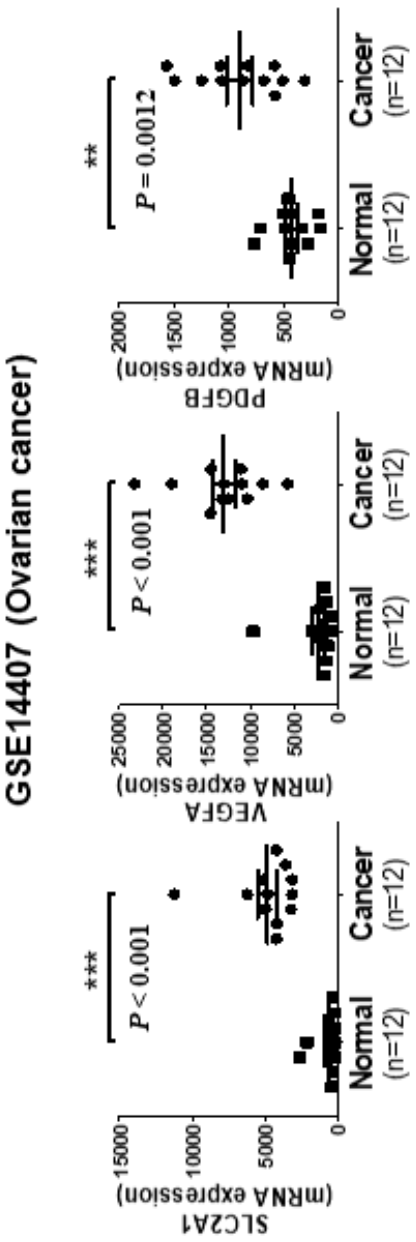
GSE14407 (Ovarian cancer)
SLC2A1
(mRNA expression)
15000
10000
5000
0
***
P < 0.001
Normal (n=12)
Cancer (n=12)
VEGFA
(mRNA expression)
25000
20000
15000
10000
5000
0
***
P < 0.001
Normal (n=12)
Cancer (n=12)
PDGFB
(mRNA expression)
2000
1500
1000
500
0
**
P = 0.0012
Normal (n=12)
Cancer (n=12)

b

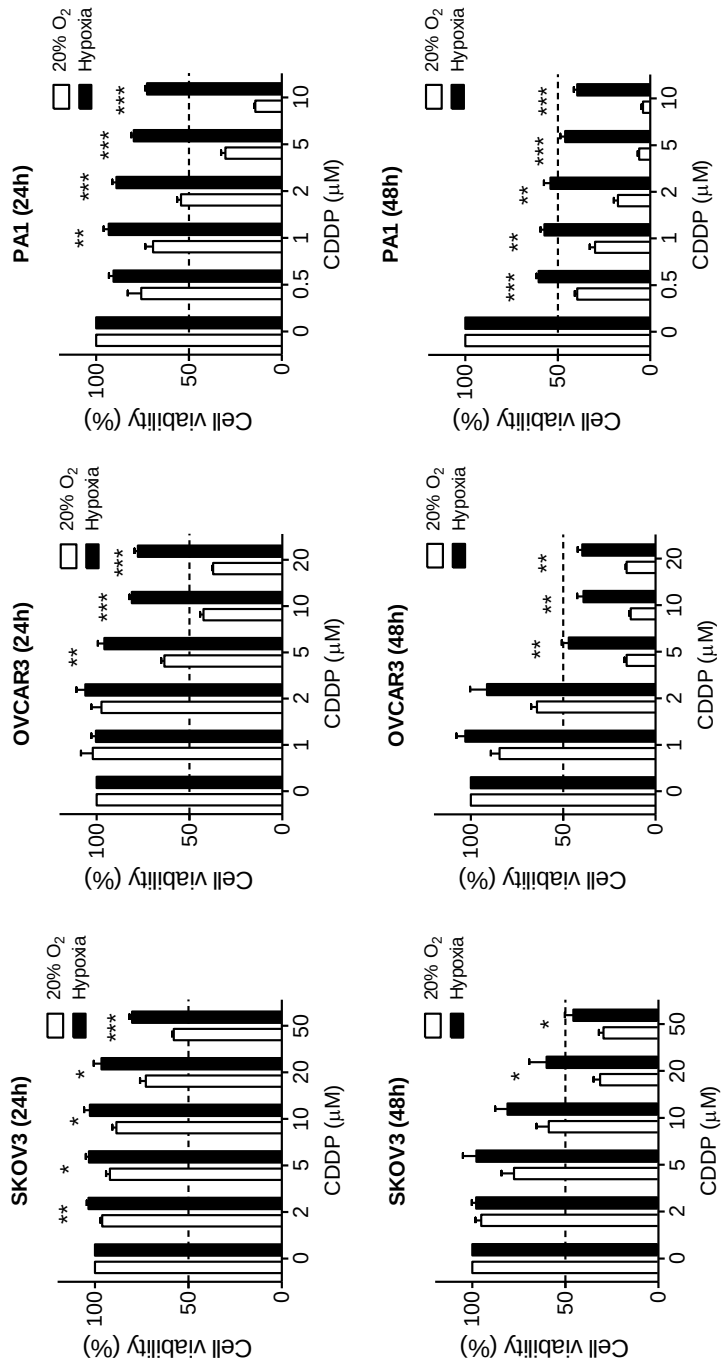
PA1 (24h)
PA1 (48h)
OVCAR3 (24h)
OVCAR3 (48h)
SKOV3 (24h)
SKOV3 (48h)
20% O2
Hypoxia
Cell viability (%)
CDDP (μM)

c

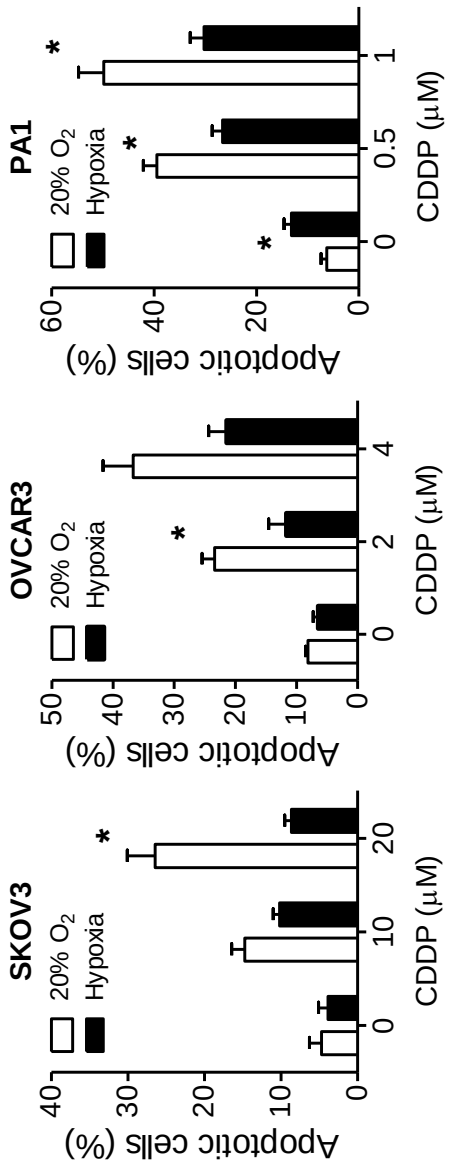

Figure 3. Hypoxia induces CDDP resistance in ovarian cancer cells.

a Expression of hypoxia markers (SLC2A1, VEGFA and PDGFB) in normal ovarian surface epithelial tissue samples (squares; n=12) and ovarian cancer tissue samples (circles; n=12) in the GEO dataset (GSE14407). Values are presented as means ± SEM (**, $P < 0.01$; ***, $P < 0.001$). **b** SKOV3, OVCAR3 and PA1 cells grown under 20% O_2 or hypoxic conditions were treated with increasing concentrations of CDDP for 24 and 48 h and the cell viability was determined by MTT assay. Means between 20% O_2 and hypoxia culture groups were compared. Values are presented as means ± SEM from three independent experiments (*, $P < 0.05$; **, $P < 0.01$; ***, $P < 0.001$). **c** SKOV3, OVCAR3 and PA1 cells cultured under 20% O_2 or hypoxia were treated with the indicated concentrations of CDDP for 48 h. Cells were stained with Annexin V-FITC/PI and analyzed using flow cytometry to measure apoptotic cells (Annexin V-FITC stained cells). Means between 20% O_2 and hypoxia culture groups were compared. Values are presented as means ± SEM from three independent experiments (*, $P < 0.05$).

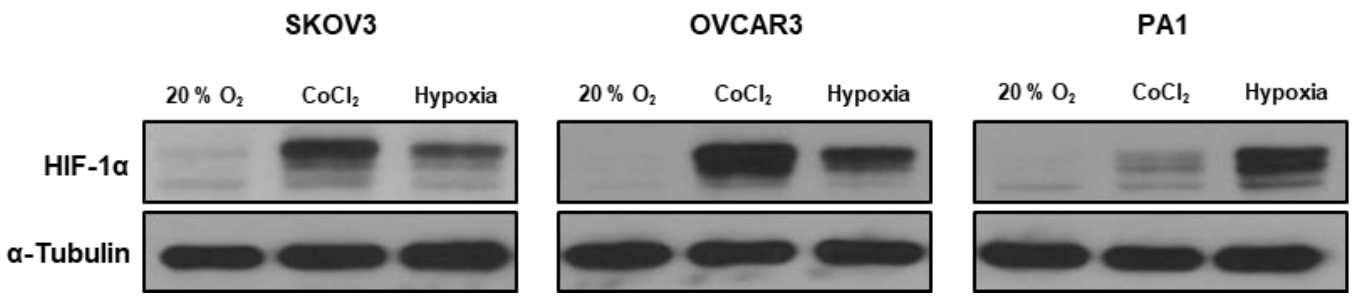
SKOV3
OVCAR3
PA1
20 % O2
CoCl2
Hypoxia
20 % O2
CoCl2
Hypoxia
20 % O2
CoCl2
Hypoxia
HIF-1α
α-Tubulin

Supplementary Fig. 1. Hypoxic culture increases HIF-1α protein contents of ovarian cancer cells.

Protein expression of HIF-1α (hypoxia marker) in ovarian cancer cells (SKOV3, OVCAR3 and PA1) grown under 20% O_2 or hypoxic conditions for 6 h was examined by Western blotting. Cobalt chloride ($CoCl_2$)-treated groups were used as positive control for HIF-1α expression. As internal control, α-tubulin expression was examined.

2.3.2 Hypoxia increases mitochondrial fission in ovarian cancer cells

Mitochondria are vital organelles of eukaryotic cells, and defective mitochondrial function is linked to the pathogenesis of various diseases including cancer (180). To explore the effect of hypoxia on phenotypic changes of the mitochondria, mitochondrial mass and activity were measured in SKOV3, OVCAR3 and PA1 cells cultured under hypoxic conditions. Mitochondrial mass showed an increasing pattern in a time-dependent manner, while retaining mitochondrial activity at the nearly constant level when hypoxia was applied. Next, to assess changes in mitochondrial activity per mass induced by hypoxia, activity to mass ratio of mitochondria was computed. Activity to mass ratio of mitochondria was significantly decreased by hypoxia in a time-dependent manner in two of the cell lines examined (OVCAR3 and PA1) and the other cell line (SKOV3) showed the time-dependent decreasing pattern. These results suggest that mitochondria may be present as a less efficient form when oxygen availability is limited (Fig. 4a).

Next, ovarian cancer cells were subjected to the analysis for morphological changes of mitochondria under hypoxia. To achieve this, SKOV3, OVCAR3 and PA1 cells cultured under hypoxia were stained with MitoSpy and fixed with 4% PFA. Representative confocal microscopic images of cancer cells exposed to hypoxia for 48 h show that fission of mitochondria was induced under hypoxia, indicated by increased numbers of small fragments of mitochondria (Fig 4b, c). Induction of mitochondrial fission by hypoxia was also observed in DsRed2-mito vector-transfected cancer cells (Supplementary Fig. 2).

a

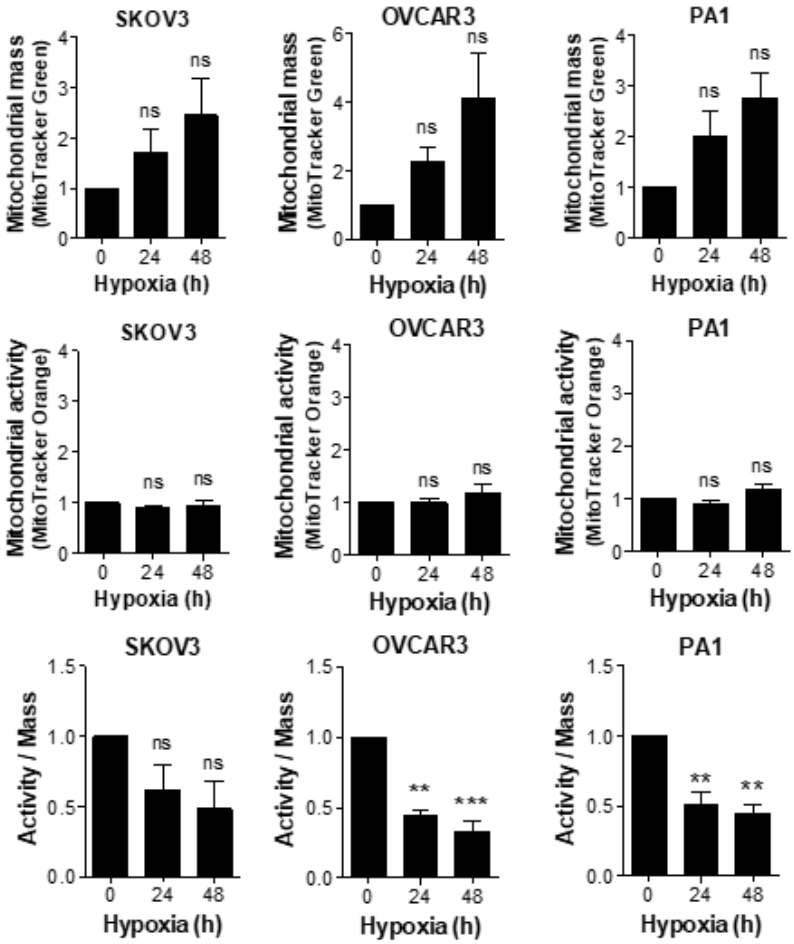
SKOV3
OVCAR3
PA1
Mitochondrial mass (MitoTracker Green)
Mitochondrial activity (MitoTracker Orange)
Activity / Mass
Hypoxia (h)
0
24
48
ns
**
***

b

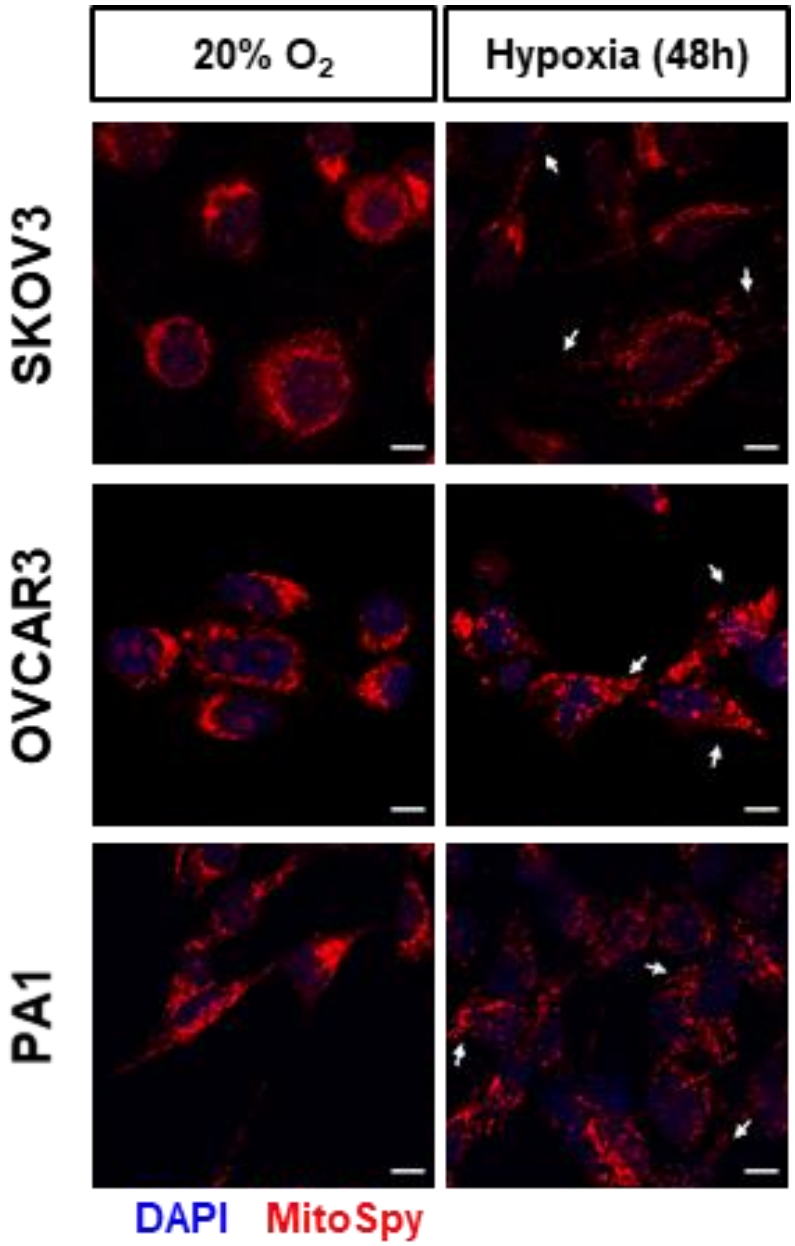

c

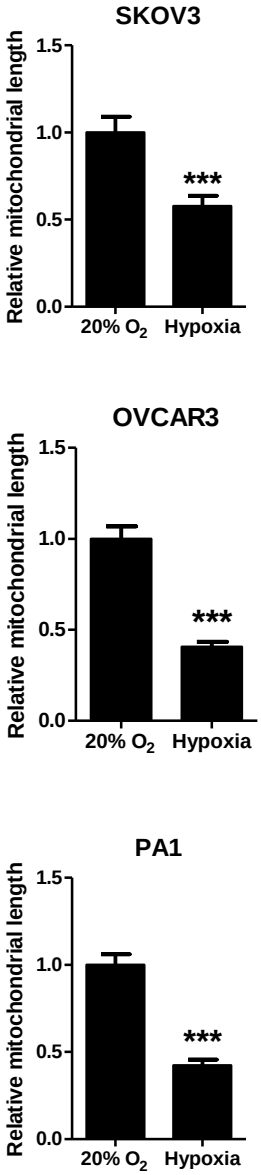
SKOV3
Relative mitochondrial length
1.5
1.0
0.5
0.0
***
20% O2
Hypoxia
OVCAR3
Relative mitochondrial length
1.5
1.0
0.5
0.0
***
20% O2
Hypoxia
PA1
Relative mitochondrial length
1.5
1.0
0.5
0.0
***
20% O2
Hypoxia

d

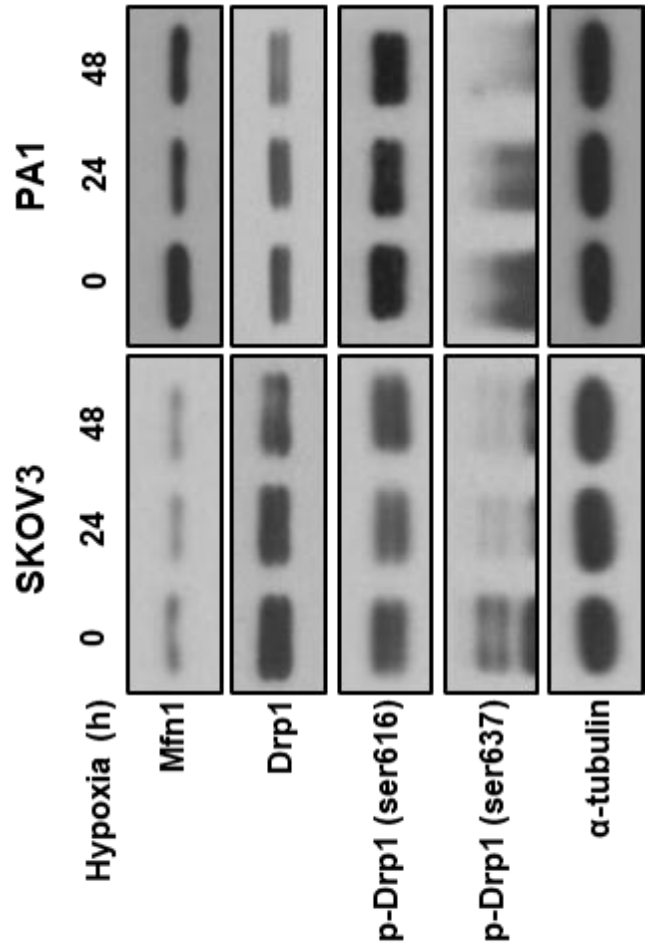
SKOV3
PA1
Hypoxia (h)
0
24
48
0
24
48
Mfn1
Drp1
p-Drp1 (ser616)
p-Drp1 (ser637)
α-tubulin

e

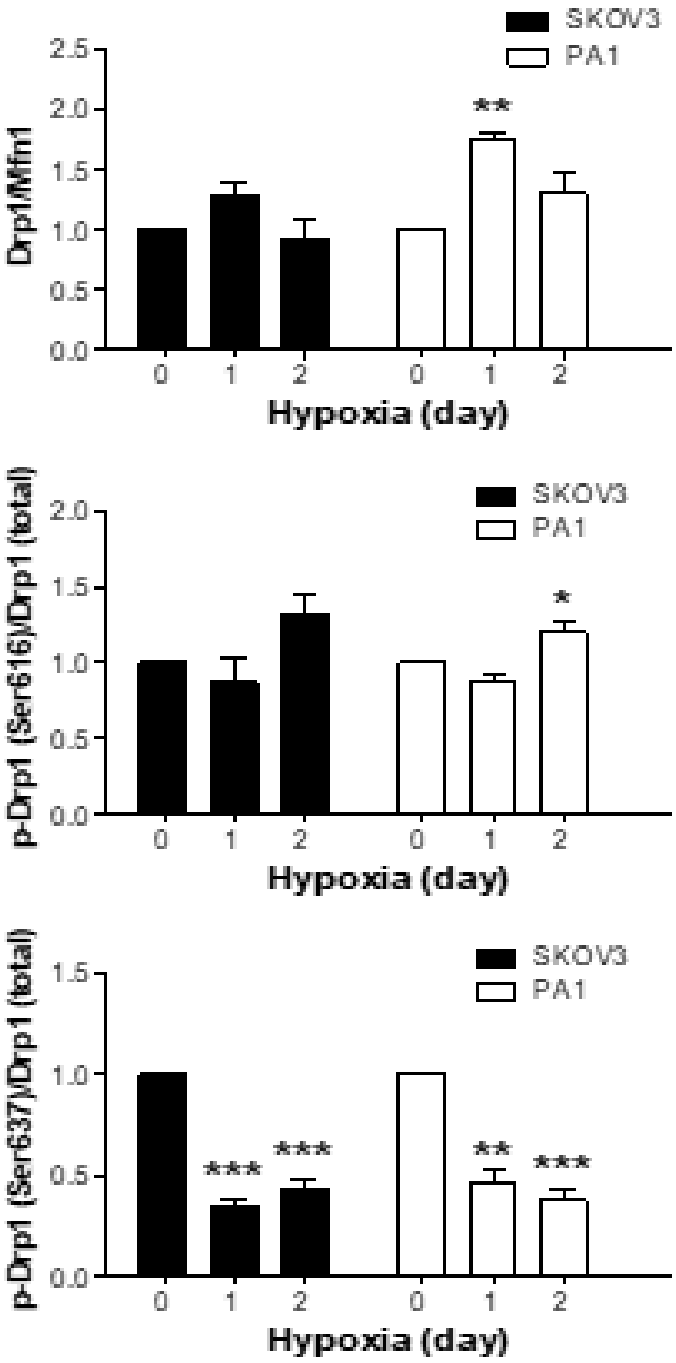
SKOV3
PA1
Drp1/Mfn1
2.5
2.0
1.5
1.0
0.5
0.0
**
0
1
2
0
1
2
Hypoxia (day)
SKOV3
PA1
p-Drp1 (Ser616)/Drp1 (total)
2.0
1.5
1.0
0.5
0.0
*
0
1
2
0
1
2
Hypoxia (day)
SKOV3
PA1
p-Drp1 (Ser637)/Drp1 (total)
1.5
1.0
0.5
0.0
***
***
**
***
0
1
2
0
1
2
Hypoxia (day)

f

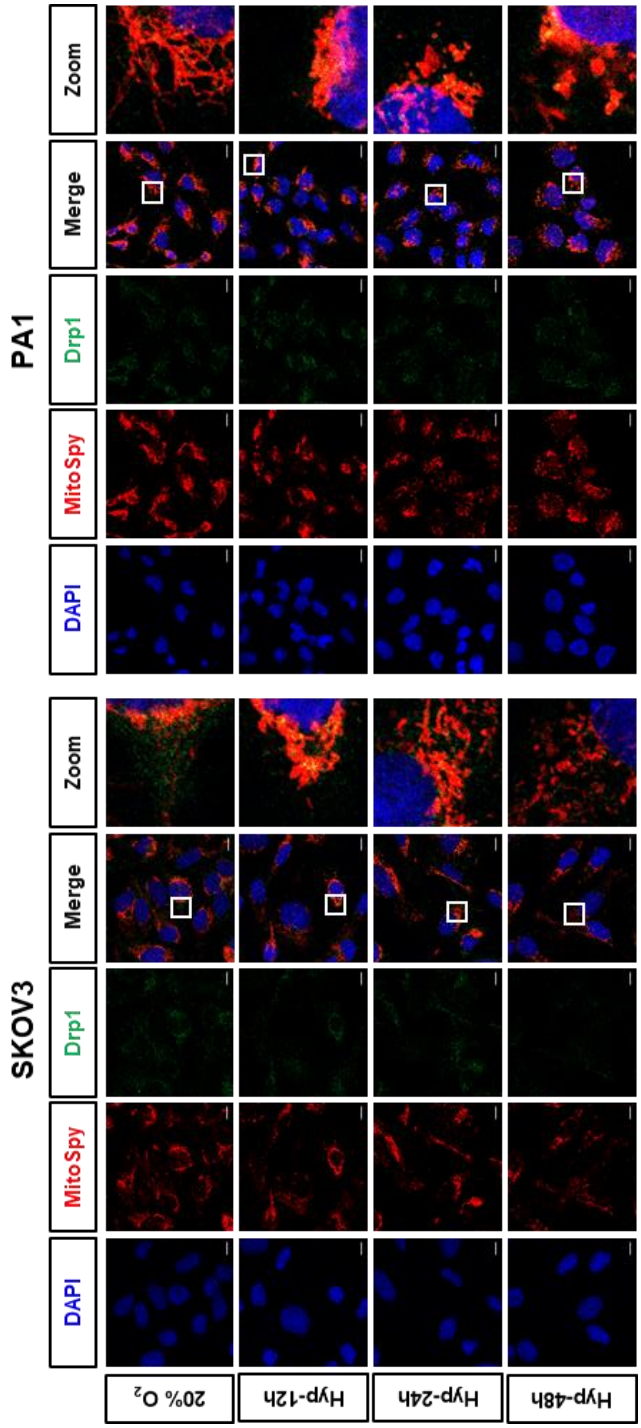
SKOV3
PA1
DAPI
MitoSpy
Drp1
Merge
Zoom
20% O2
Hyp-12h
Hyp-24h
Hyp-48h

Figure 4. Hypoxia promotes mitochondrial fission through Drp1 activation. **a** To assess mitochondrial mass, SKOV3, OVCAR3 and PA1 cells cultured under 20% O_2 or hypoxia for 24 and 48 h were stained with MitoTracker Green FM (M7514) and relative the signal intensities were analyzed using flow cytometry. To examine mitochondrial activity, relative fluorescence intensities of cancer cells stained with MitoTracker Orange (M7510) were measured to see changes in membrane potential of mitochondria. Mitochondrial activity to mitochondrial mass ratios of SKOV3, OVCAR3 and PA1 were computed to see relative changes in mitochondrial activity per mass in groups with different exposure times under hypoxia. Values are presented as means ± SEM from three independent experiments (ns, not significant; **, $P < 0.01$; ***, $P < 0.001$). **b** 20% O_2 and hypoxia-cultured SKOV3, OVCAR3 and PA1 cells were stained with MitoSpy to examine mitochondrial morphology using confocal microscopy. White arrows point at fragments of mitochondria. Length of the scale bar is 10 μm. **c** Quantification of relative mitochondrial length in cancer cells cultured under 20% O_2 and hypoxia. Error bars represent SEM (***, $P < 0.001$). **d** Protein expressions of Mfn1, Drp1, p-Drp1 (Ser616) and p-Drp1 (Ser637) from samples of SKOV3 and PA1 cells cultured under hypoxia for the indicated time periods were detected by Western blotting. As internal control, α-tubulin expression was examined. **e** To observe changes in relative expressions of mitochondrial dynamics-regulating proteins, expression ratios of Drp1/Mfn1, p-Drp1(Ser616)/Drp1 and p-Drp1(Ser637)/Drp1 were calculated using densitometric analysis of each immunoblot using ImageJ. Values are presented as means ± SEM from three independent experiments (*, $P < 0.05$; **, $P < 0.01$; ***, $P < 0.001$). **f** Representative images of SKOV3 and PA1 cells stained with MitoSpy (red), probed with anti-Drp1 (green) antibody and stained with DAPI (blue) show mitochondrial morphology and subcellular localization of Drp1 after hypoxic exposure for indicated time. Zoom indicates the enlargement of boxed region. Length of the scale bar is 10 μm.

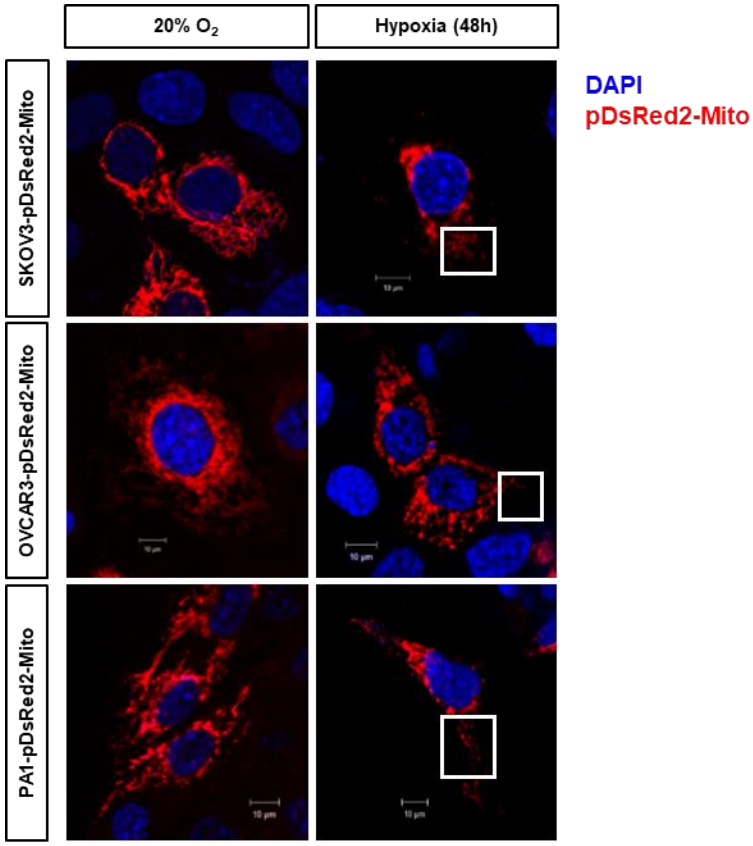
20% O2
Hypoxia (48h)
SKOV3-pDsRed2-Mito
OVCAR3-pDsRed2-Mito
PA1-pDsRed2-Mito
DAPI
pDsRed2-Mito

Supplementary Fig. 2. Mitochondrial fission is induced by hypoxia in ovarian cancer cells.

Mitochondrial morphology of 20% O_2 or hypoxia-cultured ovarian cancer cells (SKOV3, PA1 and OVCAR3) stably expressing dsRed-Mito expression construct was examined after 48 h culture under hypoxia. Morphology of mitochondrial was visualized by confocal microscopy.

2.3.3 Hypoxia changes expression and activation status of mitochondrial dynamics protein

To confirm whether mitochondrial fission and fusion proteins are responsible for mitochondrial fission induced by hypoxia, Mfn1 and Drp1 contents were assessed by Western blotting. We observed that protein contents of Mfn1 and inhibitory p-Drp1 (Ser637) were decreased under hypoxia (Fig. 4d). SKOV3 and PA1 cells cultured under hypoxia showed increased Drp1 to Mfn1 ratio which peaked at 24 h. Also, the ratio of p-Drp1 (Ser637) to Drp1 was significantly decreased in hypoxic conditions in a time-dependent manner, while an increase of p-Drp1 (Ser616) to Drp1 was observed after 48 h exposure to hypoxia (Fig. 4e).

Next, subcellular localization of Drp1 with different durations of hypoxic exposure (12, 24 and 48 h) was examined in SKOV3 and PA1 cells. Translocation of Drp1 was most notably observed after 12 h hypoxic culture indicated by the increased yellow fluorescence and decreased green fluorescence in cytosolic regions, implying Drp1-mediated mitochondrial fission occurs within 12 h under hypoxic culture conditions. Again, mitochondrial fission was observed after 24 h culture under hypoxia, indicated by the presence of many small mitochondrial fragments in the cancer cells (Fig. 4f). Collectively, these results suggest that hypoxic ovarian cancer cells undergo mitochondrial fission through Mfn1 downregulation and Drp1 activation.

2.3.4 High level of ROS exerted by hypoxia promotes mitochondrial fission

Previous studies have shown that tumor microenvironment is present with increased levels of ROS together with hypoxia. Mitochondria are major a source of ROS in eukaryotic cells, especially for hypoxic cells (106, 191). To determine the molecular mechanism by which hypoxia stimulates mitochondrial fission, we examined the impact of ROS on mitochondrial

dynamics of ovarian cancer cells. After 24 h exposure to hypoxia, SKOV3 and PA1 cells showed a significant increase in the intracellular H2O2 level compared to the 20% O2-cultured cells, whereas intracellular superoxide (O2-) level was not affected by hypoxia (Fig. 5a). To evaluate the effect of hypoxia-induced ROS on mitochondrial dynamics, H2O2 was exogenously applied to 20% O2-cultured cancer cells and NAC, a free radical scavenger, and Trolox, a water-soluble antioxidant, were treated to hypoxic cancer cells. While mitochondrial fission was promoted by exogenous H2O2 (20 μM, 6 h), hypoxia-induced mitochondrial fission was mitigated by NAC (1 mM, 6 h) and Trolox (200 μM, 6h) treatment (Fig. 5b, c and Supplementary Fig. 3). H2O2 treatment decreased Mfn1 content of SKOV3 and PA1 cells in 20% O2 culture conditions and the decrease in Mfn1 expression by hypoxia was restored by NAC and Trolox treatment. Treatment with H2O2 decreased the expressions of inhibitory p-Drp1 (Ser637) and Mfn1. The decreased p-Drp1 (Ser637) and Mfn1 expressions by hypoxia were rescued by NAC and Trolox treatment in both SKOV3 and PA1 cells (Fig. 5d). These results show that hypoxia-elicited ROS regulate Mfn1 protein level and activation status of Drp1 to promote mitochondrial fission.

a

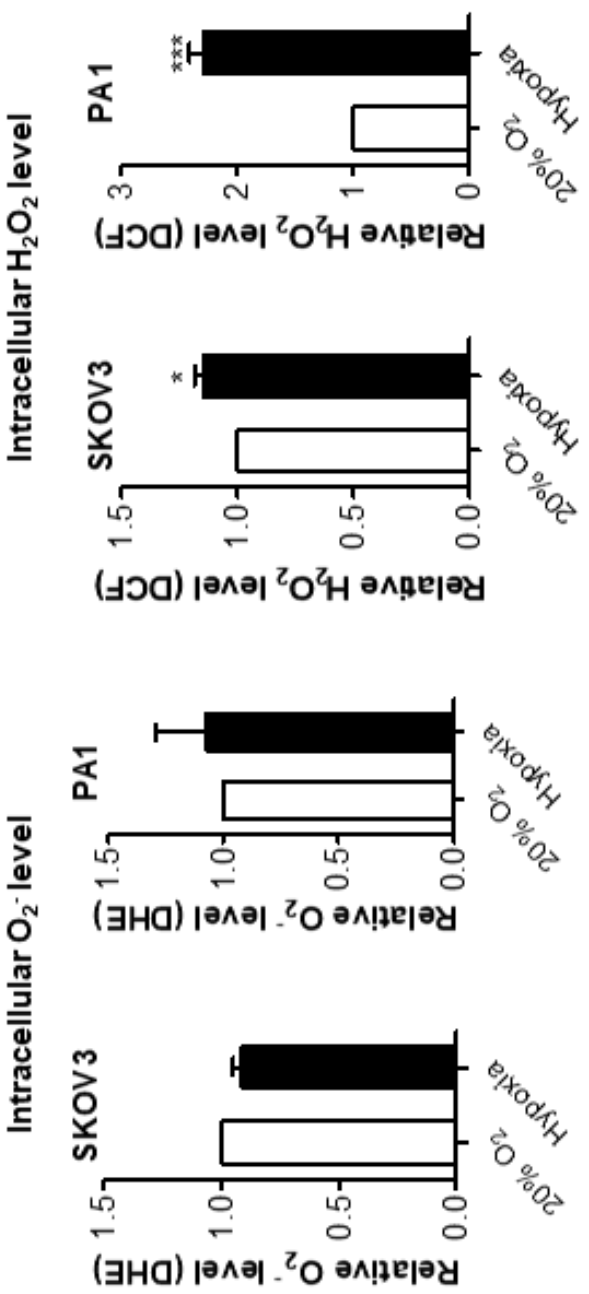
Intracellular O_2^- level
SKOV3
PA1
Relative O_2^- level (DHE)
1.5
1.0
0.5
0.0
20% O_2
Hypoxia
Intracellular H_2O_2 level
SKOV3
PA1
Relative H_2O_2 level (DCF)
3
2
1
0
1.5
1.0
0.5
0.0
*
***
20% O_2
Hypoxia

b

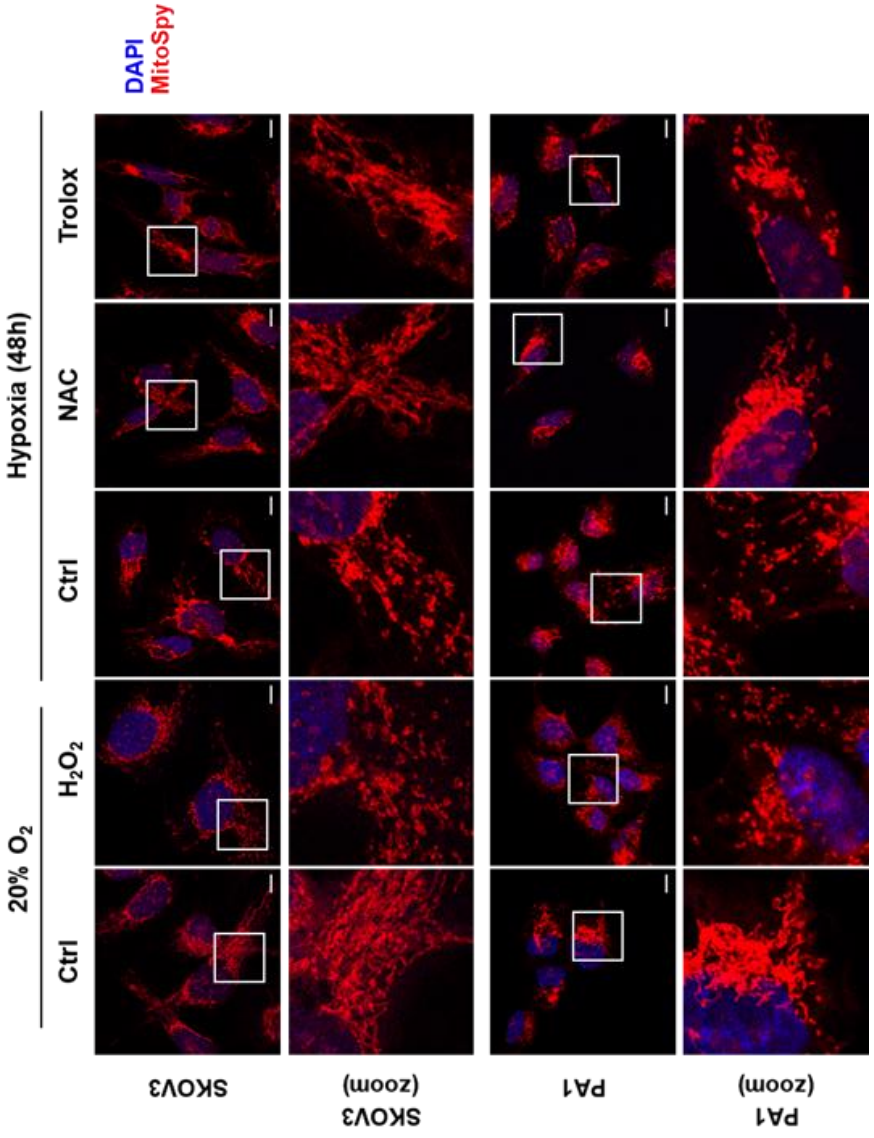
DAPI
MitoSpy
Hypoxia (48h)
20% O2
Ctrl
H2O2
Ctrl
NAC
Trolox
SKOV3
SKOV3 (zoom)
PA1
PA1 (zoom)

c

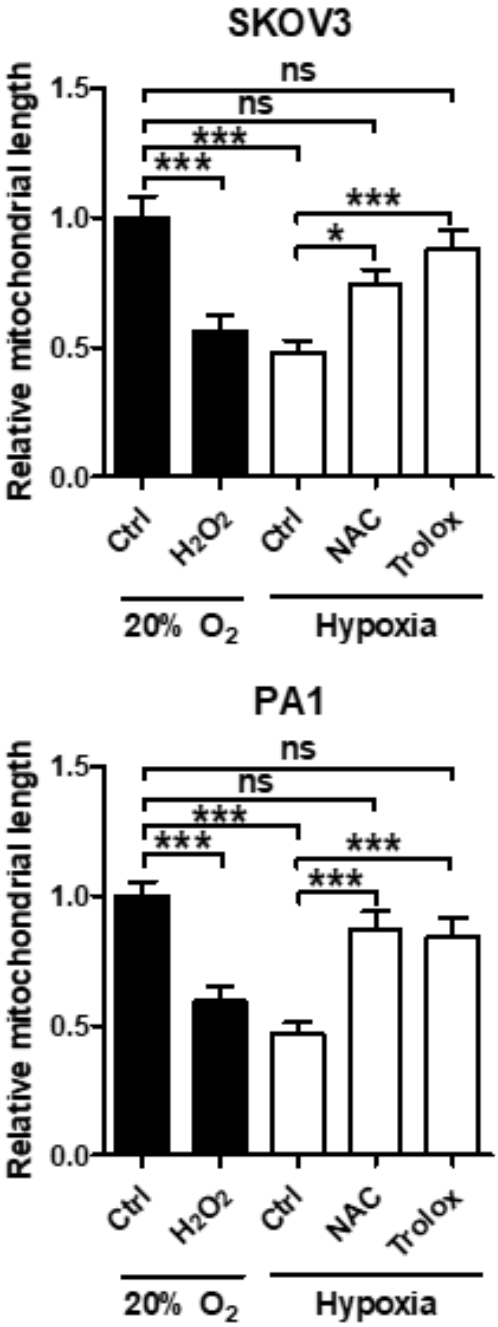
SKOV3
Relative mitochondrial length
1.5
1.0
0.5
0.0
ns
ns
***
***
***
*
Ctrl
H2O2
Ctrl
NAC
Trolox
20% O2
Hypoxia
PA1
Relative mitochondrial length
1.5
1.0
0.5
0.0
ns
ns
***
***
***
***
Ctrl
H2O2
Ctrl
NAC
Trolox
20% O2
Hypoxia

d

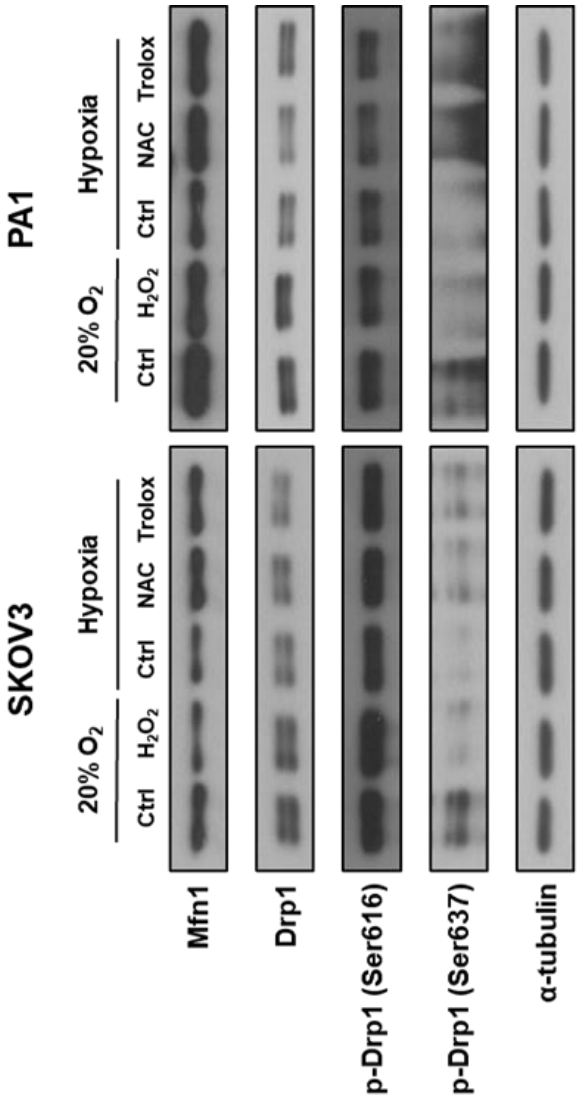
SKOV3
PA1
20% O2
Hypoxia
Ctrl
H2O2
Ctrl
NAC
Trolox
Mfn1
Drp1
p-Drp1 (Ser616)
p-Drp1 (Ser637)
α-tubulin

Figure 5. An increase of intracellular ROS by hypoxia causes mitochondrial fission.

a Relative level of intracellular ROS (O_2^- and H_2O_2) of SKOV3 and PA1 cells after 24 h exposure to hypoxia were measured. ROS levels of hypoxic cancer cells were compared against those of 20% O_2-cultured cancer cells. Values are presented as means ± SEM from three independent experiments (*, $P < 0.05$; ***, $P < 0.001$). **b** Mitochondrial morphology of SKOV3 and PA1 cells were observed by staining with MitoSpy. For H_2O_2 treated group, 20% O_2-cultured cancer cells were exposed to H_2O_2 (20 μM) for 6 h. For NAC (1 mM) and Trolox (200 μM) treated groups, hypoxia was applied for 48 h and NAC and Trolox were treated for 6 h. Length of the scale bar is 10 μm. Zoom indicates the enlargement of boxed region. **c** Mitochondrial length was quantified. Error bars represent SEM (ns, not significant; *, $P < 0.05$; ***, $P < 0.001$). **d** Protein expressions of Mfn1, Drp1, p-Drp1 (Ser616) and p-Drp1 (Ser637) were detected by Western blotting. As internal control, α-tubulin expression was examined.

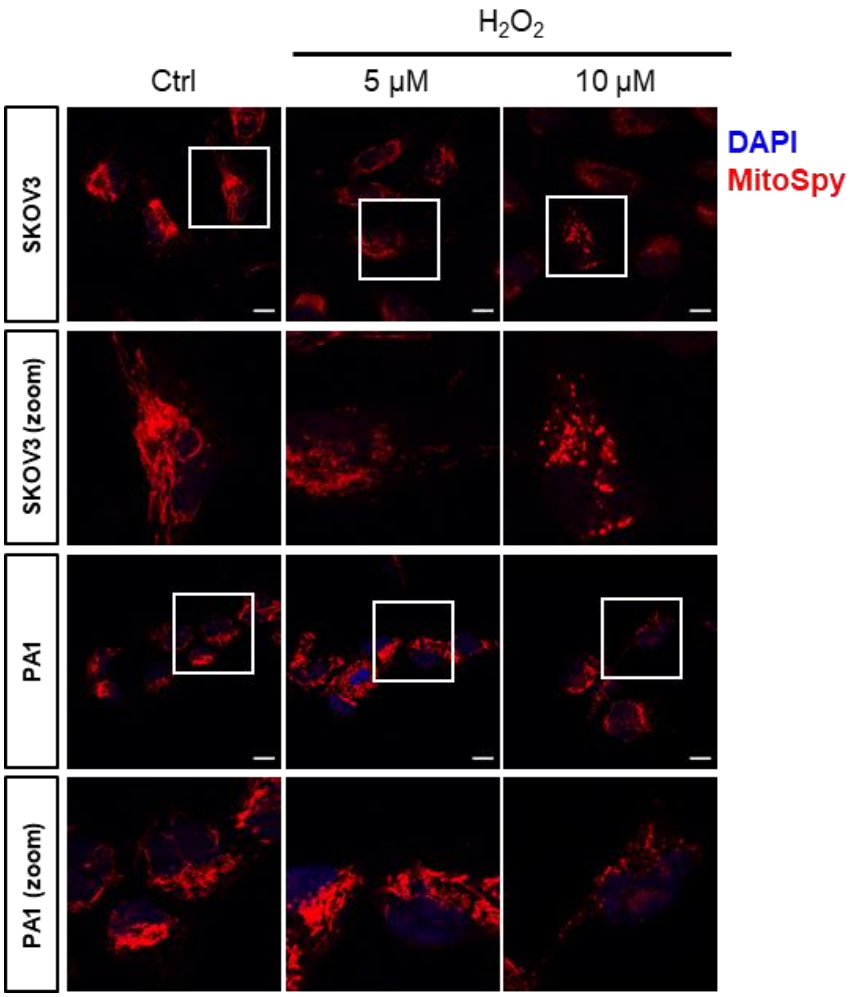
H2O2
Ctrl
5 μM
10 μM
SKOV3
SKOV3 (zoom)
PA1
PA1 (zoom)
DAPI
MitoSpy

Supplementary Fig. 3. H_2O_2 increases mitochondrial fission in ovarian cancer cells.

H_2O_2 was exogenously applied to the cancer cells with increasing doses (0, 5 and 10 μM) for 6 h. Cancer cells were stained with MitoSpy and fixed with 4% PFA. Mitochondria morphology was visualized by confocal microscopy.

2.3.5 Expression of mRNAs in cancer tissue samples from GEO dataset shows the relevance of hypoxia-induced mitochondrial fission and chemoresistance.

We compared mRNA abundance of DNM1L (the gene encodes for Drp1), Mfn1 and the ratios of Drp1/Mfn1 between normal and cancer tissues using GSE14407 dataset. Both Drp1 mRNA levels and the expression ratio were significantly higher in the cancer tissues than those in the normal tissues. Also, a positive correlation between the mRNA abundance of Drp1 and hypoxia markers (SLC2A1 and VEGFA) was observed (Fig. 6a). Cancer tissue samples (n = 12) from the GSE14407 dataset were split into two groups based on the ratio of Drp1/Mfn1 expression. Among many other gene sets in KEGG pathways, we found that 'drug metabolism cytochrome P450' and 'VEGF signaling' pathways, which are related with chemoresistance and hypoxia respectively, were significantly enriched in the high Drp1/Mfn1 ratio group compared with the low Drp1/Mfn1 ratio group (Fig. 6b). These data might imply that the hypoxia-induced mitochondrial fission event of cancer is associated with chemoresistance.

a

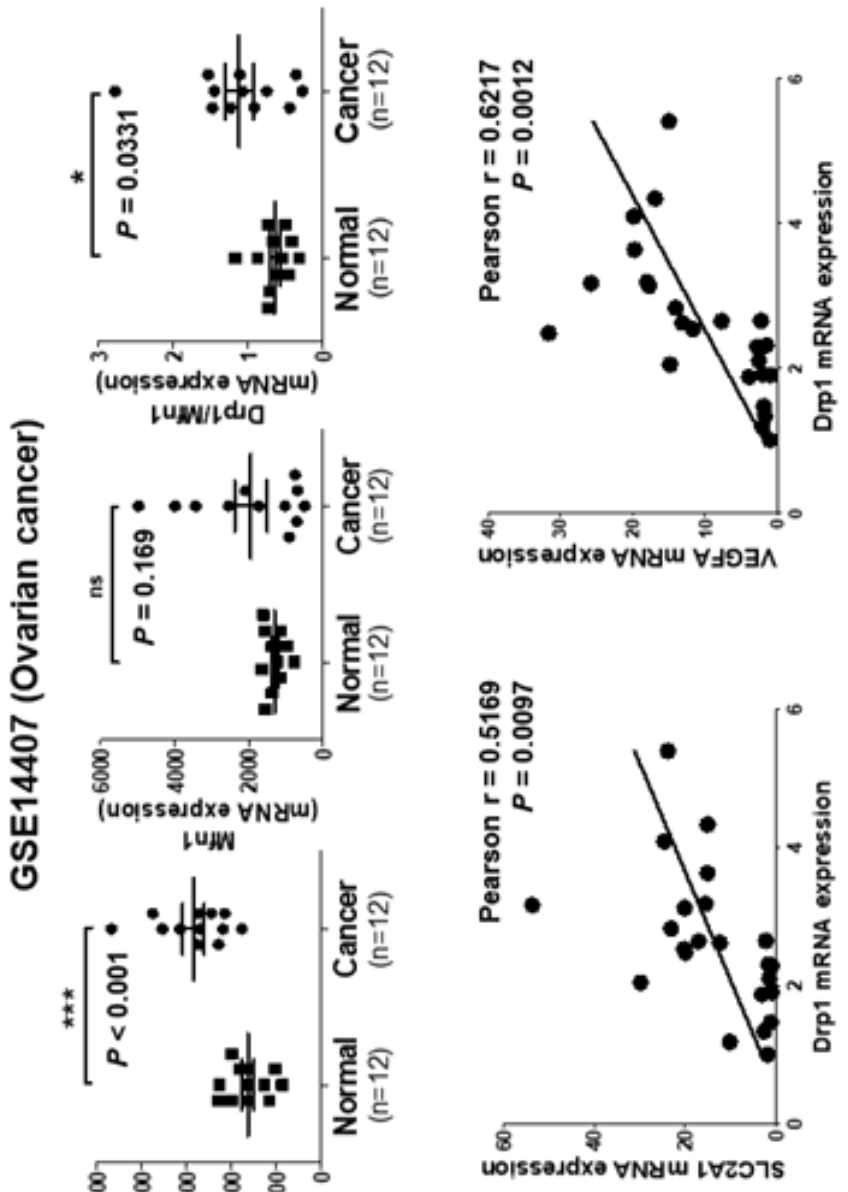
GSE14407 (Ovarian cancer)
Drp1
(mRNA expression)
2500
2000
1500
1000
500
0
***
P < 0.001
Normal (n=12)
Cancer (n=12)
Mfn1
(mRNA expression)
6000
4000
2000
0
ns
P = 0.169
Normal (n=12)
Cancer (n=12)
Drp1/Mfn1
(mRNA expression)
3
2
1
0
*
P = 0.0331
Normal (n=12)
Cancer (n=12)
SLC2A1 mRNA expression
60
40
20
0
Pearson r = 0.5169
P = 0.0097
0
2
4
6
Drp1 mRNA expression
VEGFA mRNA expression
40
30
20
10
0
Pearson r = 0.6217
P = 0.0012
0
2
4
6
Drp1 mRNA expression

b

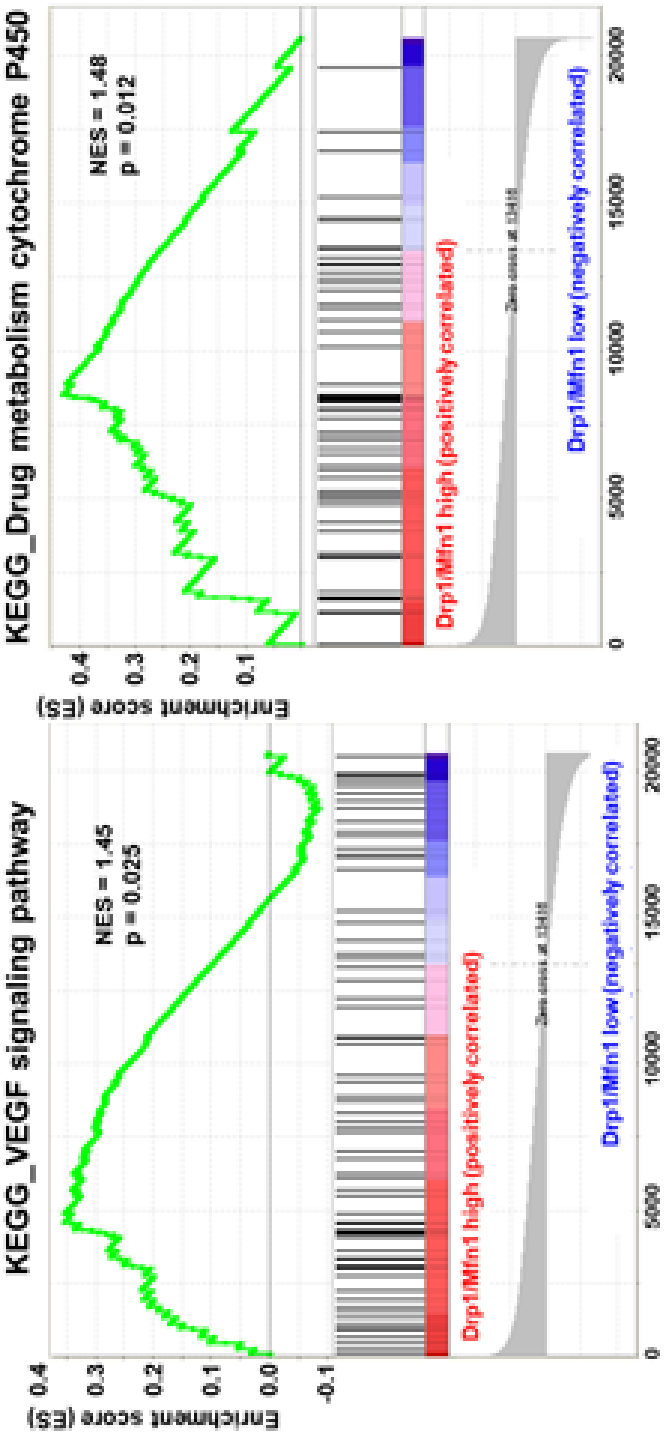
KEGG_Drug metabolism cytochrome P450
NES = 1.48
p = 0.012
Enrichment score (ES)
0.4
0.3
0.2
0.1
Drp1/Mfn1 high (positively correlated)
Drp1/Mfn1 low (negatively correlated)
0
5000
10000
15000
20000
KEGG_VEGF signaling pathway
NES = 1.45
p = 0.025
Enrichment score (ES)
0.4
0.3
0.2
0.1
0.0
-0.1
Drp1/Mfn1 high (positively correlated)
Drp1/Mfn1 low (negatively correlated)
0
5000
10000
15000
20000

Figure 6. Hypoxia-induced mitochondrial fission is related with chemoresistance.

a Transcript levels of mitochondrial dynamics-regulating proteins (Drp1, Mfn1 and Drp1/Mfn1 expression ratio) in normal tissues (squares; n=12) and ovarian cancer tissues (circles; n=12) were compared (upper panels). Values are presented as means ± SEM (ns, not significant; *, $P < 0.05$; ***, $P < 0.001$). Correlation between Drp1 mRNA expression and expression of hypoxia markers (SLC2A1 and VEGFA) in normal ovarian surface epithelial tissue samples and ovarian cancer tissue samples (n=24) were compared (lower panels). The GEO dataset, GSE14407 was utilized. **b** Enrichment profiles of two representative pathways, VEGF signaling pathway (NES = 1.45 and P = 0.025) and drug metabolism cytochrome P450 (NES = 1.48 and P = 0.012) from KEGG database are significantly enriched in the high Drp1/Mfn1 expression ratio group of epithelial ovarian cancer (n=12).

2.3.6 Inhibition of mitochondrial fission increases the sensitivity of ovarian cancer cells to CDDP in hypoxic conditions

To find whether mitochondrial fission induced by hypoxia is associated with chemoresistance in ovarian cancer cells, Mdivi-1, a small-molecule inhibitor targeting Drp1 GTPase activity was used (192). Mitochondrial fusion promoter M1 could have been incorporated into our study to prevent hypoxia-induced mitochondrial fission. However, it showed high toxicity in normal cells including adipose-derived stem cells (ASCs), immortalized ovarian surface epithelial cells (IOSE) although both Mdivi-1 and M1 showed minimal toxicity on peripheral blood mononuclear cells (PBMCs). Hence, Mdivi-1 was used for subsequent experiments to suppress mitochondrial fission induced by hypoxia (Supplementary Fig. 4).

Mdivi-1
(Fission inhibitor)
M1
(Fusion promoter)
Cancer cells
Normal cells
SKOV3
PA1
ASC
PBMC
IOSE385
Cell viability (%)
Mdivi-1 (μM)
Fusion promoter M1 (μM)
0
50
100
150
0 5 10 20
**
***
*

Supplementary Fig. 4. Treatment of Mdivi-1 and M1 on ovarian cancer cells with increasing doses.

Ovarian cancer cells (SKOV3 and PA1) and normal cells (ASC, PBMC and IOSE385) were treated with increasing doses of either Mdivi-1 (mitochondrial fission inhibitor) or mitochondrial fusion promoter M1 for 48 h and cell viability was examined by MTT assay. Values are presented as the means ± SEM of three independent experiments (*, $P < 0.05$; **, $P < 0.01$; ***; $P < 0.001$).

Treatment with ovarian cancer cells with Mdivi-1 (10 μM) 2 h prior to hypoxic exposure prevented mitochondria fission induced by hypoxia (Fig. 7a). SKOV3 and PA1 cells were treated with Mdivi-1 for 2 h and then exposed to hypoxia. After 24 h hypoxic culture, the cancer cells were then incubated with CDDP alone (50 μM for SKOV3 and 10 μM for PA1) for another 24 h. Representative micrographs of SKOV3 and PA1 cells in response to CDDP show a notable decrease in cell confluency when Mdivi-1 was treated prior to hypoxic incubation in comparison to the hypoxic cells treated with CDDP alone (Fig. 7b). Inhibition of mitochondrial fission by pre-treatment with Mdivi-1 significantly decreased the CDDP sensitivity of hypoxic ovarian cancer cells. Results from MTT assay shows 20% O_2 and hypoxic PA1 cells exhibited similar CDDP sensitivity when Mdivi-1 was treated prior to hypoxic exposure, and the viability of hypoxic SKOV3 cells in response to CDDP was markedly reduced in the Mdivi-1 pre-treatment group (Fig. 7c). Apoptotic cell death accompanies cleavage of PARP-1 and DNA damage (193, 194). The level of cleaved PARP-1 and the percentage of TUNEL positive cells in response to CDDP in hypoxic cancer cells pre-treated with Mdivi-1 were significantly increased compared to those in hypoxic cancer cells not pre-treated with Mdivi-1 (Fig. 7d-f). These results suggest that Drp1 inhibition could sensitize hypoxic ovarian cancer cells to CDDP, making hypoxic ovarian cancer cells almost as sensitive as 20% O_2-cultured cancer cells.

a

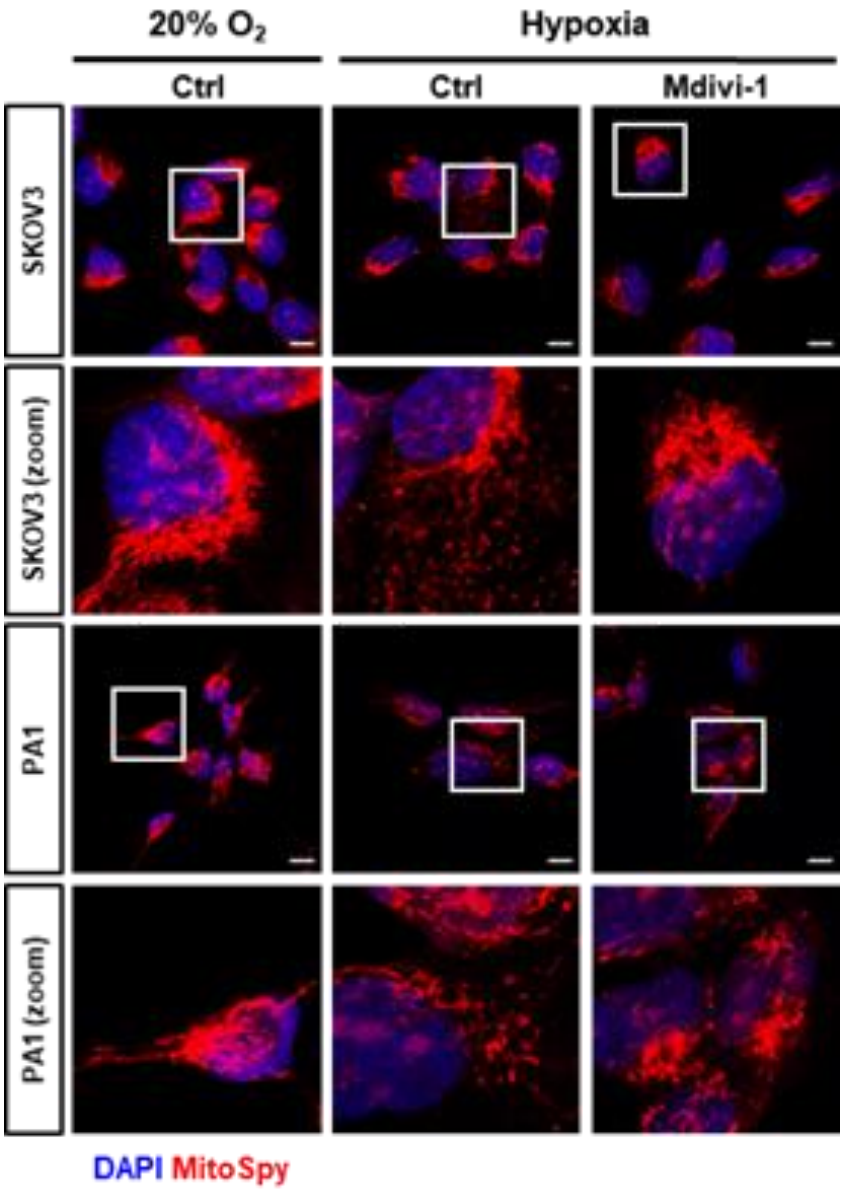
20% O2
Hypoxia
Ctrl
Ctrl
Mdivi-1
SKOV3
SKOV3 (zoom)
PA1
PA1 (zoom)
DAPI MitoSpy

b

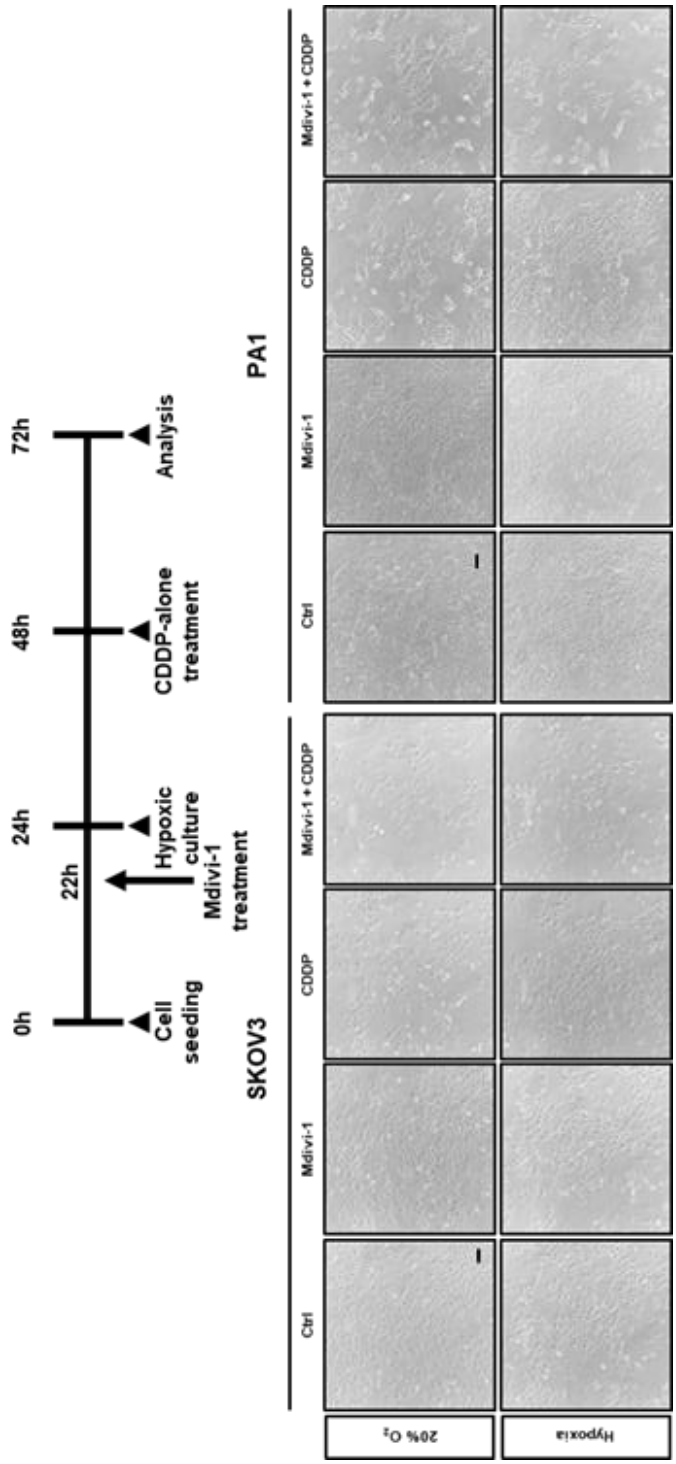
0h
24h
48h
72h
Cell seeding
22h
Hypoxic culture
Mdivi-1 treatment
CDDP-alone treatment
Analysis
SKOV3
PA1
Ctrl
Mdivi-1
CDDP
Mdivi-1 + CDDP
20% O2
Hypoxia

c

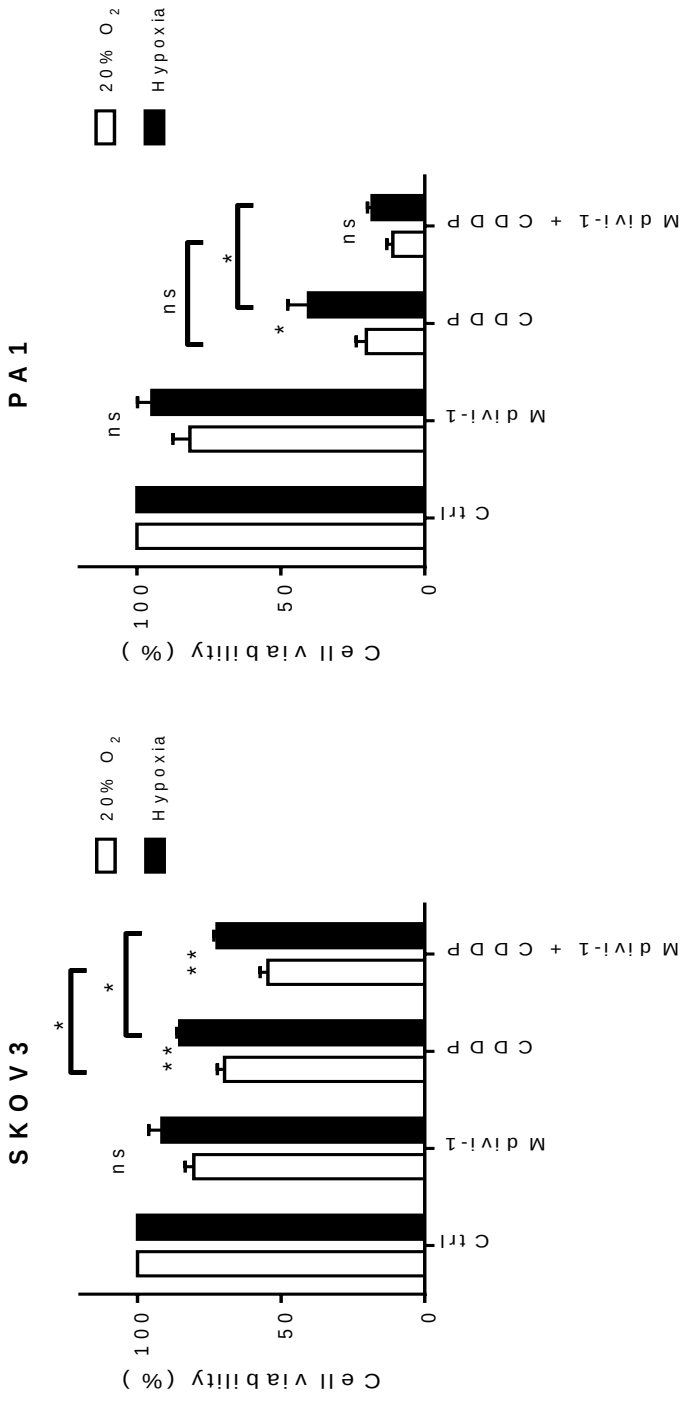
SKOV3
PA1
Cell viability (%)
0
50
100
Ctrl
Mdiv-1
CDDP
Mdiv-1 + CDDP
ns
*
**
20% O2
Hypoxia

d

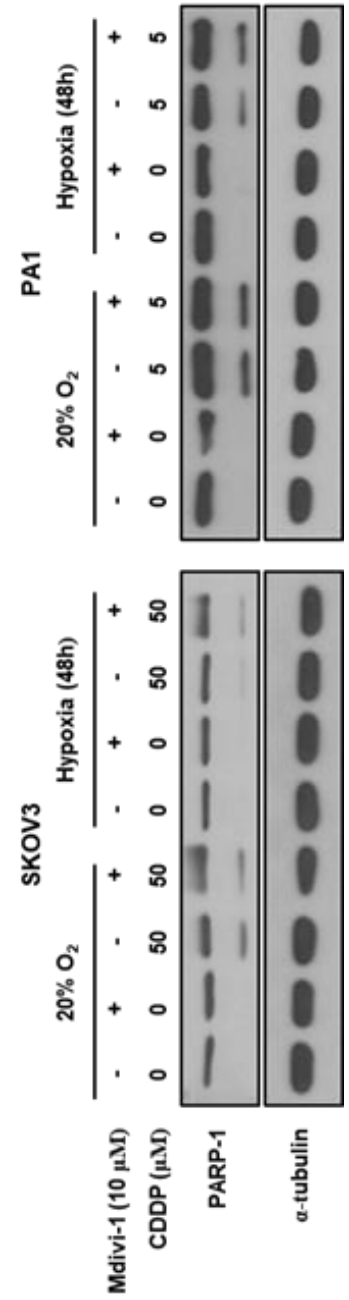
SKOV3
PA1
20% O2
Hypoxia (48h)
Mdivi-1 (10 μM)
CDDP (μM)
PARP-1
α-tubulin

e

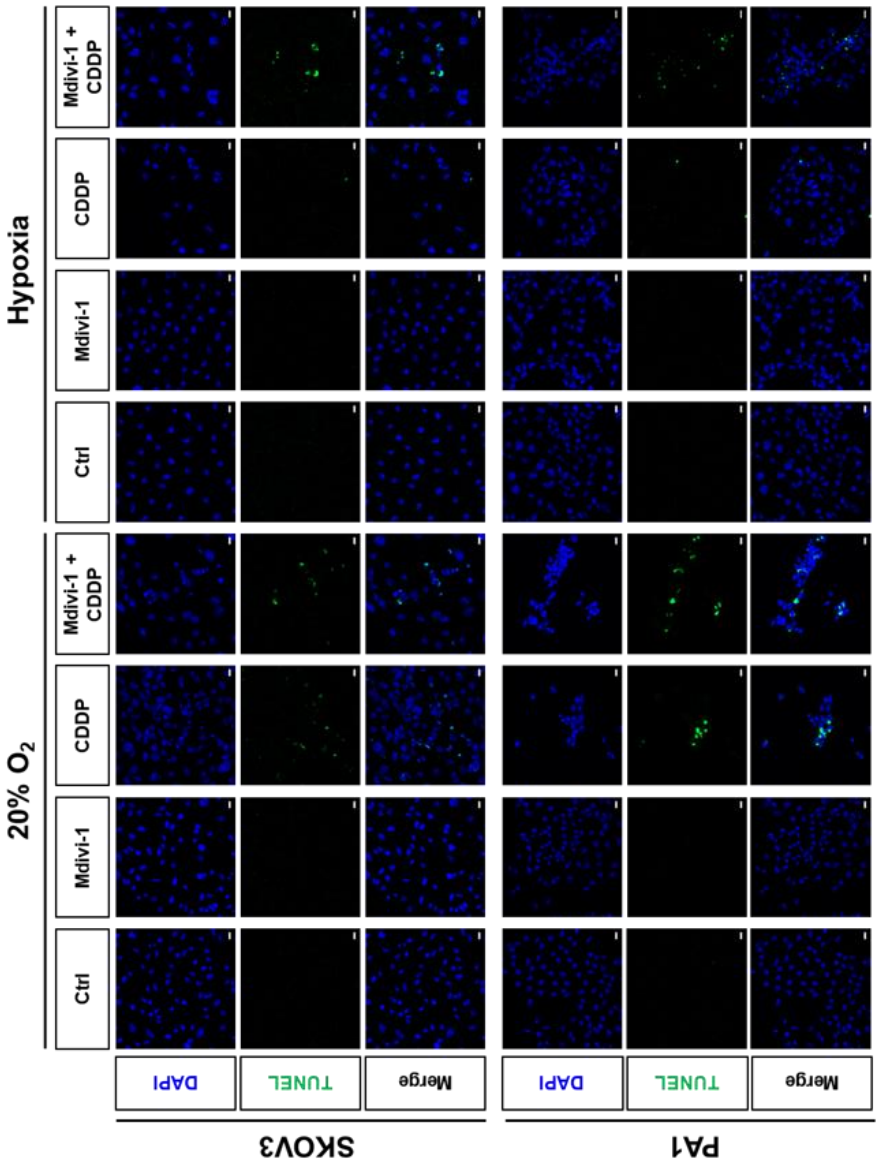
SKOV3
PA1
DAPI
TUNEL
Merge
20% O2
Hypoxia
Ctrl
Mdivi-1
CDDP
Mdivi-1 + CDDP

f

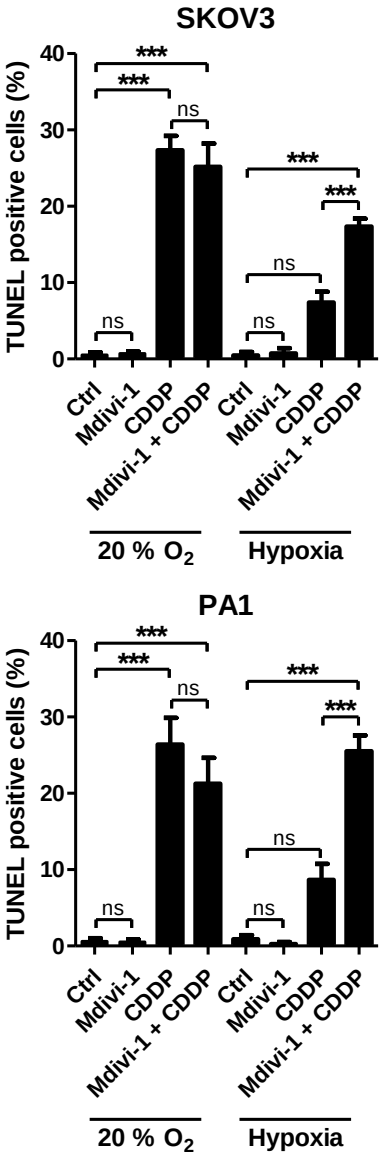
SKOV3
TUNEL positive cells (%)
40
30
20
10
0
***
***
ns
ns
ns
***
***
Ctrl
Mdivi-1
CDDP
Mdivi-1 + CDDP
Ctrl
Mdivi-1
CDDP
Mdivi-1 + CDDP
20 % O2
Hypoxia
PA1
TUNEL positive cells (%)
40
30
20
10
0
***
***
ns
ns
ns
***
***
Ctrl
Mdivi-1
CDDP
Mdivi-1 + CDDP
Ctrl
Mdivi-1
CDDP
Mdivi-1 + CDDP
20 % O2
Hypoxia

Figure 7. Inhibition of mitochondrial fission sensitizes hypoxic ovarian cancer cells to CDDP.

a Representative confocal microscopic images show the effect of Mdivi-1 pre-treatment 2 h prior to hypoxic exposure (48 h) on MitoSpy stained SKOV3 and PA1 cells. Length of the scale bar is 10 μm. Zoom indicates the enlargement of boxed region. **b** A schematic timeline (upper panel) shows specific time points of Mdivi-1 treatment, hypoxia and CDDP treatment. SKOV3 and PA1 cells were treated with 10 μM Mdivi-1 2 h prior to hypoxic exposure. After 24 h of hypoxia given to ovarian cancer cells, 24 h incubation with CDDP (50 μM for SKOV3 and 5 μM for PA1) alone was followed. Representative micrographs (lower panels) show morphological changes and confluency of SKOV3 and PA1 cells in different treatment conditions. Length of the scale bar is 100 μm. **c** Effect of Mdivi-1 pre-treatment prior to hypoxic exposure on CDDP sensitivity of SKOV3 and PA1 was analyzed by MTT assay. Means between 20% O_2 and hypoxia culture groups were compared. Values are presented as means ± SEM from three independent experiments (ns, not significant; *, $P < 0.05$; **, $P < 0.01$). **d** SKOV3 and PA1 cells were treated with Mdivi-1 2 h prior to hypoxia. CDDP (50 μM for SKOV3 and 5 μM for PA1) was treated 24 h after hypoxic exposure. Cells were harvested after 24 h incubation with CDDP alone treatment to obtain cell lysates. Cleavage of PARP-1 was assessed by Western blotting. As internal control, α-tubulin expression was examined. **e** TUNEL positive cells were observed by confocal microscopy after TUNEL (green) and DAPI (blue) staining. Length of the scale bar is 10 μm. **f** Percentage of TUNEL positive cells was calculated. Error bars represent SEM (ns, not significant; ***, $P < 0.001$).

To further confirm whether Drp1-mediated changes in mitochondrial dynamics is associated with hypoxia-induced CDDP resistance, ovarian cancer cells were transfected with si-Ctrl (50 nM) or si-Drp1 (50 nM). Cell lysates were prepared to confirm the knockdown efficiency 48 h after transfection with si-RNA by Western blotting for Drp1 protein expression (Fig. 8a). Sensitivity to CDDP was higher in the si-Drp1 transfected cancer cells than that in the si-Ctrl transfected cancer cells under hypoxia. Consistent with the result in Fig. 5B, si-Drp1 transfected SKOV3 and PA1 cells were less confluent compared to si-Ctrl transfected cancer cells after treated with CDDP under hypoxia (Fig. 8b). There was similar cisplatin sensitivity between the 20% O_2- and hypoxia-cultured cancer cells when transfected with si-Drp1 (Fig. 8c). Also, si-Drp1 transfected SKOV3 and PA1 cells showed higher level of cleaved PARP-1 compared to the si-Ctrl transfected cells after CDDP treatment in hypoxic groups. Interestingly, inhibition of Drp1 in hypoxic cancer cells treated with CDDP showed the comparable level of PARP-1 cleavage shown in the 20% O_2-cultured cancer cells treated with CDDP (Fig. 8d). Moreover, the percentages of TUNEL positive cells in response to CDDP were significant higher in ovarian cancer cells transfected with si-Drp1 than the cancer cells transfected with si-Ctrl under hypoxia (Fig 8e, f). Therefore, inhibition of hypoxia-induced mitochondrial fission could increase the sensitivity of hypoxic ovarian cancer cells to CDDP.

a

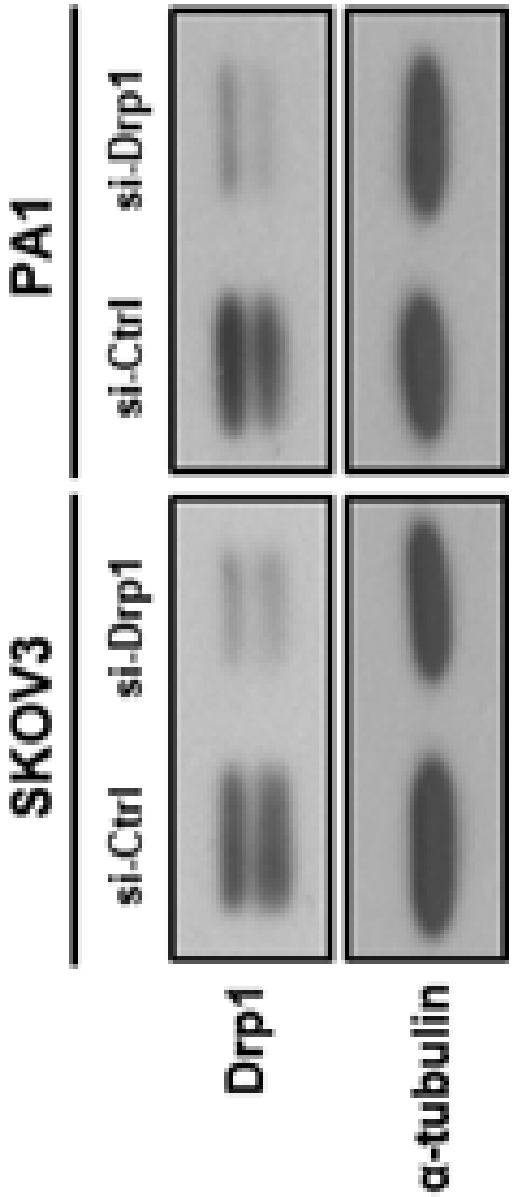

b

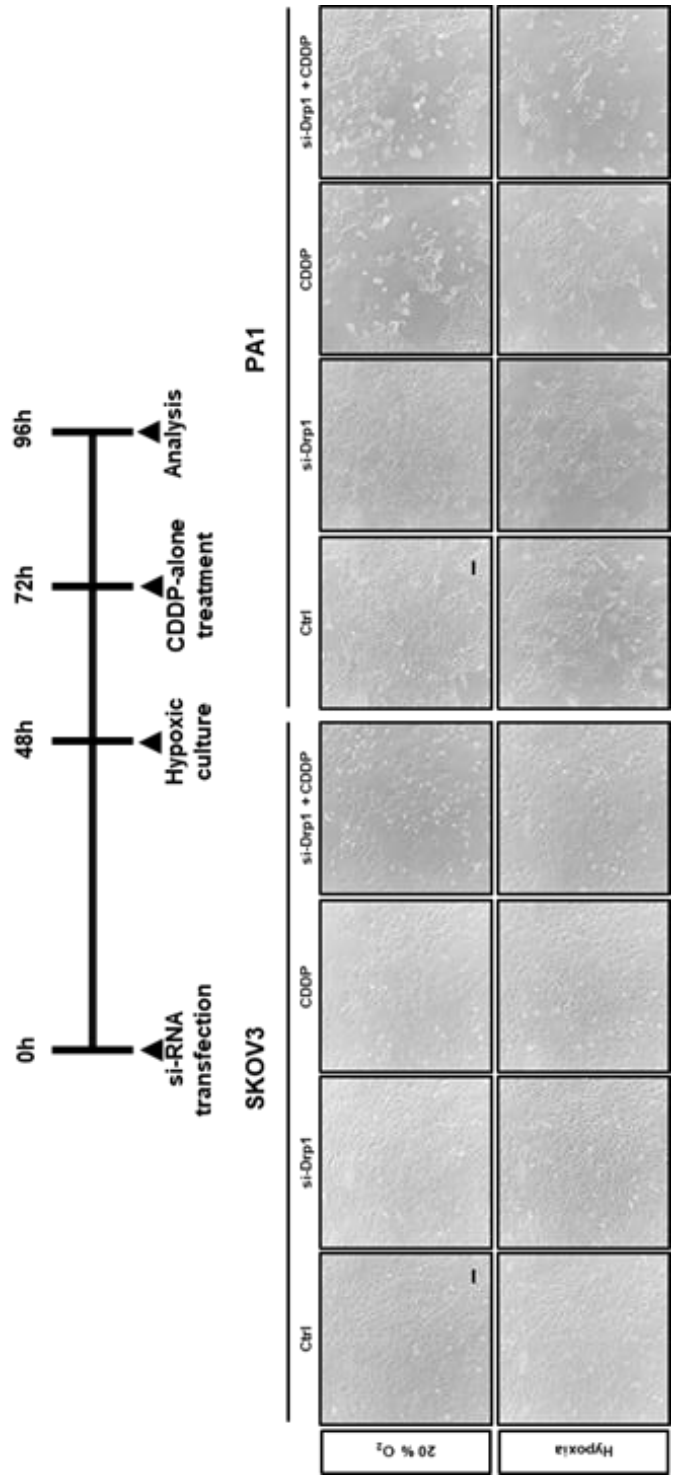
0h
48h
72h
96h
si-RNA transfection
Hypoxic culture
CDDP-alone treatment
Analysis
SKOV3
PA1
Ctrl
si-Drp1
CDDP
si-Drp1 + CDDP
20 % O2
Hypoxia

c

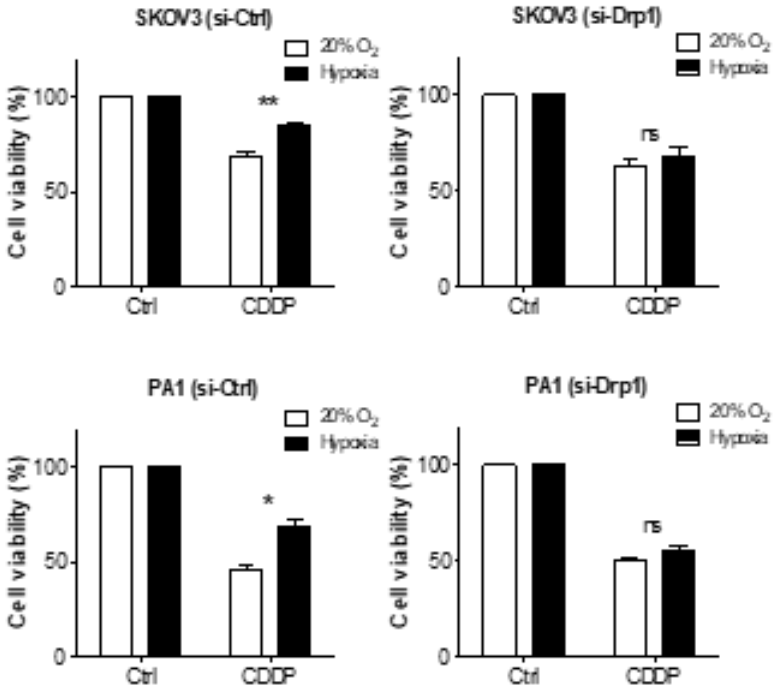
SKOV3 (si-Ctrl)
20% O2
Hypoxia
Cell viability (%)
100
50
0
**
Ctrl
CDDP
SKOV3 (si-Drp1)
20% O2
Hypoxia
Cell viability (%)
100
50
0
ns
Ctrl
CDDP
PA1 (si-Ctrl)
20% O2
Hypoxia
Cell viability (%)
100
50
0
*
Ctrl
CDDP
PA1 (si-Drp1)
20% O2
Hypoxia
Cell viability (%)
100
50
0
ns
Ctrl
CDDP

d

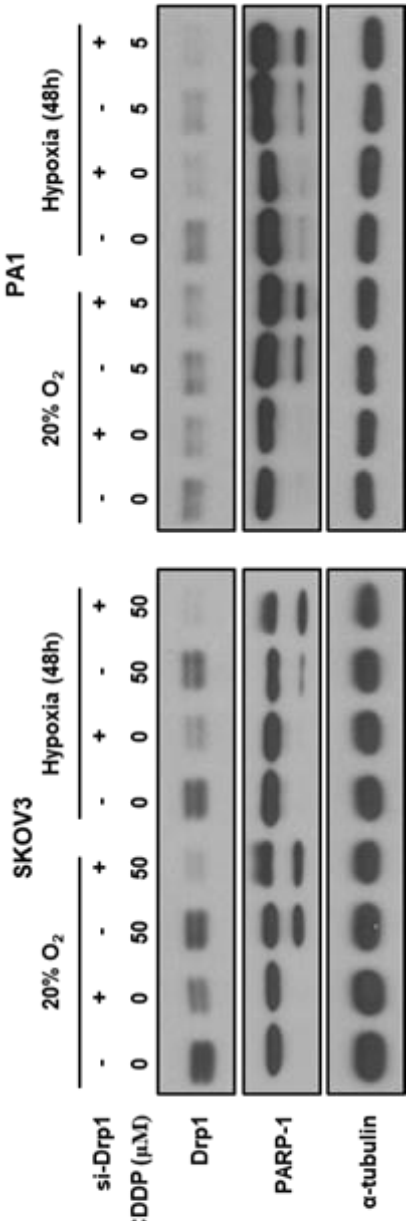
SKOV3
PA1
20% O2
Hypoxia (48h)
si-Drp1
CDDP (μM)
Drp1
PARP-1
α-tubulin

e

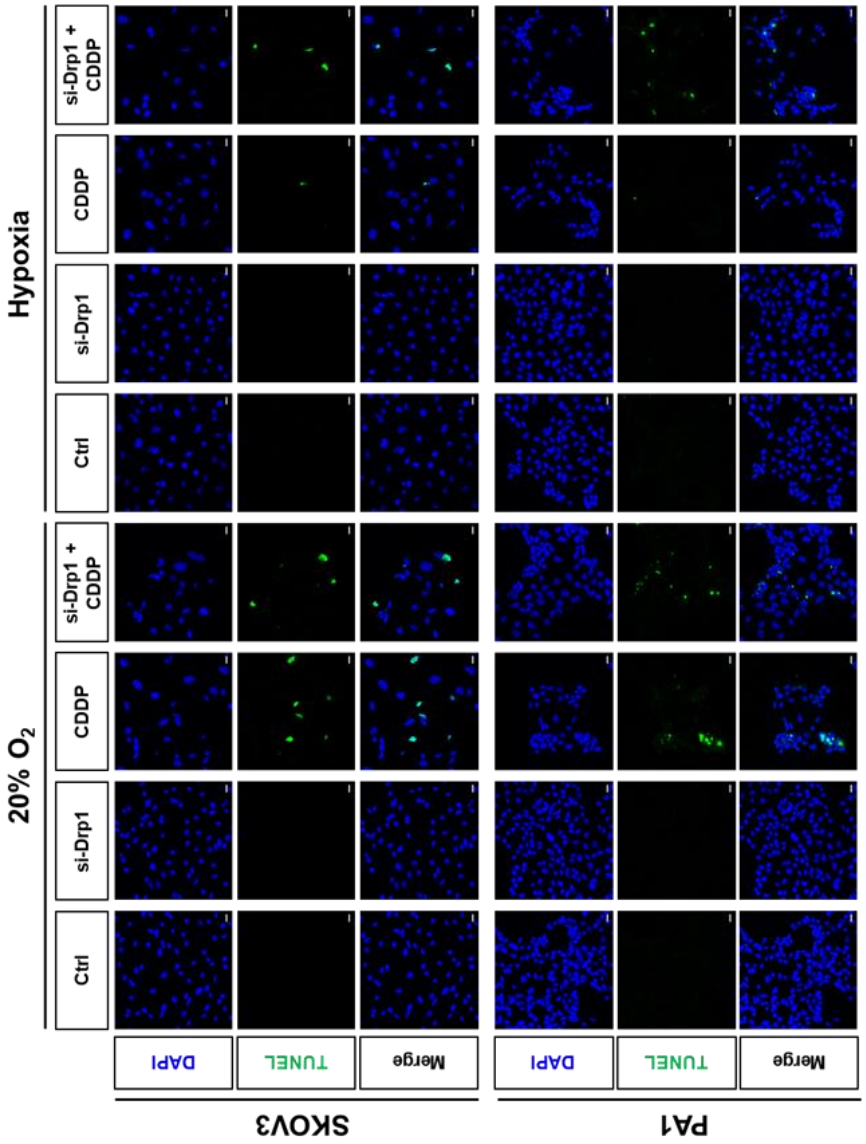
Hypoxia
20% O2
Ctrl
si-Drp1
CDDP
si-Drp1 + CDDP
DAPI
TUNEL
Merge
SKOV3
PA1

f

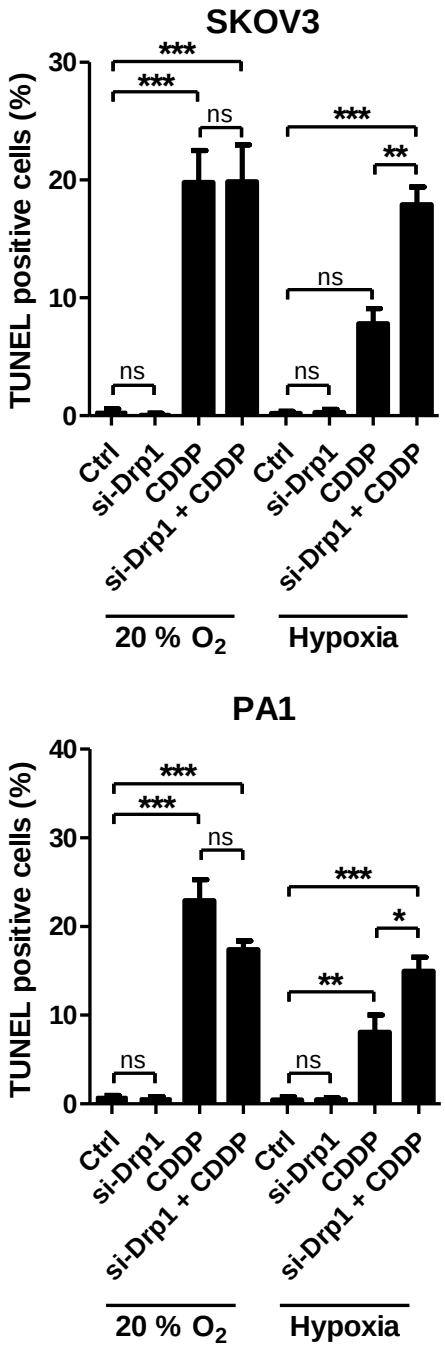
SKOV3
TUNEL positive cells (%)
30
20
10
0
***
***
ns
***
**
ns
ns
ns
Ctrl
si-Drp1
CDDP
si-Drp1 + CDDP
Ctrl
si-Drp1
CDDP
si-Drp1 + CDDP
20 % O2
Hypoxia
PA1
TUNEL positive cells (%)
40
30
20
10
0
***
***
ns
***
*
**
ns
ns
Ctrl
si-Drp1
CDDP
si-Drp1 + CDDP
Ctrl
si-Drp1
CDDP
si-Drp1 + CDDP
20 % O2
Hypoxia

Figure 8. Knockdown of Drp1 in hypoxic ovarian cancer cells sensitizes them to CDDP.

a Ovarian cancer cells were transfected with either 50 nM si-Ctrl or 50 nM si-Drp1, and expression of Drp1 was detected by Western blotting. **b** A schematic timeline (upper panel) shows time points of si-RNA transfection, hypoxia and CDDP treatment. 48 h after transfection with si-Ctrl (50 nM) or si-Drp1 (50 nM), SKOV3 and PA1 cells were exposed to hypoxia followed by CDDP (50 μM for SKOV3 and 5 μM for PA1) alone treatment. Representative micrographs (lower panels) show morphological changes and confluency of SKOV3 and PA1 cells in different treatment conditions. Length of the scale bar is 100 μm. **c** Cell viability of si-Ctrl or si-Drp1 transfected cancer cells cultured under 20% O_2 and hypoxic conditions after incubation with CDDP were examined by MTT assay. Means between 20% O_2 and hypoxia culture groups were compared. Values are presented as means ± SEM from three independent experiments (ns, not significant; **, $P < 0.01$). **d** At 48 h post-transfection, SKOV3 and PA1 cells were incubated under hypoxia. CDDP (50 μM for SKOV3 and 5 μM for PA1) was treated 24 h after hypoxic exposure. Cells were harvested after m24 h incubation with CDDP alone treatment to obtain cell lysates. Cleavage of PARP-1 was assessed by Western blotting. As internal control, α-tubulin expression was examined. **e** TUNEL positive cells were observed by confocal microscopy after TUNEL (green) and DAPI (blue) staining. Length of the scale bar is 10 μm. **f** Percentage of TUNEL positive cells was calculated. Error bars represent SEM (ns, not significant; *, $P < 0.05$; **. $P < 0.01$; ***, $P < 0.001$).

2.3.7 Mdivi-1 pre-treatment increases CDDP sensitivity of patient-derived spheroids (PDS) from tumor tissue and malignant ascites.

Next, we examined the effect of Mdivi-1 pre-treatment on CDDP sensitivity using a primary multicellular tumor spheroid model. The multicellular tumor spheroid model could be a good mimicry of complex *in vivo* tumor microenvironment that cellular components and hypoxic gradients can be retained. Compared to the mono-layered cells, multi-layered tumor spheres are characterized to be more resistant to anti-cancer agents and can form *in vivo*-like hypoxic gradient towards a center of the sphere (186, 195).

To further examine the effect of Drp1 inhibition on CDDP sensitivity, we used *in vivo*-like *in vitro* culture model employing malignant ascites samples from advanced-stage high-grade serous subtype ovarian cancer patients and primary tissue samples from advanced-stage high-grade serous and mucinous ovarian cancer patients. Patient-derived spheroids from malignant ascites (PDS #1-5) and cancer tissues (PDS #6-8) were embedded in Matrigel and cultured in tumor organoid medium. Six days after patient-derived cells were seeded 10 μM Mdivi-1 was treated. After incubation with Mdivi-1 for 24 h, 50 μM CDDP alone was added for 48 h. Representative micrographs of patient-derived spheroids (PDS #1-4) taken on day 2 and 6 show stable growth of tumor spheroids (Fig. 9a). Our previous study demonstrated that mitochondrial fission is induced in spheroids generated from ovarian cancer cells (93). Similarly, mitochondrial fission was observed in PDS. Treatment with Mdivi-1 increased mitochondrial fusion in PDS (Fig. 9b). For patient-derived spheroids from malignant ascites (PDS #1-4), Mdivi-1 pre-treatment followed by CDDP alone treatment could significantly reduce the size of the spheres (Fig 9c, d). Also, Mdivi-1 pre-treated tumor spheroids showed increased CDDP sensitivity and this was examined by MTT assay (Fig. 9e). These results demonstrate that *in vivo*-like primary tumor spheroids pre-treated with Mdivi-1 become more susceptible to CDDP.

a

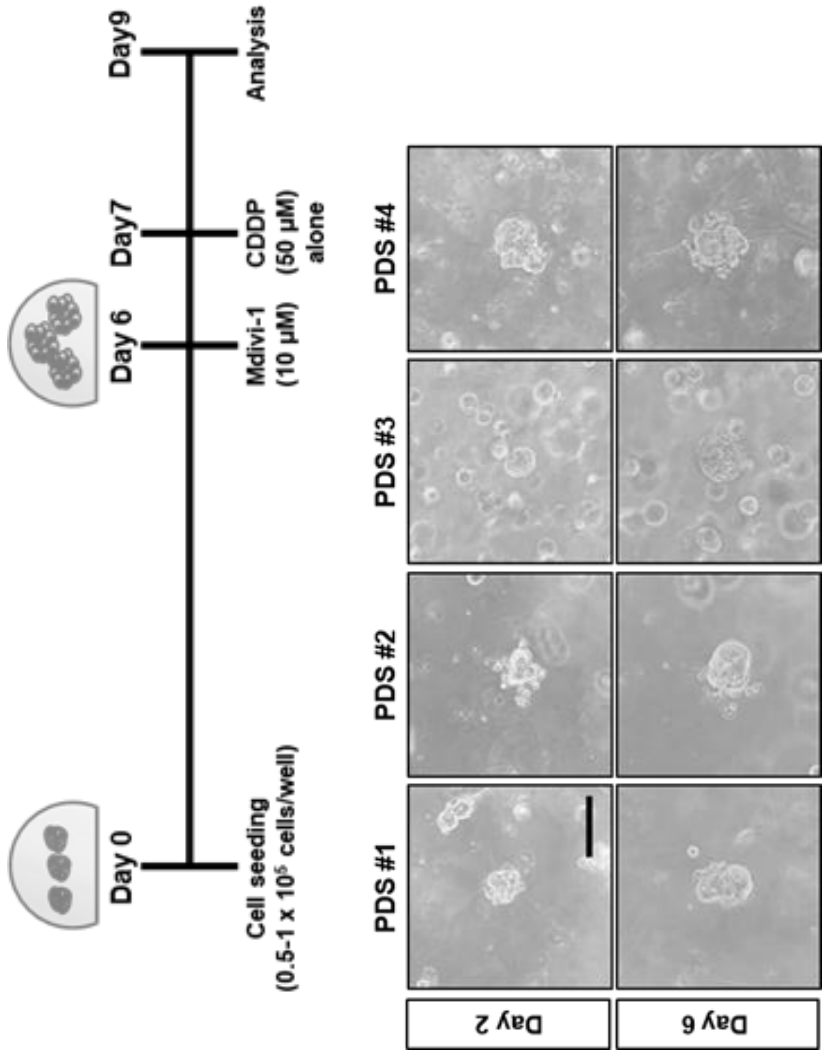
Day 0
Cell seeding
(0.5-1 x 10⁵ cells/well)
Day 6
Mdivi-1
(10 μM)
Day7
CDDP
(50 μM)
alone
Day9
Analysis
PDS #1
PDS #2
PDS #3
PDS #4
Day 2
Day 6

b

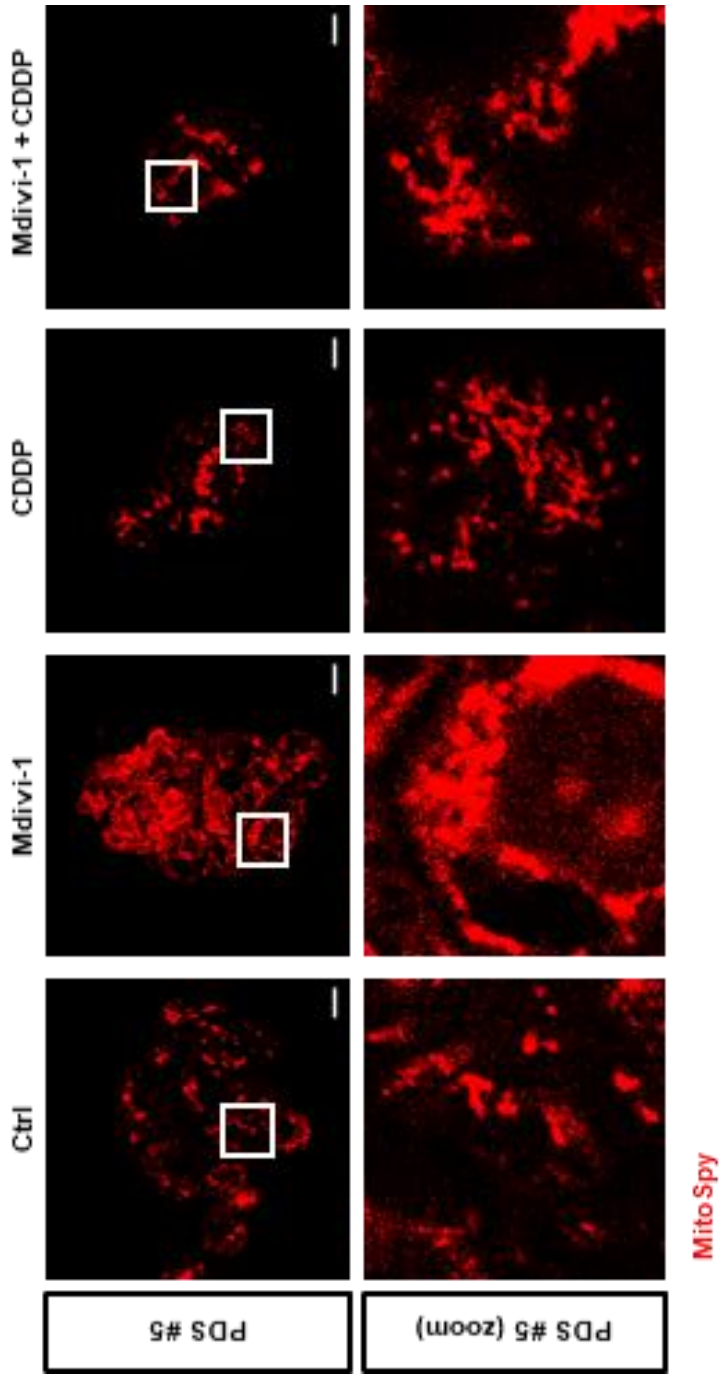

c

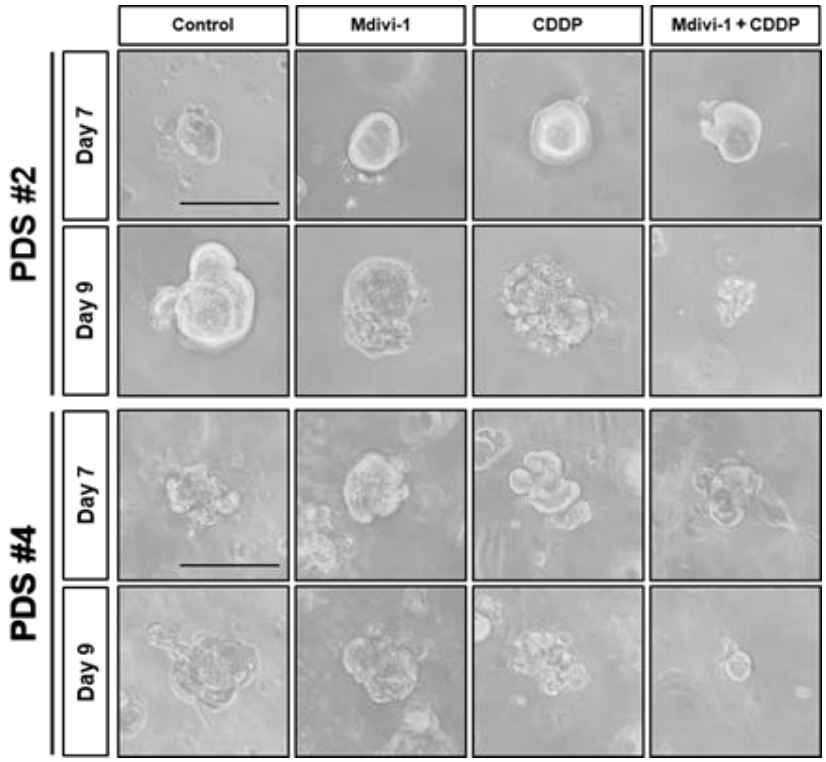
Control
Mdivi-1
CDDP
Mdivi-1 + CDDP
PDS #2
Day 7
Day 9
PDS #4
Day 7
Day 9

d

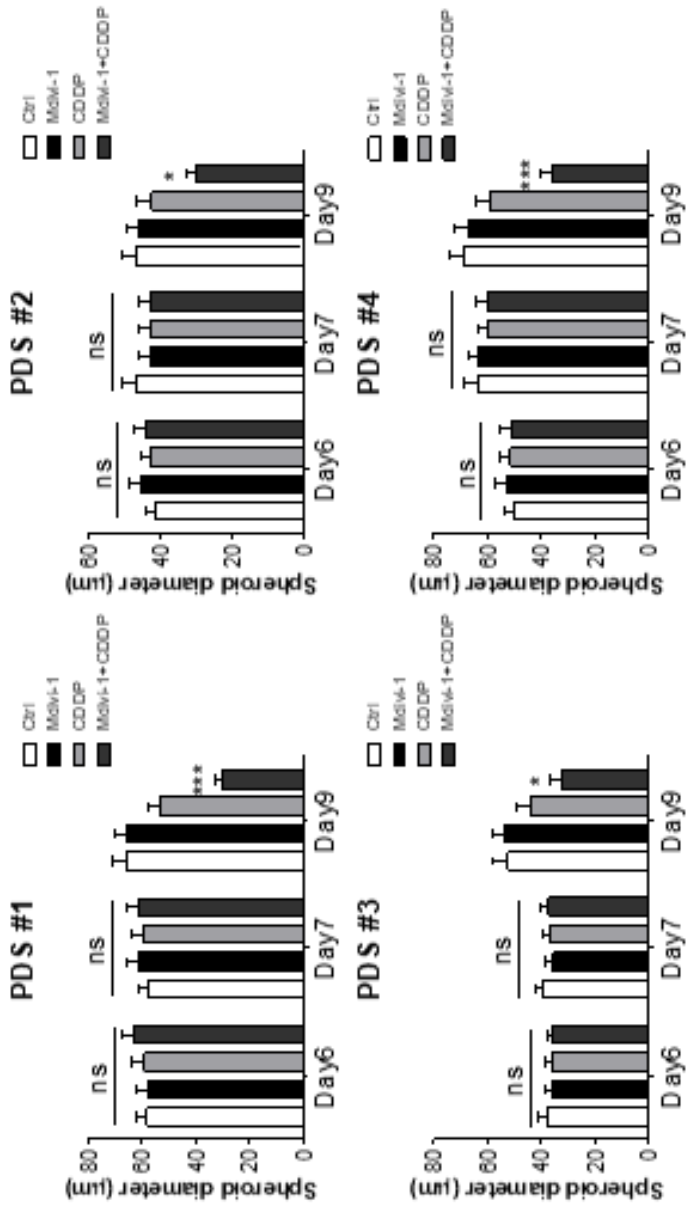
PDS #1
PDS #2
PDS #3
PDS #4
Ctrl
MdWi-1
CDDP
MdWi-1+CDDP
Spheroid diameter (μm)
0
20
40
60
80
ns
Day6
Day7
Day9
*
***

e

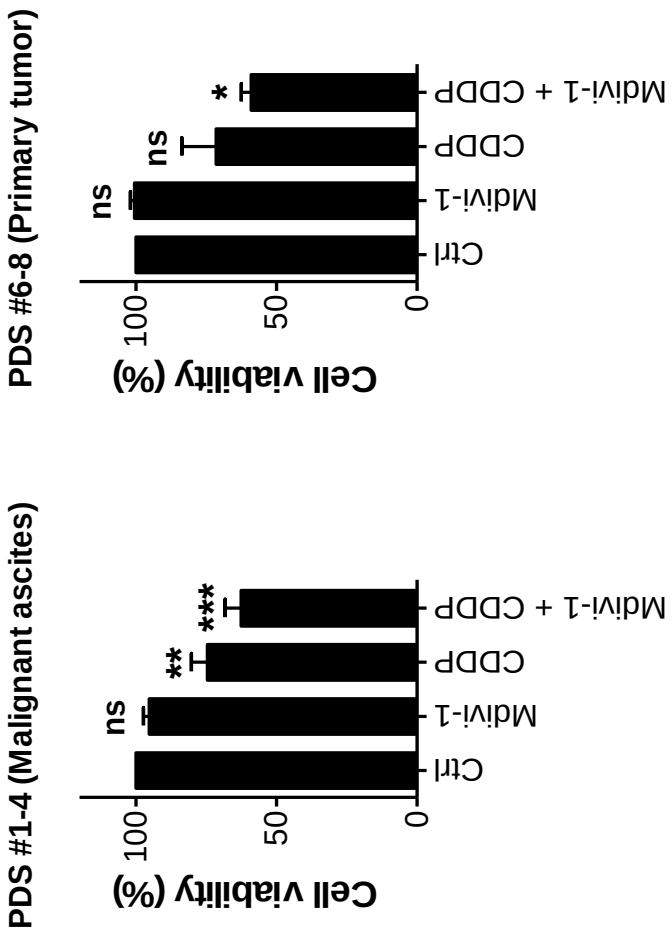
PDS #1-4 (Malignant ascites)
Cell viability (%)
0
50
100
Ctrl
Mdivi-1
CDDP
Mdivi-1 + CDDP
ns
**
***
PDS #6-8 (Primary tumor)
Cell viability (%)
0
50
100
Ctrl
Mdivi-1
CDDP
Mdivi-1 + CDDP
ns
ns
*

Figure 9. Mdivi-1 treatment increases CDDP sensitivity in ovarian cancer patient-derived spheroids.

a A schematic timeline displaying specific time points and concentrations of Mdivi-1 and CDDP treated. Primary PDS originated from tissues or ascites of different patients were isolated and grown by embedding them in the Matrigel. Micrographs of tumor spheroids were taken on day 2 and day 6. Day 0 is when the primary PDS were seeded. Representative micrographs of spheroids (PDS#1-4) show growth of tumor spheroids. Length of the scale bar is 100 μm. **b** Morphology of mitochondria in PDS was examined by MitoSpy staining. Length of the scale bar is 10 μm. **c** Representative micrographs of tumor spheroids (PDS#2 and #4) depicting changes in the size of the spheroids in different treatment conditions (mdivi-1 treatment alone, CDDP alone or Mdivi-1 pre-treatment followed by CDDP alone treatment). Length of the scale bar is 100 μm. **d** On day 6 (just before Mdivi-1 treatment), day 7 (just before CDDP treatment) and day 9 (48 h after incubation with CDDP), micrographs were taken for each experimental group and diameters of randomly chosen tumor spheroids were measured using ImageJ software (16 spheroids for each group). Values are presented as means ± SEM (ns, not significant; *, $P < 0.05$; ***, $P < 0.001$). **e** Primary tumor spheroids from malignant ascites (PDS#1-4; n=4) or primary tumor tissue (PDS#6-8; n=3), were treated with Mdivi-1 alone, CDDP alone or Mdvi-1 followed by CDDP. Relative cell viability under different experimental conditions was examined by MTT assay. Values are presented as means ± SEM from experiments with samples of different patients (ns, not significant; *, $P < 0.05$; **, $P < 0.01$; ***, $P < 0.001$).

2.4 Discussion

Adjustment of the molecular machinery under oxygen-poor condition plays an important role in ovarian cancer progression. Here, we report that mitochondrial fission is important for the acquisition of CDDP resistance under hypoxia (Fig. 10).

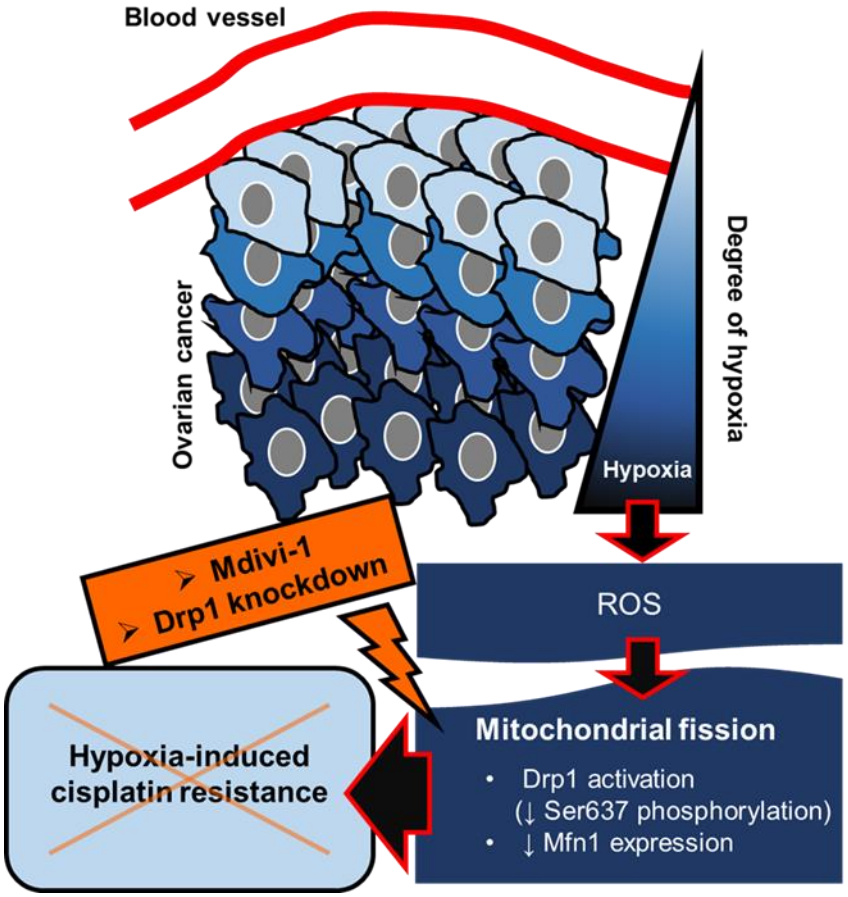

Figure 10. A schematic illustration summarizing the results of the current study.

Hypoxia is a commonly observed feature of tumor microenvironment, giving rise to resistance to CDDP, a widely used anti-cancer therapeutic agent against ovarian cancer. Drp1 activation and Mfn1 downregulation were mediated by increased level of ROS in hypoxic tumor microenvironment triggering mitochondrial fission of cancer cells. Mitochondrial fission induced by hypoxia could be targeted to maximize the efficacy of CDDP in hypoxic ovarian cancer cells.

First, we found that hypoxia promoted mitochondrial fission through the increase of ROS level. Our results are consistent with the previous study that H_2O_2 treatment increased mitochondrial fission in HeLa cells (196). Interestingly, inhibition of mitochondrial fission with Drp1 knockdown stimulated ROS production in HeLa cells (197). Similarly, our previous study showed that an excessive intracellular accumulation of ROS was accompanied by enhanced mitochondrial fission in ovarian cancer sphere cells. Therefore, mitochondrial fission possibly occurs as a part of an adaptive response to high ROS level.

Next, we showed that inhibition of mitochondrial fission prior to hypoxic exposure led to increased CDDP sensitivity in ovarian cancer cells. Although the involvement of Drp1-mediated mitochondrial fission in the intrinsic apoptotic pathway is well-recognized, the consequences of mitochondrial fission induced by hypoxia in cancer cells have not been elucidated (198, 199). Non-cancer cells are less viable in hypoxic conditions, and mitochondrial fission in these cells under hypoxia is responsible, at least in part, for cell death (106). Inhibition of mitochondrial fission suppressed hypoxia-induced cell death in pancreatic beta cells (200). These results suggest that inhibition of mitochondrial fission may prevent normal cell death and selectively increase CDDP susceptibility of cancer cells in the hypoxic tumor microenvironment

Accumulating evidence suggests that several factors existing in tumor microenvironment could regulate mitochondrial function and dynamics. In our previous study, we showed that increased metastatic potential of ovarian cancer cells is mediated by inflammatory signaling of tumor necrosis factor-α (TNF-α) secreted from pro-inflammatory M1 macrophages (96). Interestingly, in cardiomyocytes, TNF-α stimulates mitochondrial fission through Drp1 activation (201). Melatonin mainly secreted by the pineal gland is also produced in other organs including ovary and has been shown to suppress the metastatic potential of ovarian cancer stem cells (202). Pre-treatment of cortical neurons with melatonin inhibits mitochondrial fragmentation induced by cadmium (203). Gynecologic cancer cell lines under atmospheric oxygen culture conditions displayed tubular or well-connected morphology of

mitochondria (135). Whereas, under hypoxia, mitochondrial fission is induced along with the activation of HIF-1α in different types of cancer including gynecologic cancer, thyroid cancer and glioblastoma cells (135, 204, 205). Also, hypoxia promoted mitochondrial fission in breast cancer cells in a Drp1-dependent manner (113). Taken together, tumor microenvironment could alter the regulation of mitochondrial dynamics causing tumor progression.

Recently, the association between malignant properties and mitochondrial dynamics of cancer has been reported (161). In highly invasive breast cancer cells, treatment with Drp1 inhibitor suppressed cell migration (113). Treatment with PI3K inhibitor induced mitochondrial trafficking and fission, increasing migration and invasion in prostate and brain cancer cells (206). Additionally, increased mitochondrial fragmentation and Mfn2 downregulation in breast cancer are correlated with poor prognosis (207). Also, activation of Drp1 correlated with poor survival outcomes of brain cancer patients (208).

We have previously reported the role of heterogeneous cellular components in chemoresistance associated with epithelial ovarian cancer (209-211). As tumor heterogeneity and hypoxia are important factors in cancer progression, we used patient-derived tumor spheroids to confirm the association of hypoxia-induced mitochondrial fission with chemoresistance to CDDP. Instead of testing drug efficacy on a mouse xenograft model, primary tissues and malignant ascites directly obtained from debulking surgery could be used for generation of *in vivo*-like conditions, recapitulating cellular and physiological microenvironment of cancer. Patient-derived tumor spheroids have been shown to retain intra-tumoral heterogeneity (186, 195). Thus, it could be the ideal model to test drug efficacy in cancer, achieving personalized medicine in cancer treatment (212).

Given that prognosis of ovarian cancer patients varies between individuals, considerable efforts have been made to identify proteomic, transcriptomic, genomic and epigenetic disparities between tumors from individuals associated with therapeutic outcomes of ovarian cancer. One possible approach to improve therapeutic outcomes of cancer would be targeting the pro-tumorigenic changes in cancer cells elicited by the landscape of tumor microenvironment. In this

context, we demonstrated that mitochondrial fission induced by hypoxia through Drp1 activation could give rise to chemoresistance in ovarian cancer cells. We propose that the molecular signaling of mitochondrial dynamics as a target of ovarian cancer cells to enhance the sensitivity of hypoxic cancer cells to CDDP. Therefore, the current study could open up new avenues for the development of novel therapeutic strategies against cancer cells in hypoxic tumor microenvironment. Future research on other external signals in the tumor microenvironment that regulate mitochondrial dynamics and their association with cancer progression is warranted.

3. Chapter III: RELB stimulated by TNFα promotes invasive capacity of ovarian cancer cells through secretion of urokinase (PLAU/uPa)

3.1 Introduction

Ovarian cancer, the most lethal type of gynecologic malignancy, metastasizes to secondary organs mainly through peritoneal cavity forming malignant ascites (213, 214). A number of studies suggest multicellular detachment from primary site to peritoneal cavity is the main mechanism of ovarian cancer dispersal unlike other cancer that relocate its niche thorough vascular system (215). Hence, epithelial-to-mesenchymal transition (EMT) might not be a critical process for metastasizing ovarian cancer cells which take advantage of peritoneal cavity as a route of metastasis. Rather, various proteases that help detachment of multicellular tumor aggregates from the site of origin might be more important in both initial and final steps of spreading.

Many studies have uncovered oncogenic roles of a pro-inflammatory cytokine, TNF (216). Our group and others have shown that TNF activates canonical NFκB pathway involving RelA and NFκB1 increasing metastatic potential of ovarian cancer (217). However, the role of non-canonical NFκB pathway is relatively less explored. Also, only few studies have investigated TNF-mediated non-canonical NFκB pathway involving RelB in cancer. Recently, the fundamental role of RelB in cancer stemness, radioresistance and metastatic potential has been reported in ovarian, prostate and breast cancer studies, suggesting that RelB confers malignant phenotypes as an oncogenic signaling regulator (218-220).

We have previously reported oncogenic roles of proinflammatory cytokines such as TNF and IL-6 in ovarian cancer (104, 183, 217). Extending from those finding, we further investigated key molecular mechanisms associated with inflammatory signaling-associated metastatic potential of ovarian cancer. We also aimed to reveal the role of RelB in acquisition of metastatic phenotypes of ovarian cancer cells. Our hypothesis was that TNF would promote invasion of ovarian cancer cells resistant to TNF-induced cell death via RelB-regulated secretion ECM-degrading molecules. We showed that ovarian malignancy which shows the tumor microenvironment with high levels of TNF exhibits increased RelB expression. Increased RelB expression, in turn, promotes

secretion of prometastatic proteases. Targeting TNF-mediated RelB expression by RNAi suppressed malignant phenotypes of ovarian cancer cells. Therefore, utilizing the inflammatory tumor microenvironment of ovarian cancer shaped by TNF could be a promising treatment strategy.

3.2 Materials and Methods

3.2.1 Cell culture

Ovarian cancer cell lines used in this study were obtained from the American Type Culture Collection ATCC (Rockville, MD). These cell lines were grown in RPMI1640 (WelGENE, Seoul, Korea) supplemented with 10% FBS (Gibco-BRL, Gaithersberg, MD), and penicillin-streptomycin (Invitorogen, Carlsbard, CA). All the cell lines used in this study were authenticated and tested for mycoplasma. Cells were maintained in 5% CO2 humidified incubator at 37 ºC. ASCs were cultured in MesenPRO RS medium (Gibco) containing 1% GlutaMAX (Gibco), 100 U/mL penicillin and 100 μg/mL streptomycin (Invitrogen).

3.2.2 Invasion assay

To examine the effect of TNF, the Boyden chamber assay (transparent PET membrane with 8 μm pore size, BD bioscience) was used. Inserts were pre-coated with growth factor reduced Matrigel (BD Biosciences). Cells were serum starved overnight and 5,000-20,000 cells were seeded to the upper chamber. The inserts were then carefully placed onto the serum containing medium. Inserts were washed with PBS for three times and fixed with 4% formaldehyde for 1 hr at room temperature. For visualization and counting of cells, cells were stained with 0.5% crystal violet. Cotton swabs were used to remove the Matrigel. The invaded cells were counted using the ImageJ software.

3.2.3 Cell cycle analysis

Cell cycle analysis was conducted using flow cytometry. Cells were harvested by trypsinization and wished with PBS three times by centrifugation. Cell pellets were re-suspended with 70% ethanol at - 20 ºC overnight. Ethanol-fixed cells were then washed with PBS three times. Pellets were then suspended in PBS containing RNase A (Invitrogen) and incubated at the room temperature for 15 min. PI was added in each sample and flow cytometry analyses were conducted.

3.2.4 Reagents and antibodies

Primary antibodies used for this study were purchased from SantaCruz Biotechnology (P50, RelB, PARP-1, CyclinD1, CDK6, CDK4, CyclinE, CDK2, CyclinA and CyclinB), Sigma-Aldrich (α-tubulin) and Cell Signaling Technology (P65, P-P65 and P100/P52).

3.2.5 Cell viability assay

Cell viabilities were evaluated by MTT assay. Cells were seeding 96-well plate. Cells were incubated with 50 μL MTT (2mg/mL; 3hr) in the humidified incubator with 5% CO_2 and 37 ºC. After the incubation, metabolized formazan by mitochondrial reductase was solubilized in DMSO (100 μL /well). The optical density at 540 nm was determined using an spectrophotometer.

3.2.6 Transfection of siRNA

For RelB silencing, SKOV3, ES2, TOV21G and PA1 cells were transfected with 100 nM si-RelB #1-3 (Bioneer, Korea), using RNAiMax (Invitrogen). In a negative control group, 50 nM scramble siRNA (mBioTech, Korea) was transfected. At 24 h post-transfection, cells were harvested and reseeded for assays.

3.2.7 Western blotting

Protein lysates were prepared as described in the method section of the chapter 2. Briefly, proteins were separated by SDS-PAGE with 6-12% gel depending on the size of proteins examined. Then the gel was transferred onto the nitrocellulose membranes and probed with the indicated antibodies.

Bioinformatics analysis

3.2.8 Bioinformatics analysis

The GEO datasets were retrieved from NCBI website and used to analyze

mRNA levels. For gene set enrichment analysis (GSEA), mRNA expression of ovarian cancer tissue samples was used, and a formatted GCT file was used as an input for the GSEA algorithm v3.0 (broadinstitute.org/gsea). Patient prognosis depending on the expression of genes were analyzed using KM plotter. For dichotomization of the sample based on RelB and PLAU expression, 'split patient by' tab was set at 'auto select best cutoff'. (http://kmplot.com/analysis/). The mRNA expression data from both TCGA (cancer) and GTEx (normal ovary) cohorts were incorporated (http://gepia.cancer-pku.cn). The cut-off for P-value was set at 0.01. UALCAN is a web-based tool available at http://ualcan.path.uab.edu and was used to compare PLAU expression in different stages of ovarian cancer.

3.2.9 Proteome profiler array

Secretion of proteases was examined by Human Protease Array Kit. Experiment was conducted according to the protocol provided by the manufacturer.

3.2.10 Statistical analysis

Data were presented as mean $\pm$ SEM of the triplicate experiments. One-way ANOVA and student's t-test were used for the statistical analysis. Significant difference among experimental groups were assessed by Bonferroni's post hoc test. Data analysis was performed using IBM SPSS statistics 25 (SPSS Inc., Chicago, IL) and the GraphPad Prism 5 software. A P value < 0.05 was considered statistically significant.

3.3 Results

3.3.1 TNF is highly expressed in ovarian malignancy compared with other types of solid malignancies

We have previously shown that invasive capacities could be dictated by the tumor microenvironment, specifically pro-inflammatory cytokines, in ovarian cancer cells. Also, it has been now well-conceptualized that the role of inflammatory tumor microenvironment is critical for the cancer cell behaviors. Among the gene encoding inflammatory cytokines (TNFα, IL6 and IL1β) investigated using the TCGA RNA sequencing dataset, TNF expression was markedly higher in ovarian cancer tissue in comparison to that in the other solid tumors (Figure 11A). This may indicate that TNF could be a critical pro-inflammatory cytokine associated with ovarian cancer tumorigenesis and progression.

3.3.2 TNF promotes ovarian cancer cell growth through cell cycle progression

Next, increasing concentrations (0-10 ng/mL) of recombinant TNF were treated to the ovarian cancer cell lines (high-grade serous, clear cell and teratoma subtypes) and normal cells (ASCs and IOSE385). While TNF treatment for 24h show did not affect the viability in the most of normal and cancer cells, PA1 showed decreased cell viability as displayed in the MTT assay data but did not show significant changes in the results from CyTox-Glo assay. Also at the higher concentration of TNF (10 ng/mL), PA1 cells showed increased cleavage of PARP-1. Interestingly, ES2 cells showed increased cell viability despite short exposure time (24h) to TNF (Figure 11B and C). This results may indicate that ovarian cancer cells are generally resistant to TNF-induced cell death and PA1 cells are relatively sensitive to TNF-induced cell death.

To investigate cell cycle regulation, protein expression of cell cycle regulators and PI staining of fixed cell followed by flow cytometric analysis

was conducted. SKOV3 and PA1 cells showed increased cyclin D1 and/or Cyclin B expression at the protein level (Figure 11D) and proportions of cells in G2/M phases of cell cycle were increased (Figure 11E). Data from colony-forming assay to examine the long-term growth of TNF-exposed ovarian cancer cells show that TNF treatment increased colony forming capacity of ovarian cancer cells. This data support that TNF a critical role in ovarian cancer growth.

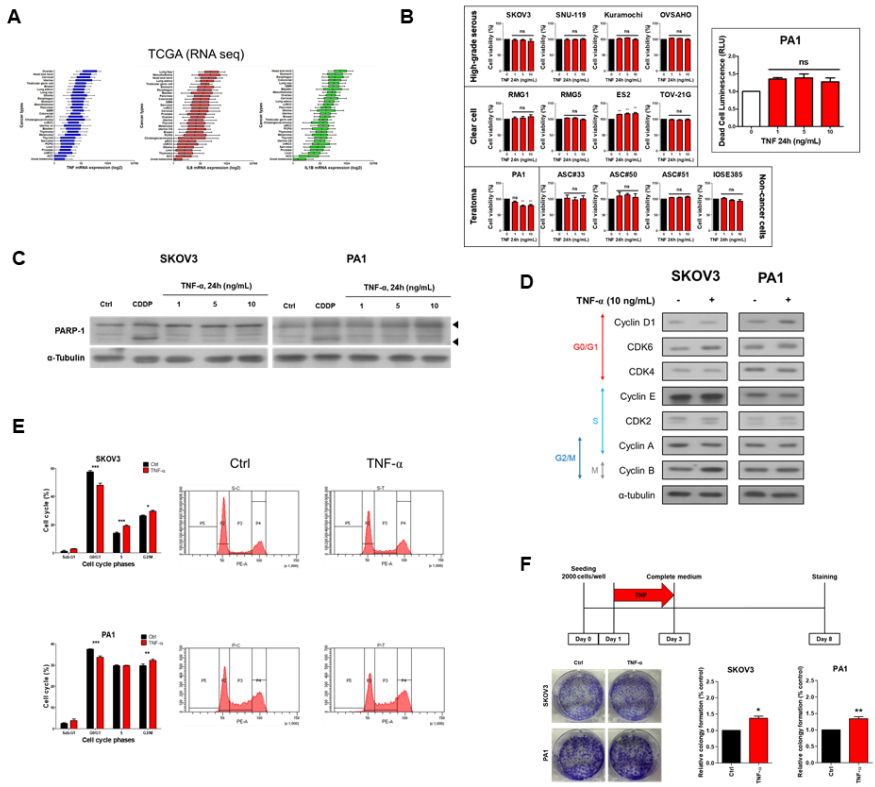

Figure 11. TNF is highly expressed in ovarian tumors promoting cancer proliferation through cell cycle progression.

A Transcript levels of genes encoding inflammatory cytokines (TNFα, IL6 and IL1β) were compared in different types of solid cancer. GSE38666 dataset was used. **B** Cell viability of ovarian cancer cells were compared after treatment of increasing doses of TNFα. Values are presented as means ± SEM (ns, not significant; **, $P < 0.01$). **C** PARP-1 expression was analyzed after treatment with TNFα for 24h at different doses. CDDP-treated group was included as a positive control. **D** Protein expression of cell cycle regulators were examined to see the effect of TNFα. **E** Cell cycle analysis was conducted after exposing cancer cells to TNFα. **F** Colony formation assay was done to examine the long term growth of the cancer cells exposed to TNFα. Values are presented as means ± SEM (*, $P < 0.05$; **, $P < 0.01$).

3.3.3 TNF enhances invasion of ovarian cancer cells

The representative results from GSEA analysis shows that high TNF expression is associated with metastatic and invasive phenotypes in ovarian cancer (Figure 12A). Also expression of TNF and TNF receptors (TNFR1 and TNFR2) were upregulated in the secondary/metastatic sites of tumors (Figure 12B and C). On the basis of these results we conducted migration and invasion assay on cancer cells to see changes in their metastatic capacity upon TNF exposure. While TNF did not affect migration capacity of ovarian cancer cells, invasive capacity of ovarian cancer cells was increased in response to TNF (Figure 12 D and E).

3.3.4 TNF increases expression of RelB, an alternative NFκB pathway gene, predicting poor prognosis in ovarian cancer patients.

TNF-enriched tumor tissues showed elevated levels of NFκB pathway genes

3.3.5 Knockdown of RelB prevents TNF induced invasion of ovarian cancer cells

To assess whether RelB is involved in TNF-induced invasion of ovarian cancer cells, si-RelB was transfected to the ovarian cancer cells (Figure 14A). Knockdown of RelB notably mitigated TNF-induced invasion of the ovarian cancer cells (Figure 14B). Also compared to the primary sites (left and right ovaries), RelB is highly expressed at the metastatic sites (ascites, omentum and peritoneum indicating that RelB could be a critical regulator of metastasis in ovarian cancer (Figure 14C).

A

NAME	SIZE	ES	NES
WANG_TUMOR_INVASIVENESS_UP	350	0.382113	1.765945
ROESSLER_LIVER_CANCER_METASTASIS_UP	102	0.526939	1.735292
WU_CELL_MIGRATION	180	0.696863	1.710815
ALONSO_METASTASIS_EMT_UP	33	0.710023	1.697845

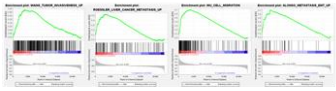

B

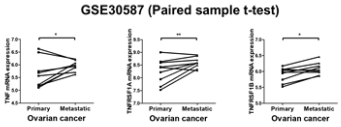

C

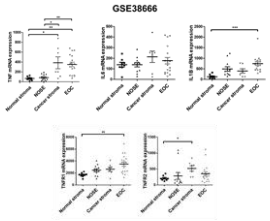

D

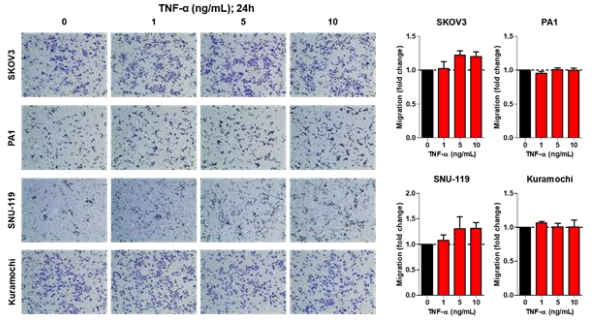

E

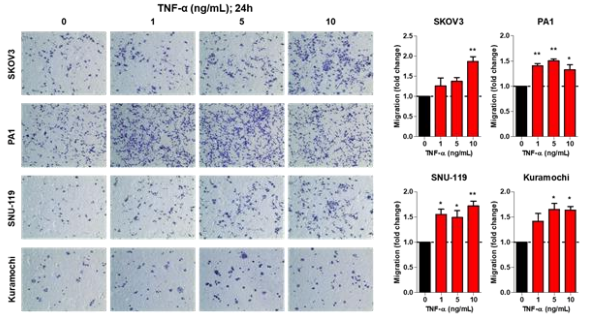

Figure 12. TNF enhances invasive capacity of ovarian cancer cells.

A Enrichment profiles of four representative pathways in TNF-high versus TNF-low groups of tissues (N=285). **B** Paired sample t-test done for expression of TNF, TNFR1 and TNFR2 in primary versus metastatic tissues. Values are presented as means ± SEM (*, $P < 0.05$; **, $P < 0.01$). **C** Transcript levels of genes encoding inflammatory cytokines (TNF, IL6 and IL1β) and TNF receptors (TNFR1 and TNFR2) were compared in different tissue groups (normal stroma, normal ovarian surface epithelium, cancer stroma and epithelial ovarian cancer). GSE38666 dataset was used. Values are presented as means ± SEM (*, $P < 0.05$; **, $P < 0.01$; ***, $P < 0.001$). **D** Migration assay was done using insert wells. **E** Invasion assay was done using insert wells. Values are presented as means ± SEM (*, $P < 0.05$; **, $P < 0.01$).

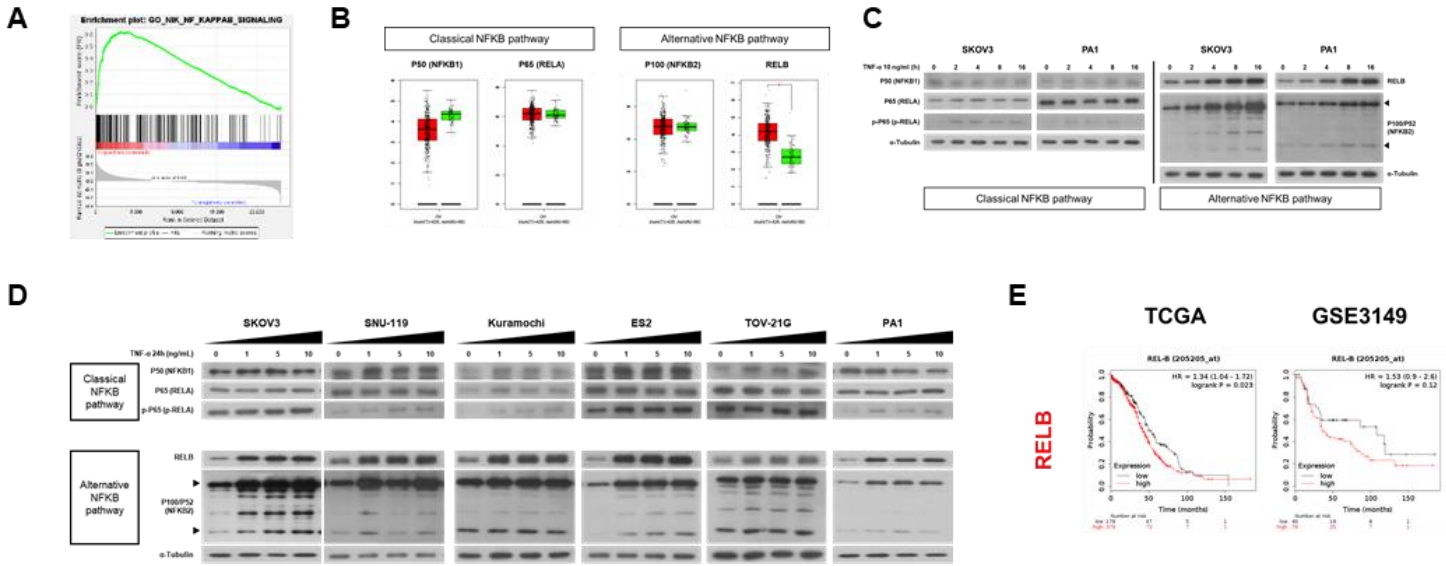
A
Enrichment plot: GO_NIK_NF_KAPPAB_SIGNALING
B
Classical NFKB pathway
Alternative NFKB pathway
P50 (NFKB1)
P65 (RELA)
P100 (NFKB2)
RELB
C
SKOV3
PA1
SKOV3
PA1
TNF-α 10 ng/ml (h)
0 2 4 8 16 0 2 4 8 16 0 2 4 8 16 0 2 4 8 16
P50 (NFKB1)
P65 (RELA)
p-P65 (p-RELA)
α-Tubulin
RELB
P100/P52 (NFKB2)
α-Tubulin
Classical NFKB pathway
Alternative NFKB pathway
D
SKOV3
SNU-119
Kuramochi
ES2
TOV-21G
PA1
TNF-α 24h (ng/mL)
0 1 5 10 0 1 5 10 0 1 5 10 0 1 5 10 0 1 5 10 0 1 5 10
Classical NFKB pathway
P50 (NFKB1)
P65 (RELA)
p-P65 (p-RELA)
Alternative NFKB pathway
RELB
P100/P52 (NFKB2)
α-Tubulin
E
TCGA
GSE3149
RELB
REL-B (205205_at)
HR = 1.34 (1.04 - 1.72)
logrank P = 0.023
REL-B (205205_at)
HR = 1.53 (0.9 - 2.6)
logrank P = 0.12
Probability
Expression
low
high
Time (months)

Figure 13. TNF increases RelB expression which predicts poor prognosis in ovarian cancer.

A Enrichment profiles of a representative pathway in TNF-high versus TNF-low groups of tissues (N=285). **B** Classical and alternative NFκB pathway genes were examined in the normal (green box) and cancer (red box) tissues using TCGA and GTEx datasets. **C** Protein expression of classical and alternative NFκB pathway genes were examined after treatment of TNFα for different time **D** Protein expression of classical and alternative NFκB pathway genes were examined after treatment of TNFα for different doses **E** Higher expression of SDC4 was associated with poor overall survival of ovarian cancer patients. Ovarian cancer public datasets from TCGA and GSE3149 (GEO data) were used.

A
SKOV3
PA1
ES2
TOV21G
TNF-α 10 ng/ml (24h)
Blank
si-Ctrl
si-RelB #1
si-RelB #2
si-RelB #3
si-RelB #4
RelB
α-tubulin
B
si-ctrl
si-Ctrl + TNF-α
si-RelB #1 + TNF-α
SKOV3
PA1
ES2
TOV21G
C
GSE85296
RELB mRNA expression (Z-scores)
0.2
0.1
0.0
-0.1
-0.2
-0.3
*
Left ovary
Right ovary
Ascites
Omentum
Peritoneum

Figure 14. RELB is associated with TNF triggered invasion of ovarian cancer cells.

A Protein expression of RelB was assessed after si-RelB transfection in the indicated ovarian cancer cell lines. **B** Transcript expression level of RelB was examined in the ovarian cancer tissue samples from different tissues of orgins. GSE85296 dataset was used for the analysis. Values are presented as means ± SEM (*, $P < 0.05$). **C** Insert-well invasion asssy was conducted to observe the effect of TNFα treatment in the ovarian cancer cell lines after si-ctrl or si-RelB transfection.

3.3.6 TNF induces secretion of prometastatic proteases through RelB signaling

It has been shown that MMP-2 and MMP-9 are pro-invasion enzymes degrading ECM components and are regulated by RelB. We found that TNF treatment increased MMP-2 and MMP-9 expressions at the transcript level (Figure 15A). Proteases profiling array data suggest that MMP1, MMP-9, MMP-13 and PLAU/uPA are secreted in response to TNF treatment. Among those secretory factors regulated by TNF, MMP9 and PLAU secretion were mediated by RelB (Figure 15B). Interestingly, Cancer tissues showed elevated levels of MMP-9 and PLAU expression than normal tissues (Figure 15C). Also PLAU expression was up regulated in the late stages (stages 3 and 4) in ovarian cancer patient tissues than in earlier stage (Figure 15D). Lastly, high PLAU expression was significantly associated with Poor progression-free and overall survivals in ovarian cancer patients (Figure 15E).

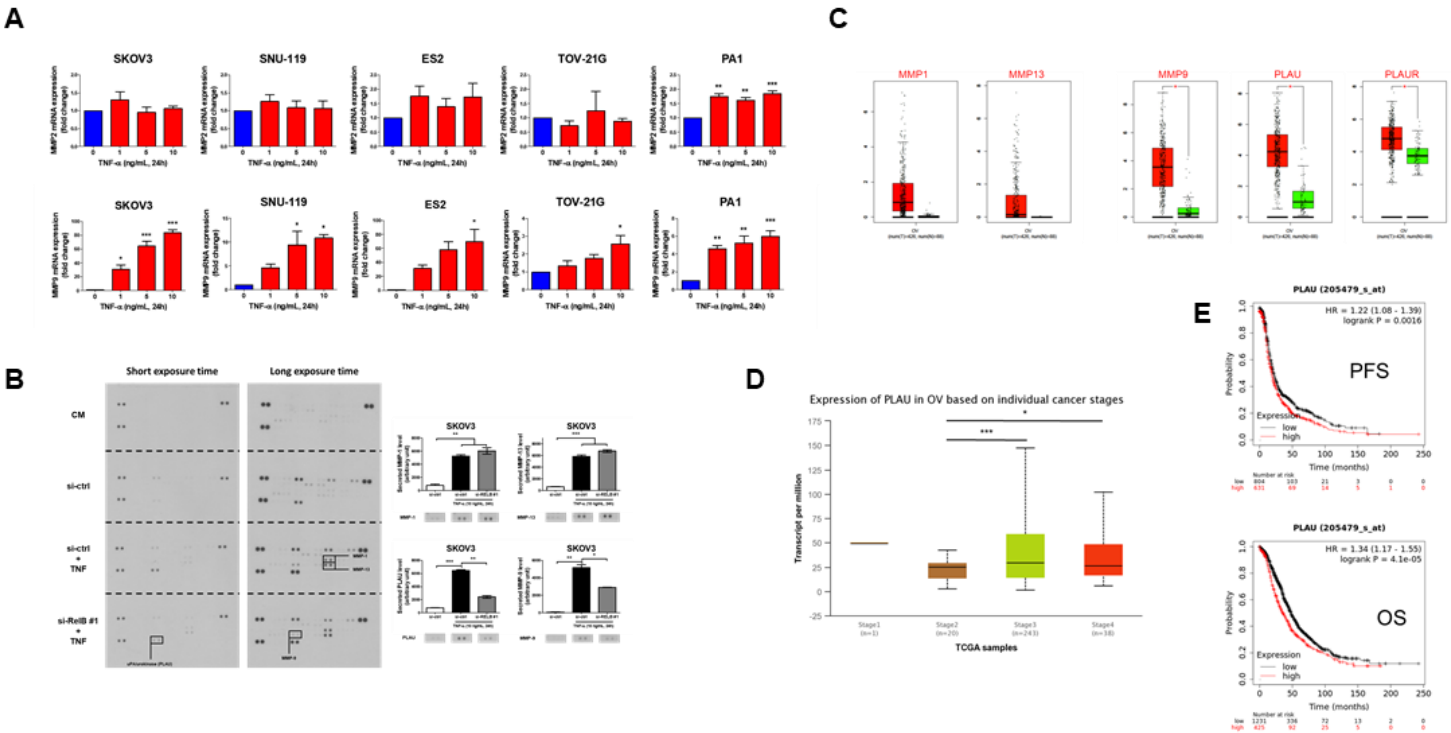
A
SKOV3
SNU-119
ES2
TOV-21G
PA1
MMP2 mRNA expression (fold change)
MMP9 mRNA expression (fold change)
TNF-α (ng/mL, 24h)
B
Short exposure time
Long exposure time
CM
si-ctrl
si-ctrl + TNF
si-RelB #1 + TNF
C
MMP1
MMP13
MMP9
PLAU
PLAUR
D
Expression of PLAU in OV based on individual cancer stages
Transcript per million
TCGA samples
Stage1
Stage2
Stage3
Stage4
E
PLAU (205479_s_at)
HR = 1.22 (1.08 - 1.39)
logrank P = 0.0016
PFS
HR = 1.34 (1.17 - 1.55)
logrank P = 4.1e-05
OS
Probability
Time (months)
Expression
low
high
Number at risk

Figure 15. TNF induces secretion PLAU/uPa through RelB.

A qRT-PCR was done to examine expression levels of MMP-2 and MMP-9 genes after exposing ovarian cancer cells to TNFα for 24h at indicated doses. **B** Protease array result of conditioned medium from the complete medium (CM) without cells seeded, si-ctrl SKOV3 cells, si-ctrl SKOV3 cells treated with TNF and si-RelB #1 transfected SKOV3 cells treated with TNF. **C** Expression levels of secreted proteins (MMP-1, MMP-13, MMP-9 and PLAU) were compared between normal and cancer tissues using TCGA and GTEx datasets. **D** The PLAU/uPA expression is significantly upregulated in the cancer tissues from stages III and IV patients. UALCAN was used to analyze the association of stages with RelB expression. **E** Higher expression of PLAU is associated with poor prognosis in ovarian cancer patients.

3.4 Discussion

In this study, we showed that the inflammatory signaling mediated activation of RelB promotes ovarian cancer cell metastasis. Our analysis of data from public databases show that TNF could be an important pro-inflammatory cytokine for oncogenesis and progression of ovarian cancer cells. Among many other ECM-degrading enzyme secreted by cancer cells shown to be regulated by RelB, our results suggest that RelB induces PLAU secretion under TNF treated conditions (Figure 16).

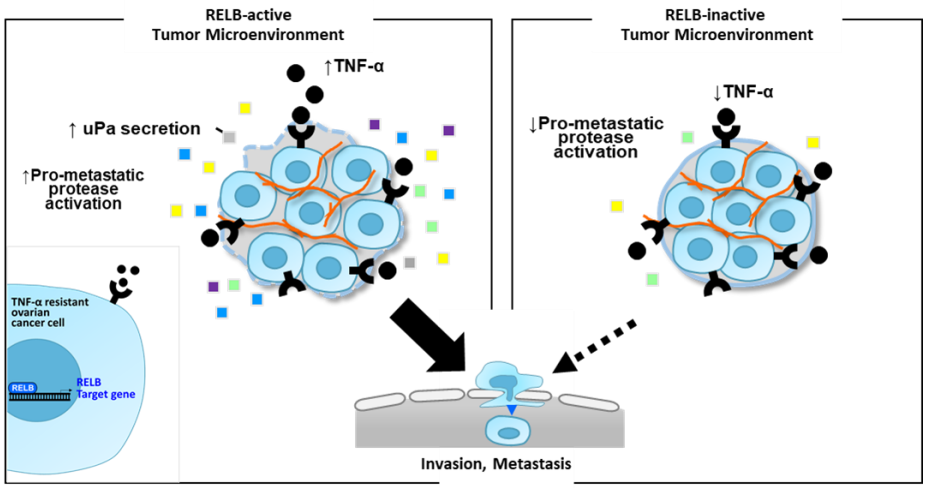

Figure 16. Graphical summary study in the chapter 3.

Even though a number of studies have suggested the involvement of classical/canonical NFκB pathway involving P50 and P65, recent studies show RelB can induce malignant progression of many types of cancer (221, 222). Recent study by Wang et al., suggests that RelB highly expressed in triple-negative breast cancer aggressive breast cancer tissues and promotes proliferation and metastasis through EMT and MMP-1 expression in breast cancer cells (223). In prostate cancer, expression of RelB triggers growth, migration and invasion. Knockdown of RelB inhibited metastatic potential and radio-sensitivity of prostate cancer cells In the same study they showed that RelB induced increased invasion capacity is associatted wih MMP-2 and MMP-9 expression (218). Also, in DLD1 colon cancer cells, relB promotes chemoresistance to 5-FU through down regulation of AKT/mTOR signlaing pathway. Also the study revealed that RelB knockdown in the colon cancer cells showed attenuation of MMP-2, MMP-9 and integrin β-1 expression (219). However, another study showed contrasting results that in breast cancer, low RelB exprssion is associated with poor overall and progression-free survival. Therefore, RelB might act differently depending on clinicopathological features of cancer in different cancer types. Further study would be necessary to fully elucidate mechanistic aspects of classical and non-cannonical NFκB pathways in cancer progression (222).

Additionally, PLAU is an interesting molecule and could be a critical secreted protein as shown by several recent evidence. Overexpression of PLAU showed poor prognosis in gastric cancer patients (224). Moreover, PLAU has recently shown its potential to act as a prognostic biomarker in head and neck squamous carcinoma (225). PLAU has been shown to be a secreted molecule with a multi-faceted role. First, it can act as an activator of ECM degrading enzymes including various kinds of metalloproteases (MMPs). In glioblastoma, PLAU has been shown to directly activates MMP-9 enabling invasion. Along with MMP-9 many other MMPs could be activated by PLAU at the extracellular regions (226). In breast cancer cells, fluid shear stress significantly upregulates PLAU expression and increases urokinase activity supporting its role in metastatic processes of cancer cells (227).

All in all, our data suggest that TNF induced RelB plays a significant role in metastatic processes of ovarian cancer cells. These processes could be critical, at least in part, for the early dissemination of ovarian cancer cells from their primary sites and/or micro-invasion to various organs in the peritoneal cavity. Therefore, PLAU secretion via TNF-induced RelB could give an insight into a novel therapeutic target for inhibiting ovarian cancer progression.

4. Chapter IV: Communication between immune and cancer cells in ovarian cancer ascites through CCL5-SDC4 interaction

4.1 Introduction

Ovarian cancer is the most lethal type of gynecological malignancy with a five-year survival rate below 50% (228). For the past three decades, there has been only a slight increase in the ovarian cancer survival outcome. Early detection is difficult because no specific symptoms of ovarian cancer as well as no effective detection markers with high accuracy are available. In addition to the fact that the vast majority of patients are diagnosed at advanced stages, the current gold standard of care for advanced ovarian cancer is a primary debulking surgery followed by taxol/platinum-based chemotherapy, which has not changed for many years. Patients are treated irrespective of histologic subtypes and genetic background, and chemoresistance is highly prevalent in this cancer (229). With the recent advances of sequencing at single-cell resolution, our understanding of molecular mechanisms underlying cancer progression has significantly increased. Accumulating evidence supports the importance of tumor microenvironment (TME) in facilitating the oncogenic behavior of cancer cells, but its precise role in cancer progression remains poorly understood. A deeper understanding of interactions between diverse cells in the cancer tissue may allow the identification of novel diagnostic biomarkers and therapeutic targets of ovarian cancer.

The major route of metastasis in ovarian cancer is transcoelomic dissemination causing the accumulation of fluid, malignant ascites (230). Malignant ascites could act as a vehicle and reservoir for ovarian cancer metastases to various secondary sites. Malignant ascites accumulates in the peritoneal cavity during ovarian cancer progression, providing a niche for disseminated cancer cells (231). The majority of patients in the advanced stage of the disease have malignant ascites, which is associated with poor survival (232). Therefore, it is of prime importance to understand the role of ascites TME in ovarian cancer progression.

In our previous studies, we focused on acelluar components (IL-6 and cholesterol) that are enriched in malignant ascites and their effects on ovarian cancer progression (233, 234). In the current study, we postulated that cellular

components within the malignant ascites could be highly heterogeneous and asked what types of cellular components and interactions are enriched in the ascites TME. To answer this question, we conducted a scRNA-seq on malignant ascites-derived cells isolated from an ovarian cancer patient with the advanced stage (stage IV). Our scRNA-seq data were analyzed along with previously reported data from Schelker et al. (2017) (235) to dissect cellular heterogeneity and interactions in the malignant ascites. Understanding cellular heterogeneity and ligand-receptor interactions within malignant ascites may yield novel therapeutic targets for cancer metastasis and cell survival in ovarian cancer.

4.2 Materials and Methods

4.2.1 Patient samples and sample processing

Malignant ascites (a25) was obtained from the 58-year-old high-grade serous ovarian cancer patient (stage IV). Isolation of cellular components from malignant ascites was described previously (236). Briefly, ascitic fluid was centrifuged at 1,400 x g for 10 min at 4°C. To remove erythrocytes, density-gradient centrifugation with Ficoll was performed. Isolated cells were stored in liquid nitrogen until further analysis. The experimental protocol was approved by the Institutional Review Board (IRB) of Seoul National University Hospital (IRB no. 1409-154-616) and conducted in accordance with the Declaration of Helsinki.

4.2.2 scRNA-seq library preparation and data pre-processing

A total of 1,086 cells from a25 patient were sequenced to a read depth of ~ 120,000 per cell and run through the 10x Genomics cell ranger platform. Single-cell suspensions were prepared as outlined by the 10x Genomics Single Cell 3' v2 Reagent kit user guide. In brief, single cell suspensions were loaded into a 10x Chromium Controller (10x Genomics, Pleasanton, CA, USA) and aimed for 5,000 cells. Following Gem capturing and lysis, cDNA was synthesized and amplified to construct sequencing libraries.

4.2.3 scRNA-seq Data analysis

The sequenced data were processed into expression matrices with the Cell Ranger Single Cell software 1.3.1 by 10x Genomics (http://10xgenomics.com/). The libraries were sequenced on the Illumina HiSeq 2500 platform, and sequencing reads were aligned with

STAR to the human transcriptome using the human reference transcriptome GRCh38. From the gene expression matrix, the downstream analysis was

carried out with R version 3.6.3 (2020-02-29). Quality control, data pre-processing, integration of multiple scRNA-seq datasets from two different technologies and visualization, and the differential expression analysis was carried out using Seurat version 3.1.5 package (237, 238). For each individual dataset, genes expressed in less than 3 cells as well as cells with < 200 genes and any cells with > 10% UMIs mapped to mitochondrial genes were removed from the gene expression matrix. Based on these criteria, 26,669 genes across 7,343 samples remained for downstream analysis. We performed PCA on the gene expression matrix and used the first 15 principal components for clustering and visualization. Unsupervised shared nearest neighbor (SNN) clustering was performed with a resolution of 0.15 and we employed UMAP (uniform manifold approximation and projection) for dimensionality reduction and visualization. Differentially expressed genes were identified using Seurat's "FindAllMarkers" to process all clusters combined with the MAST test (239) with logFC threshold > 0.25 and expressed in at least 10% of the cells in the cluster. The expression profile of each cluster's top 10 genes based on average log FC were visualized as a heatmap.

4.2.4 MacSpectrum analysis

A total of 1,868 differentially expressed genes between macrophage subclusters were selected and expression levels of each genes per cell were extracted to generate MPI and AMDI values using MacSpectrum analyzer Release v1.0.1 (https://macspectrum.uconn.edu/) (240). MPI and AMDI values were added to the metadata slot of Seurat objects for further categorization of macrophage subtypes.

4.2.5 Pathway enrichment analysis

GSEA(241) was applied to identify enriched pathways between the groups stated in Figure 3 and Figure S2. We used hallmark gene sets (h.all.v7.1.symbols.gmt) from Molecular Signature Database (MSigDB, https://www.gsea-msigdb.org/gsea/downloads.jsp) (242). Genes were ranked

by the average log fold change and p value was calculated using pre-ranked gene set enrichment analysis method fgsea (https://github.com/ctlab/fgsea) (243) package with hundred thousand gene set permutations.

4.2.6 NicheNet analysis - ligand-receptor communication prediction model

To predict the potential ligand-receptor communication between ovarian cancer cells and niche cells in ascites TME, we used a pre-built prior model, the NicheNet method (244, 245). In brief, we defined a ligand or receptor as expressed in a particular cell type when it is expressed in at least 30% of the cells in that cluster. To perform NichNet ligand activity analysis, we've defined the geneset of interest by combining two GO terms, negative regulation of anoikis (GO:2000811) and negative regulation of programmed cell death (GO:0043069) for anoikis related ligand-receptor communication prediction model and used all genes expressed in ovarian cancer cells as background of genes.

4.2.7 TCGA, GEO and GTEx dataset analysis

Patient prognosis depending on the expression of syndecan4 (SDC4, also known as SYND4) was analyzed using KM plotter. For dichotomization of the sample based on SDC4 expression, 'split patient by' tab was set at 'auto select best cutoff'. TCGA and GEO cohorts (GSE9891, GSE3149, GSE26193 and GSE63885) were utilized for the analysis (http://kmplot.com/analysis/) (246). The Pearson correlation between expression of MET and SDC4 and the expression of SDC4 in normal and cancer tissues were analyzed using the GEPIA (Gene Expression Profiling Interactive Analysis) online database. The mRNA expression data from both TCGA (cancer) and GTEx (normal ovary) cohorts were incorporated (http://gepia.cancer-pku.cn) (247). The cut-off for P-value was set at 0.01. UALCAN is a web-based tool available at http://ualcan.path.uab.edu and was used to compare SDC4 expression in different stages of ovarian cancer (248).

4.2.8 Statistical analysis

Significant differences were defined at $P < 0.05$ or adj.$P < 0.05$, where applicable. Survival analysis by KM plotter was performed using a Kaplan-Meier and the hazard ratio with 95% confidence intervals, and logrank P values are computed. Pearson correlation coefficient (Pearson's r) was used for co-expression test and automatically calculated by the GEPIA tool. Statistical significance was calculated by using GraphPad Prism 5 software for the correlation analysis when applicable.

4.3 Results

4.3.1 Clustering of single-cell transcriptomic data identifies cellular heterogeneity of malignant ascites

To investigate the cellular populations of malignant ascites, scRNA-seq was conducted on malignant ascites-derived cells using the 10x Genomics Chromium platform. Malignant ascites (a25) from the high-grade serous patient (stage IV) was collected before the patient received chemotherapy and underwent surgery at Seoul National University Hospital (SNUH). After quality control, 1,082 cells were retained for analysis. Mean reads per cell were 118,862 and median genes per cell was 3,109. scRNA-seq data from a25 and data from a previous study (235) (7873M, 7882M, 7892M, 7890M2) were incorporated for the subsequent analysis. From ascites samples, 7,343 cells were analyzed. To eliminate the batch-specific variations between different datasets, batch-correction was executed prior to the subsequent analysis (Figure 17A, left panel). For comprehensive visualization of transcriptomic likeness between cells from the five ascites samples, UMAP analysis was performed with the batch-corrected dataset. Ten major clusters were revealed, indicating the existence of transcriptomically distinct cellular profiles within malignant ascites (Figure 17A, right panel).

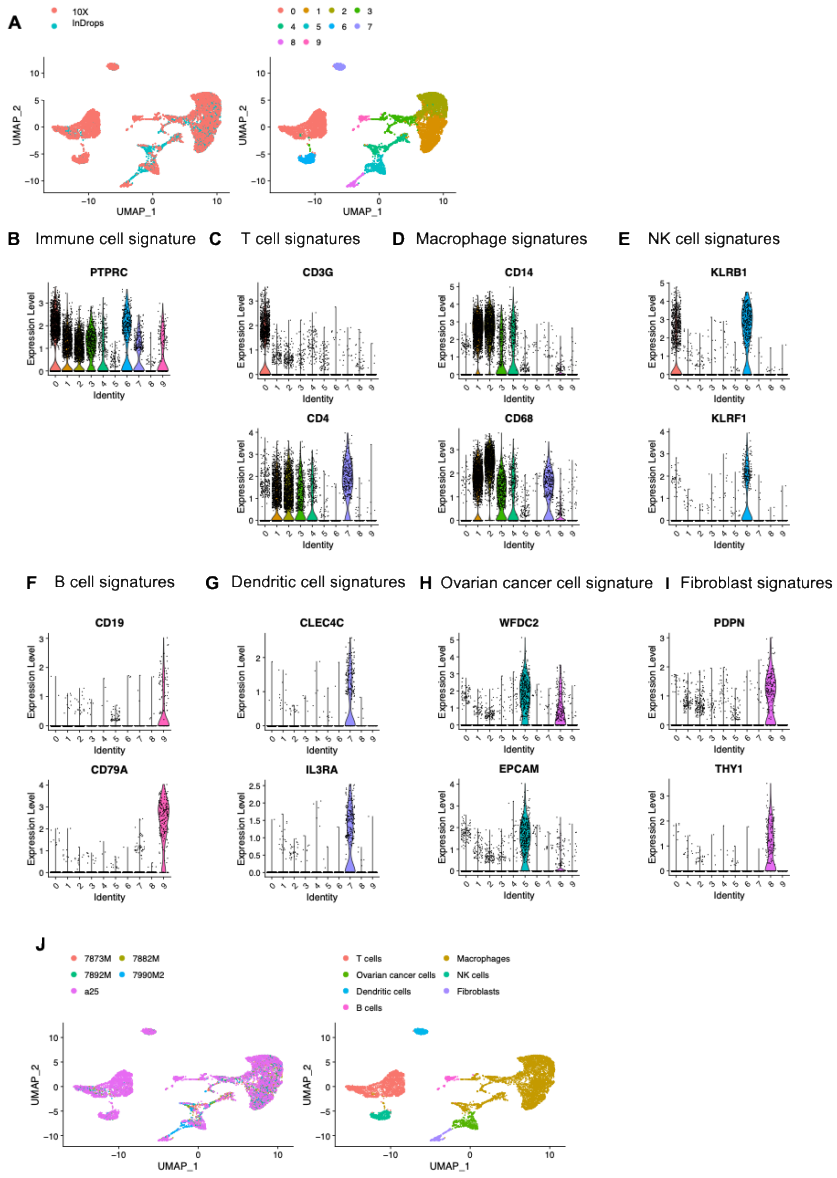

K

50,501 genes in 7,343 cells							
Cell type	T cells	Macrophages	Ovarian cancer cells	NK cells	Dendritic cells	Fibroblasts	B cells
Cell count	1756	4073	404	397	308	212	193

Figure 17. Identification of cellular components of ovarian cancer patient derived ascites.

(A) Batch corrected unsupervised clustering of ascites cellular components. UMAP dimensional reduction analysis identified 10 major clusters. (B-I) Expression of cluster defining genes. (B-G) Immune cell signatures (PTPRC, CD3G, CD4, CD14, CD68, KLRB1, KLRF1, CD19, CD79A, CLEC4C, IL3RA). (H-I) non-immune cell signatures, ovarian cancer cell signatures (WFDC2, EPCAM) and fibroblast signatures (PDPN, THY1), visualized by Violin plots (left) and Feature plots (right). (J) UMAP plots of ascites cellular components from 5 patient samples with cell types labeled. (K) Number of cells counted in each cell types.

We then used the expression of known genetic markers to identify cell types within the malignant ascites. Expression levels of T cell, macrophage, NK cell, B cell and dendritic cell signatures were investigated to characterize immune cells. Based on the expression level of the pan-immune marker, PTPRC (also known as CD45), the clusters fell into two large groups, immune-related and non-immune related clusters, with the latter expressing mostly ovarian cancer and fibroblast signatures. We identified 8 distinct immune cell clusters including a T cell cluster (cluster 0 highly expressing CD3G; low level of CD4+ cells was found), four macrophage clusters (clusters 1, 2, 3, 4 highly expressing CD14 and CD68), an NK cell cluster (cluster 6 highly expressing KLRB1 and KLRF1), a B cell cluster (cluster 9 highly expressing CD19 and CD79A), and a dendritic cell cluster (cluster 7 highly expressing CLEC4C and IL3RA) (Figure 17B-G). However, we could not detect cell clusters expressing polymorphonuclear leukocytes (e.g., mast cells, eosinophils, basophils and neutrophils). The two non-immune cell populations based on low PTPRC levels were characterized by an ovarian cancer cell signature (cluster 5 highly expressing WFDC2 and EPCAM) and a fibroblast signature (cluster 8 highly expressing COL1A1 and THY1) (Figure 17H, I). About 5.5% of cells derived from malignant ascites were expressing ovarian cancer cell signatures (WFDC2 and EPCAM). A small fraction of cells (2.6%) was expressing fibroblast markers (PDPN and THY1) (Figure 17J, K). These results show that different cell types (immune cells, ovarian cancer cells and fibroblasts) exist in the malignant ascites TME.

Overall, seven distinct cell types were identified by the expression levels of cell type-specific signatures in the malignant ascites TME (Figure 17J, K). Preprocessing of the samples using Ficoll-density gradient centrifugation, enriched mononuclear cells in our ascites samples. Data from analysis of immune cell signatures suggest that the vast majority of the cells within ascites are immune cells. Notably, macrophages (55.5%) were the most abundant cell type, followed by T cells (23.9%), NK cells (5.4%), Dendritic cells (4.2%), B cells (2.6%). Among these immune cells, macrophages are the dominant cells in the ascites TME and are noticeably scattered in the UMAP plot, implying

that the cells expressing macrophage markers are highly heterogeneous.

4.3.2 Profiling of macrophage polarization states in ascites TME of ovarian cancer patients with MacSpectrum analysis

As mentioned above, macrophages comprised the most abundant population found in multiple UMAP clusters in our dataset. This may imply that macrophages are the most heterogeneous immune cell population within the malignant ascites. The heterogeneity of macrophages in ascites TME is not simply characterized by the conventional M1 and M2 subtypes (Figure S5). To characterize macrophage heterogeneity in ascites TME, macrophages were re-clustered, and 13 Seurat defined clusters were identified (Figure 18A, left panel). There was no notable difference in transcriptomic expression pattern in macrophages across the patient samples (Figure 18A, right panel).

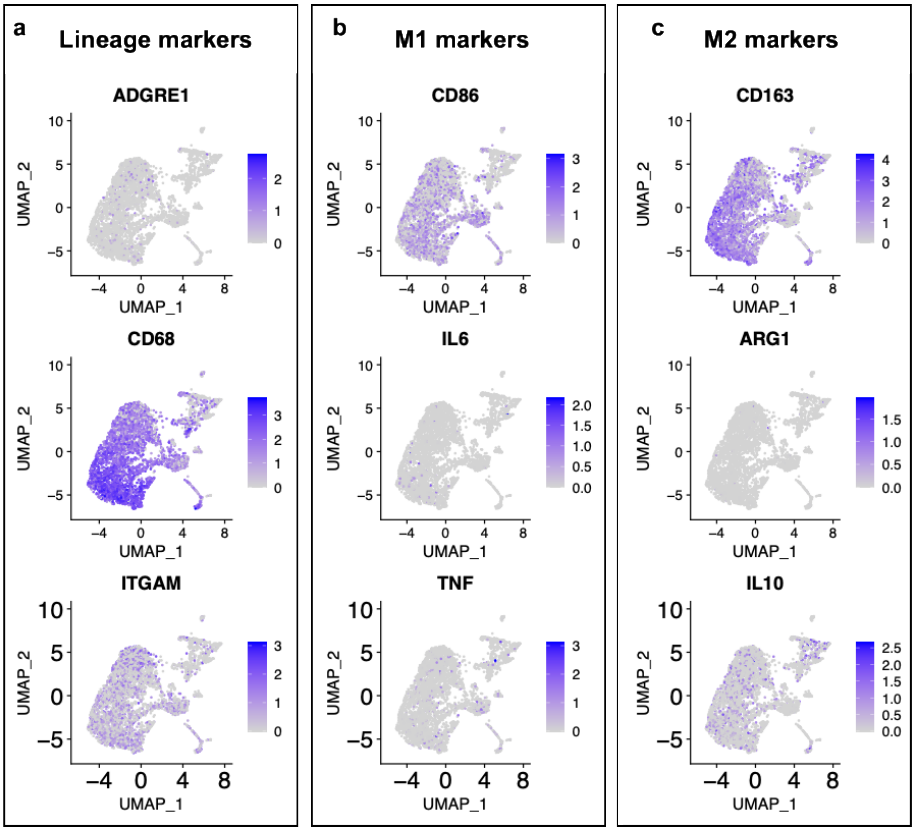

Fig. S5 Macrophage subcluster analysis using well-known markers.

Expression of macrophage lineage markers: (**a**) M1 markers (**b**), and M2 markers (**c**) by UMAP plots.

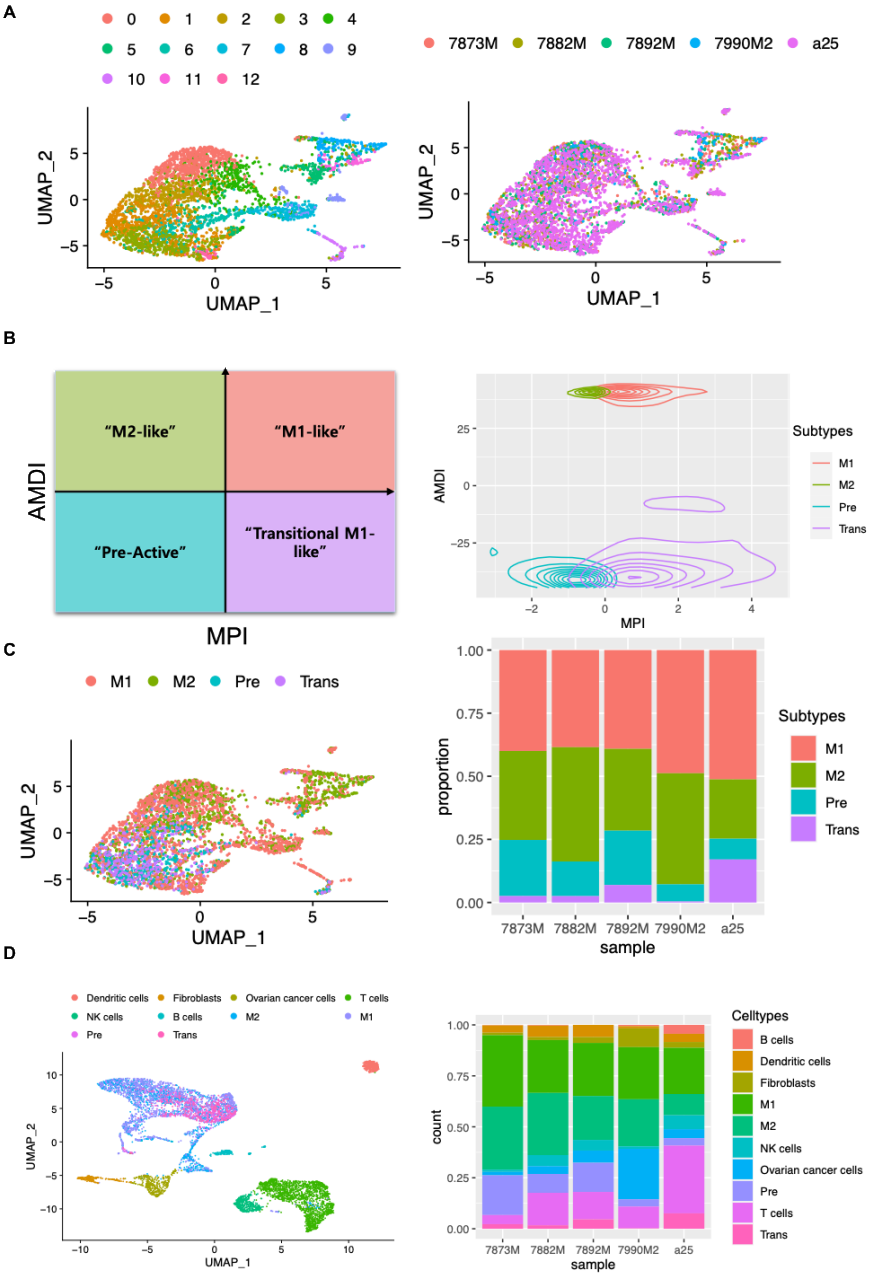
A
0 1 2 3 4
5 6 7 8 9
10 11 12
UMAP_2
UMAP_1
7873M 7882M 7892M 7990M2 a25
B
"M2-like"
"M1-like"
"Pre-Active"
"Transitional M1-like"
AMDI
MPI
Subtypes
M1
M2
Pre
Trans
C
M1 M2 Pre Trans
proportion
sample
D
Dendritic cells
Fibroblasts
Ovarian cancer cells
T cells
NK cells
B cells
M2
M1
Pre
Trans
count
Celltypes
B cells
Dendritic cells
Fibroblasts
M1
M2
NK cells
Ovarian cancer cells
Pre
T cells
Trans

Figure 18. Macrophage subtype annotation using MacSpectrum.

(A) Unsupervised clustering of macrophages (4,073 cells) of ascites from five patients (colored by patient; left panel). UMAP dimensional reduction analysis identified 13 clusters (colored by subclusters; right panel). (B) Macrophage Polarization Index (MPI)/Activation induced Macrophage Differentiation Index (AMDI) plot illustrating separation of M1 (M1-like), M2 (M2-like), Pre (Pre-active) and Trans (Transitional M1-like) macrophages by MacSpectrum. (C) Macrophages colored by subtypes (M1, M2, Pre and Trans) and displayed with UMAP (left) and proportional barplot of macrophage subtypes from 5 patient samples (right). (D) UMAP embedding macrophage subtypes with all cells, colored by cell types (left) and proportional barplot of cell types present in ascites for each patient sample (right).

Macrophage polarization status in ascites TME was further characterized using the MacSpectrum analysis tool, which allows a comprehensive analysis of multifaceted activation states of macrophages under various conditions. We have used differentially expressed gene (DEG) lists from 13 Seurat clusters (2552 genes in total) to generate a Macrophage Polarization Index (MPI) and an Activation-induced Macrophage Differentiation Index (AMDI) (Figure 18B). MacSpectrum analysis defined macrophages into four subtypes, Pre- (low MPI/low AMDI), Trans-(high MPI/low AMDI), M2- (low MPI/high AMDI) and M1- (high MPI/high AMDI) (Figure 18B, left panel). MacSpectrum defined macrophage subtypes were superimposed on a Seurat-defined UMAP plot (Figure 18C, left panel), which revealed that M1 polarized macrophages comprised the largest subtype in ascites TME followed by M2, Pre and Trans macrophages (Figure 18C, right panel).

To further characterize the macrophage subpopulation in ascites TME, we performed DEG analysis and gene set enrichment (GSEA) analysis on each macrophage subtype. The M1 macrophage cluster expressed relatively higher levels of antigen presentation genes (HLA class II genes), HLA-DPA1, HLA-DPB1, HLA-DQA1, HLA-DQB1 and classic inflammatory pathways, such as interferon-gamma, IL6 and NFkB were strongly upregulated (Figure S6A, S6B). The M2 macrophage cluster was enriched with anti-apoptotic genes, MTRNR2L1, MTRNR2L6, MTRNR2L8, MTRNR2L11, MTRNR2L12 and the Wnt/beta-catenin signaling pathway was strongly enriched (Figure S6B, S6F), which has been previously reported to promote M2 macrophage polarization (249, 250). The Pre-macrophage cluster was enriched with PI3K-Akt signaling pathway, which regulates macrophage survival, migration and proliferation (251), whereas the Trans-macrophage cluster was in an intermediate state enriched with innate immune response-related pathways, including interferon alpha, interferon gamma and complement pathways (Figure S6C, S6D, S6G, S6H). GSEA analysis of subtype-specific genes supports MacSpectrum analysis based macrophage subtype annotation and reveals the existence of unique, macrophage subtype-specific functions in ascites TME.

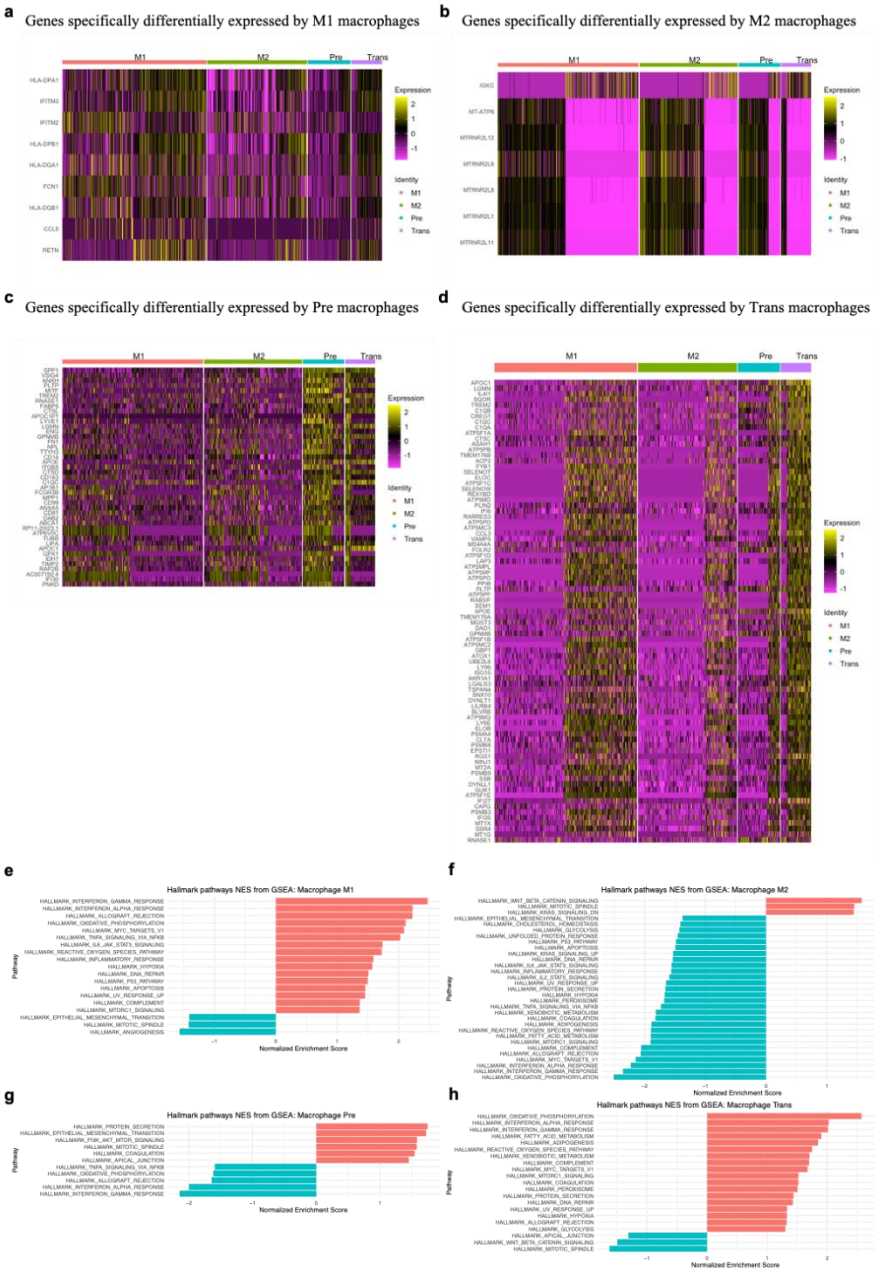
a
Genes specifically differentially expressed by M1 macrophages
b
Genes specifically differentially expressed by M2 macrophages
c
Genes specifically differentially expressed by Pre macrophages
d
Genes specifically differentially expressed by Trans macrophages
M1
M2
Pre
Trans
Expression
Identity
e
Hallmark pathways NES from GSEA: Macrophage M1
f
Hallmark pathways NES from GSEA: Macrophage M2
g
Hallmark pathways NES from GSEA: Macrophage Pre
h
Hallmark pathways NES from GSEA: Macrophage Trans
Pathway
Normalized Enrichment Score

Fig. S6 MacSpectrum annotated macrophage subtype analysis.

(**a-d)** Heatmap shows enriched genes of 4 macrophage subtypes: M1 macrophage enriched genes (**a**), M2 macrophage enriched genes (**b**), Pre-macrophage enriched genes (**c**), Trans-macrophage enriched genes (**d**). (**e-h)** Gene set enrichment analysis between macrophage subtypes using hallmark geneset. Pathway enrichment is expressed as Normalized Enrichment Score (NES), showing statistically significant pathways (FDR < 0.05).

Adaptive immune cells (T cells and B cells), innate immune cells (NK cells, dendritic cells and macrophage subtypes), fibroblasts and ovarian cancer cells were re-plotted with UMAP analysis. The proportion of each cell type was compared among the samples. Markedly higher proportion of T cells was observed in the a25 sample, while the percentage of M2 in a25 was the lowest among the samples analyzed (Figure 18D). These results that there is significant heterogeneity in the distribution of cell types in malignant ascites.

4.3.3 Comparison of molecular pathways enriched in ovarian cancer cell clusters in malignant ascites reveals intra- and inter-patient heterogeneity

We identified the intratumor-heterogeneity of ovarian cancer cells in ascites TME, showing 3 Seurat-defined subclusters (Figure 19A). We analyzed a list of putative ovarian cancer stem cell markers documented in a recent review (252). We found that all ovarian cancer cell sub-clusters showed high expression levels of CD24 and EPCAM (Figure S7), which were recently highlighted as unique markers to cancer cells with the highest sensitivity (253). Noteworthy was the low expression of other putative stem cell markers, including the most frequently used ovarian cancer biomarker, CA125 (254) and the highly documented side-population of ovarian cancer stem-like cell markers, ALDH1A1 and ABCG2 (255). These observations suggest that ovarian cancer stem-like cells are rare and highly heterogeneous at the transcript level in the malignant ascites.

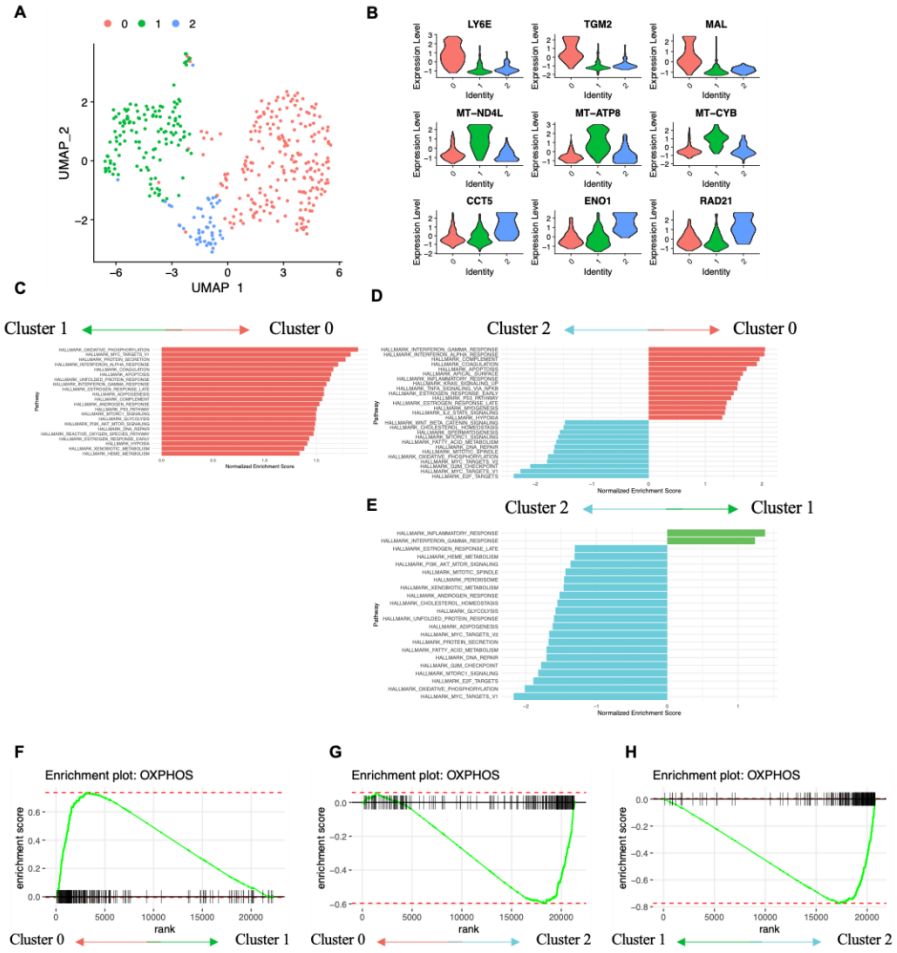
A
0 1 2
UMAP_2
UMAP_1
B
LY6E
TGM2
MAL
MT-ND4L
MT-ATP8
MT-CYB
CCT5
ENO1
RAD21
Expression Level
Identity
C
Cluster 1
Cluster 0
Normalized Enrichment Score
D
Cluster 2
Cluster 0
Normalized Enrichment Score
E
Cluster 2
Cluster 1
Normalized Enrichment Score
F
Enrichment plot: OXPHOS
enrichment score
rank
Cluster 0
Cluster 1
G
Enrichment plot: OXPHOS
enrichment score
rank
Cluster 0
Cluster 2
H
Enrichment plot: OXPHOS
enrichment score
rank
Cluster 1
Cluster 2

Figure 19. Analysis of cancer cell heterogeneity and enriched molecular pathways.

(A) Subclustering analysis of ovarian cancer cells identified 3 clusters. (B) Ovarian cancer subcluster 0 showed high expression of stem cell related genes LY6E, TGM2 and MAL, subcluster 1 showed high expression of mitochondrial genes MT-ND4L, MT-ATP8 and MT-CYB, and subcluster 2 showed high expression of CCT5, ENO1 and RAD21. (C-E) Gene set enrichment analysis between ovarian cancer cell subclusters using hallmark genesets. Pathway enrichment is expressed as Normalized Enrichment Score (NES), and the graphs display statistically significant pathways (FDR < 0.05). (F-H) Enrichment plot showing OXPHOS heterogeneity in ovarian cancer cells. (F) Enrichment plot of the gene set OXPHOS in cluster 0 vs cluster 1. (G) Enrichment plot of the gene set OXPHOS in cluster 0 vs cluster 2. (H) Enrichment plot of the gene set OXPHOS in cluster 1 vs cluster 2.

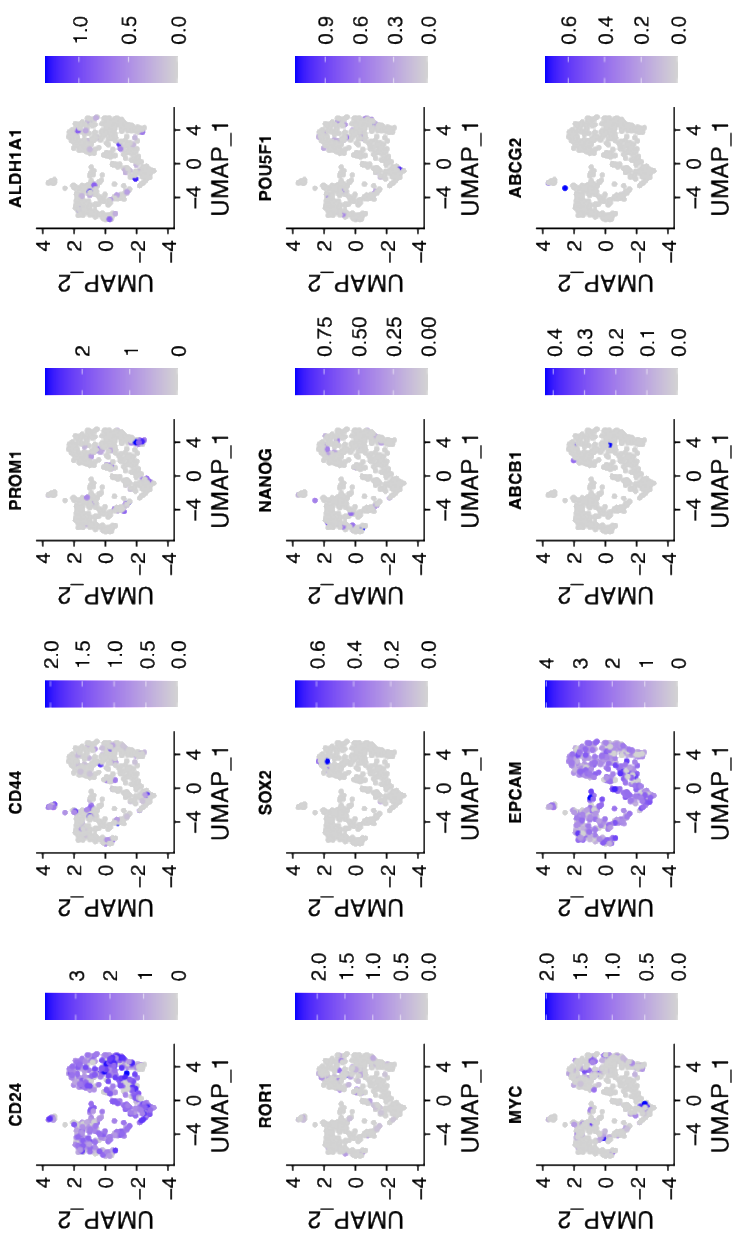

Fig. S7 UMAP plots of well-known stem cell markers expression in ovarian cancer cells.

The most differentially expressed genes between ovarian cancer cell subclusters were closely related to the self-renewal, respiration and proliferation. Subcluster 0 exhibited enrichment of many stem cell-related genes, such as LY6E, TGM2, MAL and CD55 (Figure 19B). Mitochondrial genes, for example MT-ATP8, MT-CYB, MT-ND4L, MT-ND3 and MT-ND6, are expressed throughout the majority of ovarian cancer cell subclusters, but are particularly enriched in subcluster 1 (Figure 19B and Figure S8A). Subcluster 2 expressed genes such as CCT5, HSP90AB1, PPIA and ENO1 and was transcriptionally the most unique subcluster. Hallmark gene sets were used for the analysis of pathways enriched between subclusters of ovarian cancer cells (Figure 19C-E). Ovarian cancer cell subcluster 0 showed enrichment of several metabolic pathways such as 'oxidative phosphorylation', 'unfolded protein response', 'adipogenesis', 'xenobiotic metabolism' and 'heme metabolism', when compared to the ovarian cancer cell subcluster 1 (Figure 19C, F). Additionally, we observed an enrichment of inflammation-related pathways in subcluster 0, including 'interferon gamma response', 'interferon alpha response', 'complement', 'inflammatory response', 'TNFA signaling via NFKB' and 'IL2-STAT5' signaling when compared to subcluster 2 (Figure 19D, G). Subcluster 1 exhibited enrichment of two gene sets compared to the subcluster 2, including inflammation-related signaling pathways ('inflammatory response' and 'interferon gamma response) (Figure 19E). Subcluster 2 showed relatively higher expression levels of genes related to several pathways including 'E2F targets', 'G2M checkpoint', 'MYC targets', 'oxidative phosphorylation', 'mitotic spindle', 'DNA repair', 'fatty acid metabolism' and 'MTORC1 signaling' than subcluster 0 or 1 (Figure 19D, E, G, H). Overall, GSEA analysis of ovarian cancer cell subclusters further highlighted the presence of metabolic heterogeneity in relation to oxidative phosphorylation (Figure 19C-H). These data support the presence of ovarian cancer cell subgroups, with varying degrees of disparities in metabolic programming of cancer cells.

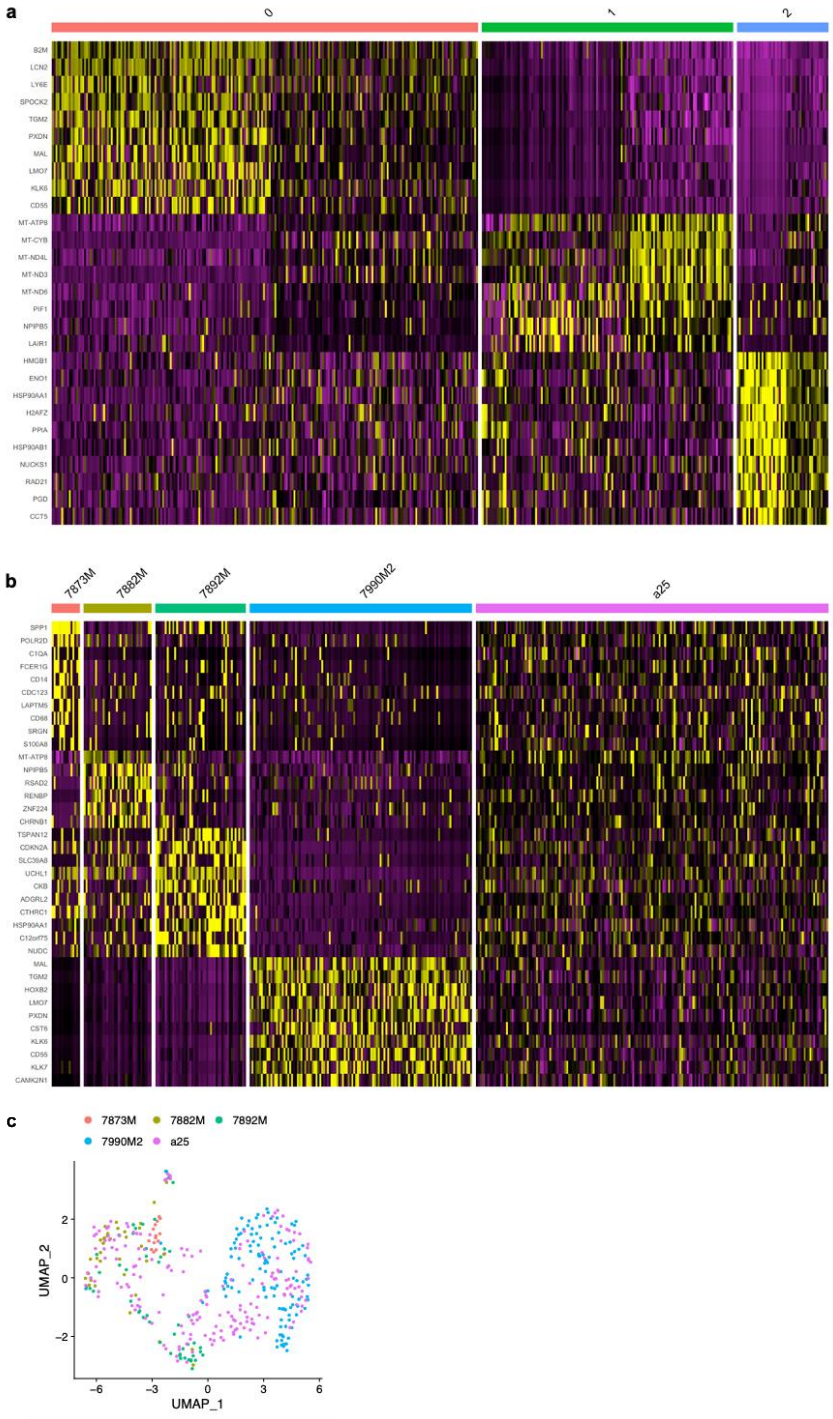
a
0
1
2
B2M
LCN2
LY6E
SPOCK2
TGM2
PXDN
MAL
LMO7
KLK8
CD55
MT-ATP8
MT-CYB
MT-ND4L
MT-ND3
MT-ND6
PIF1
NPIPB5
LAIR1
HMGB1
ENO1
HSP90AA1
H2AFZ
PPIA
HSP90AB1
NUCKS1
RAD21
PGD
CCT5
b
7873M
7882M
7892M
7990M2
a25
SPP1
POLR2D
C1QA
FCER1G
CD14
CDC123
LAPTM5
CD68
SRGN
S100A8
MT-ATP8
NPIPB5
RSAD2
RENBP
ZNF224
OHRNB1
TSPAN12
CDKN2A
SLC39A8
UCHL1
CKB
ADGRL2
CTHRC1
HSP90AA1
C12orf75
NUDC
MAL
TGM2
HOXB2
LMO7
PXDN
CST6
KLK8
CD55
KLK7
CAMK2N1
c
7873M
7882M
7892M
7990M2
a25
UMAP_2
2
0
−2
−6
−3
0
3
6
UMAP_1

Fig. S8 Heatmaps of top 10 enriched gene expression for each cluster of cells.

(a) Heatmaps for ovarian cancer cell subclusters. (**b)** UMAP plot showing ovarian cancer cell subclusters overlaid with patient samples. **(c)** Heatmaps for ovarian cancer cells in each patient sample.

Though the subclustering analysis showed a low degree of inter-patient variability among the samples we have analyzed and cluster 0 was over-represented by the sample 7990M2, there were several genes significantly upregulated in every sample (Figure S8B). To identify genes from cancer cells that vary among the ascites samples, a heatmap was generated for comprehensive visualization of differences at the transcript level (Figure S8C). Cancer cells from the 7873M sample showed enrichment of several genes related to inflammatory responses (SPP1, C1QA, FCER1G, CD14, LAPTM5, CD68, SRGN and S100A8), translation and cell cycle (CDC123) and a RNA polymerase (POLR2D). We found that the cancer cells in the 7873M sample showed higher expression of CD68 than those from other samples. As observed in the UMAP plots presenting different cell types within the ascites sample, cancer cells in the ascites samples were trancriptomically similar to macrophage populations. This may suggest the presence of trans-differentiated or macrophage-ovarian cancer hybrid-like cells in the ascites TME, reported in previous studies (256, 257). Cancer cells in 7882M sample showed enrichment of a subunit of mitochondrial ATP synthase (MT-ATP8), a nuclear pore complex gene (NPIPB5), an anti-viral gene (RSAD2), a renin inhibiting gene (RENBP), a transcription factor (ZNF224) and a gene coding for an acetylcholine receptor subunit (CHRNB1). The cancer cells from the 7892M sample showed higher expression of tumor suppressor genes CDKN2A, which codes for two proteins, p16 and p14. Along with CDKN2A, other genes enriched in the 7892M sample were a cancer-fibroblast interaction mediator (TSPAN12), a metal cation transporter gene (SLC39A8), a ubiquitin-producing gene (UCHL1), a creatine kinase (CKB), a cell adhesion gene (ADGRL2), a tissue repairing gene (CTHRC1), a chaperone (HSP90AA1), a colon carcinoma-associated gene (C12orf75) and a cytokinesis regulator (NUDC). Interestingly, the cancer cells in the 7890M2 sample, which contained the highest proportion of fibroblasts, showed increased expression of extracellular proteases, kallikreins (KLK6 and KLK7). Aside from kallikreins, genes coding for a membrane-integrated protein (MAL), an oncogenic enzyme (TGM2), a homeobox protein (HOXB2), a mediator of protein-protein interaction (LMO7), bromine metabolism

(PXDN), a cysteine protease inhibitor (CST6), a regulator of the complement system (CD55) and an inhibitor of CaMKII (CAMK2N1) were upregulated in the 7890M2 (Figure S8B). The increased kallikreins might be due to the adaptive responses of cancer cells to retain their invasiveness in the fibroblast-rich ascites TME of the sample 7890M2.

We observed that the a25 sample overlapped and spanned all three subclusters found in ovarian cancer cells (Figure S8C). The differences may reflect sampling bias due to the differences in scRNA-seq techniques used across the patient samples. The SNUH a25 sample was processed with 10X genomics, which outperforms InDrop technique in terms of sensitivity and coverage. This could also be due to the true differences between patient samples reflecting the inter-patient heterogeneity. Altogether, we observed that each patient sample harbored cancer cells expressing distinct gene that may play a role in sample-specific molecular mechanisms of cancer cell dissemination, survival and invasiveness in the ascites TME and the cancer cells from the a25 sample showed the most diverse gene expression pattern.

4.3.4 Elevated expression of ligands related to the anoikis-resistant phenotype may provide survival advantages to cancer cells in the malignant ascites

To examine cellular crosstalk between ovarian cancer cells and the niche cells in ascites TME, NichNet was used to predict the ligand-receptor pairs that could potentially induce the transcriptomic changes in ovarian cancer cells. We were interested in the anoikis resistance process, as it has been previously reported that the acquisition of anoikis resistance is a critical cellular process driving cancer progression (258). We combined two gene sets, negative regulation of programmed cell death (GO:0043069) and negative regulation of anoikis (GO:2000811) for NicheNet analysis. Potential immune cell-derived ligands included CCL5 (a chemokine involved in an inflammatory response, cancer cell migration, survival and proliferation), TNF family members TNFSF13B and LTB, and immune response genes ITGB2 and ICAM1 (Figure

20A). CCL5 was the most highly expressed ligand by T cells and NK cells (Figure 20B) and across patients (Figure S9). The top 5 potential receptors for CCL5 in ovarian cancer cells included ACKR3, LPAR2, SDC1, CDH1 and SDC4 (Figure 20C). Finally, among the potential receptors in ovarian cancer cells, SDC4 was the most highly expressed across the patient samples (Figure 20D). A circosplot shows the overall ligand-receptor links between predicted ligands from immune cells and receptors found on ovarian cancer cells, where the transparency of the inner lines represents the degree of ligand activity (Figure 4E). Expression levels of CCL5 and SDC4 were visualized using Violin plots and Feature plots (Figure 20F, G), demonstrating that the ligand CCL5 is expressed exclusively in T cells and NK cells and that the receptor SDC4 is expressed in ovarian cancer cells and fibroblasts. To evaluate CCL5-SDC4 axis, we tested our model with recently published scRNA-seq data from 6 additional ovarian cancer patient-derived ascites (GSE146026). Of those, one patient had no ovarian cancer cells and was excluded from the analysis. Intriguingly, the evaluation of CCL5 and SDC4 expression across 5 patients, further supports our identification (Figure S10A-S10C). Overall, NicheNet highlighted the CCL5-SDC4 axis as a potential mechanism for ovarian cancer cells to acquire anoikis resistance in ascites TME.

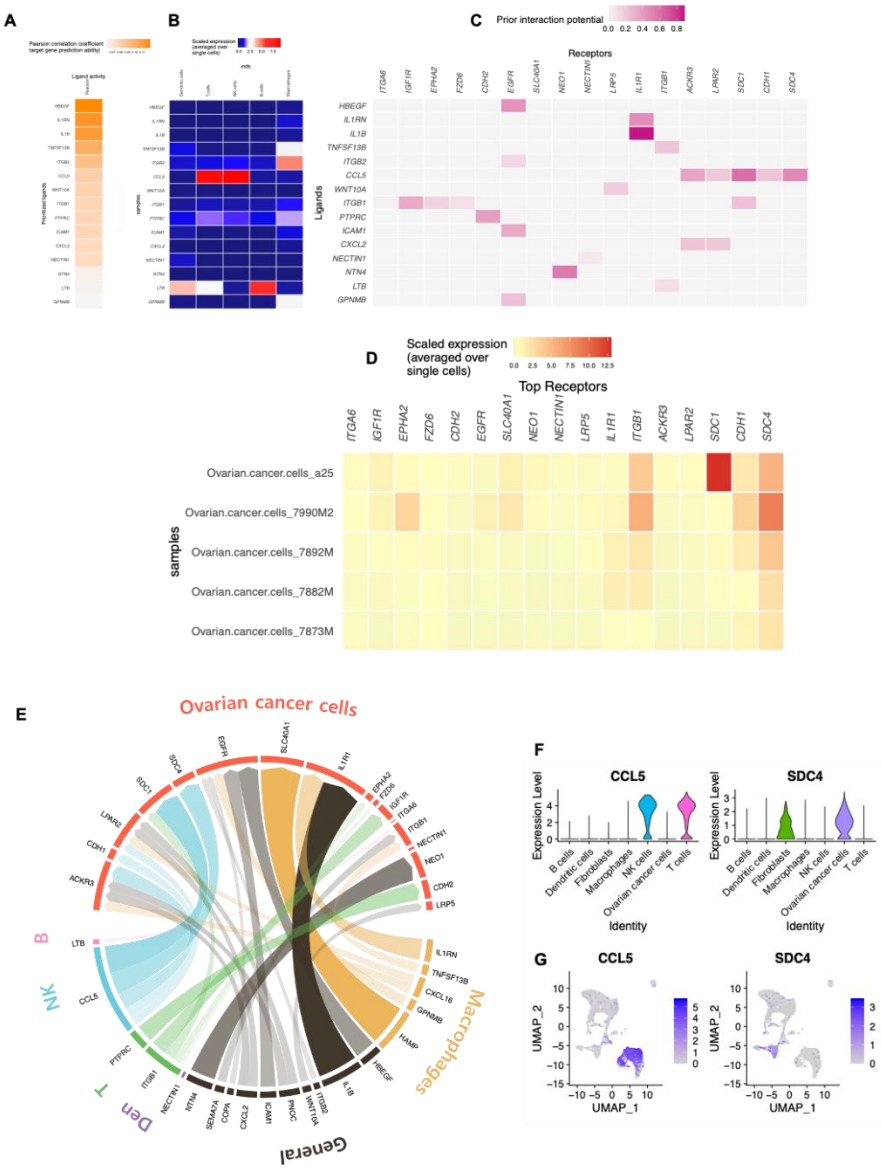
A
B
C
Prior interaction potential
Receptors
Ligands
D
Scaled expression (averaged over single cells)
Top Receptors
samples
Ovarian.cancer.cells_a25
Ovarian.cancer.cells_7990M2
Ovarian.cancer.cells_7892M
Ovarian.cancer.cells_7882M
Ovarian.cancer.cells_7873M
E
Ovarian cancer cells
Macrophages
NK
B
T
Dendritic
General
F
CCL5
SDC4
Expression Level
Identity
B cells
Dendritic cells
Fibroblasts
Macrophages
NK cells
Ovarian cancer cells
T cells
G
UMAP_1
UMAP_2

Figure 20. CCL5 - SDC4 axis serve as a potential upstream ligand-receptor signal inducing anoikis resistance in ovarian cancer cells.

(A, B) NicheNet analysis of ligand-receptor pairs inducing the anoikis resistance in ovarian cancer. Ligand activity analysis (A) Average expression of the ligands (B) by the different immune cell types. (C) Receptors of prioritized ligands expressed by ovarian cancer cells. (D) Average expression of potential receptors in ovarian cancer cells across patient samples. (E) Circos plot showing links between predicted ligands from immune cell types with their associated receptors found on ovarian cancer cells. The degree of transparency indicates the prior interaction weight of the ligand-receptor interaction. (F,G) Expression of CCL5 and SDC4 in cellular components of ascites TME visualized by (F) Violin plots and (G) Feature plots.

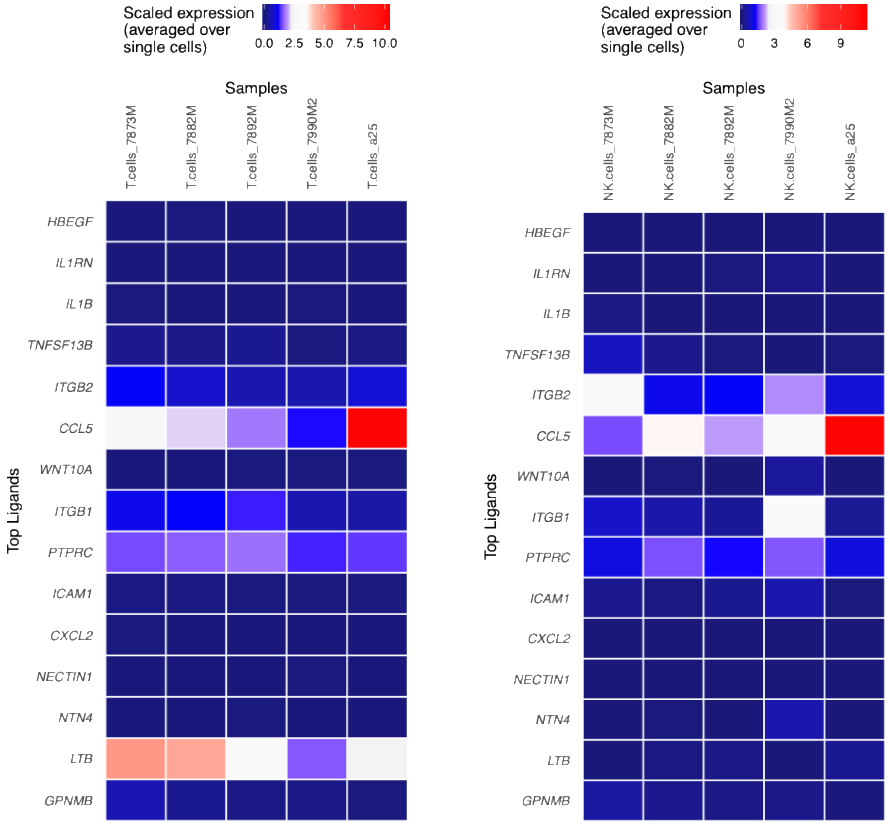

Fig. S9 Heatmap showing average expression of the upstream ligands inducing anoikis resistance in ovarian cancer cells (shown in Fig. 20) in T cells (left) and NK cells (right) across patient samples.

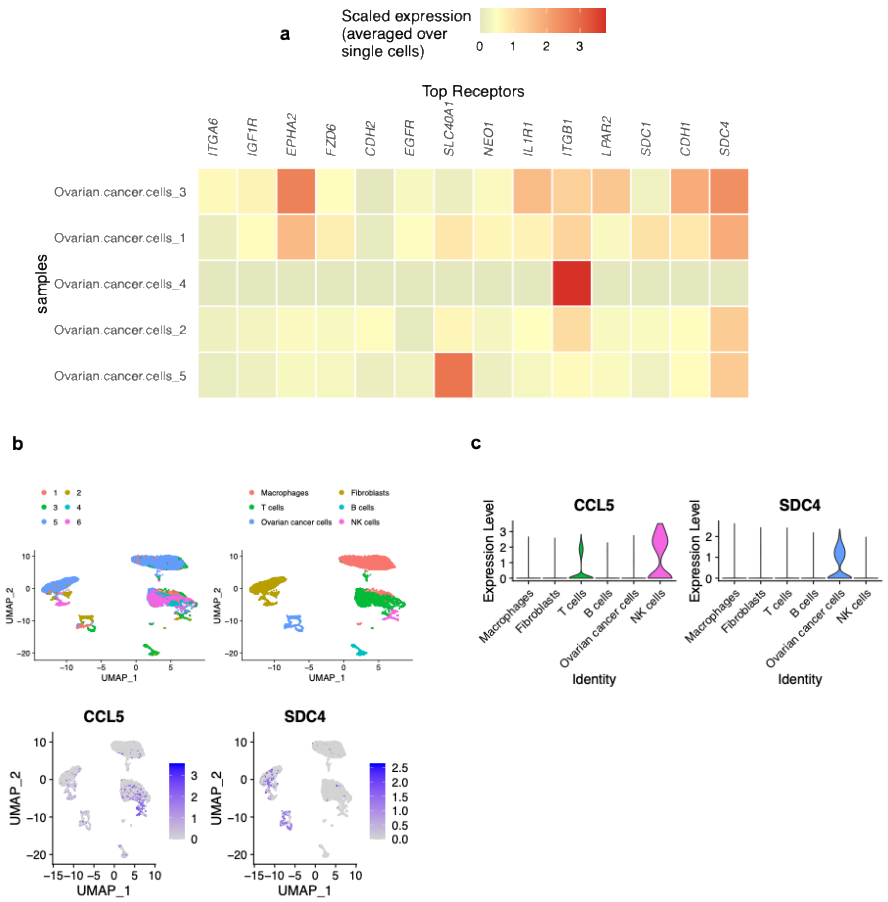
a
Scaled expression (averaged over single cells)
0 1 2 3
Top Receptors
ITGA6
IGF1R
EPHA2
FZD6
CDH2
EGFR
SLC40A1
NEO1
IL1R1
ITGB1
LPAR2
SDC1
CDH1
SDC4
samples
Ovarian.cancer.cells_3
Ovarian.cancer.cells_1
Ovarian.cancer.cells_4
Ovarian.cancer.cells_2
Ovarian.cancer.cells_5
b
1 2 3 4 5 6
Macrophages
Fibroblasts
T cells
B cells
Ovarian cancer cells
NK cells
UMAP_1
UMAP_2
CCL5
SDC4
c
CCL5
SDC4
Expression Level
Macrophages
Fibroblasts
T cells
B cells
Ovarian cancer cells
NK cells
Identity

Fig. S10 CCL5-SDC4 axis in malignant ascites TME (additional ovarian cancer patient-derived ascites single cell RNA seq datasets were downloaded from GSE146026).

(**a)** Average expression of NicheNet predicted receptors from Figure 4 were compared across the patient samples. (**b, c)** Ascites cellular components shown in UMAP plots with patient sample IDs (**b**, upper left panel) and cell types (**b**, upper right panel). CCL5 and SDC4 expressions visualized by Feature plots (**b**, bottom panels) and Violin plots (**c**).

4.3.5 Effector and exhausted CD8+ T cells and NK cells highly express CCL5 in the malignant ascites

To examine the complexity of T cell and NK cell subsets found in ascites TME, each cell types were re-clustered, and 5 and 3 Seurat defined clusters were identified in T cell and NK cell populations, respectively (Figure 21A and Figure S11A). Expression profiles were similar across subclusters in both T cell and NK cell (Figure 21A and Figure S11B). Interestingly, co-expression analysis of CD4 and CD8A with CCL5 in T cell subsets revealed that cluster 0 and 1 are CD8+ T cell with high CCL5 co-expression, whereas clusters 2 and 3 are CD4+ T cell with low CCL5 co-expression (Figure 21C, D). T cell subsets were further characterized by functional markers reported in a recent study (259). Expression profiles of T cell subclusters revealed that subcluster 0 is CD8+ effector T cell cluster, with high expression of cytokines and effector molecules, GZMA, GNLY, PRFA, GZMB, GZMK, NKG7. Whereas, subcluster 1 is CD8+ exhausted T cell cluster, with exhaustion marker expression, LAG3, TIGIT, PDCD1 and HAVCR213 (Figure 21E). NK cell subsets analysis show that all subclusters highly express KLRB1 with high CCL5 co-expression (Figure S11C). These results suggest that CCL5 is exclusively expressed in effector and exhausted CD8+ T cell subsets and NK cells in malignant ascites TME.

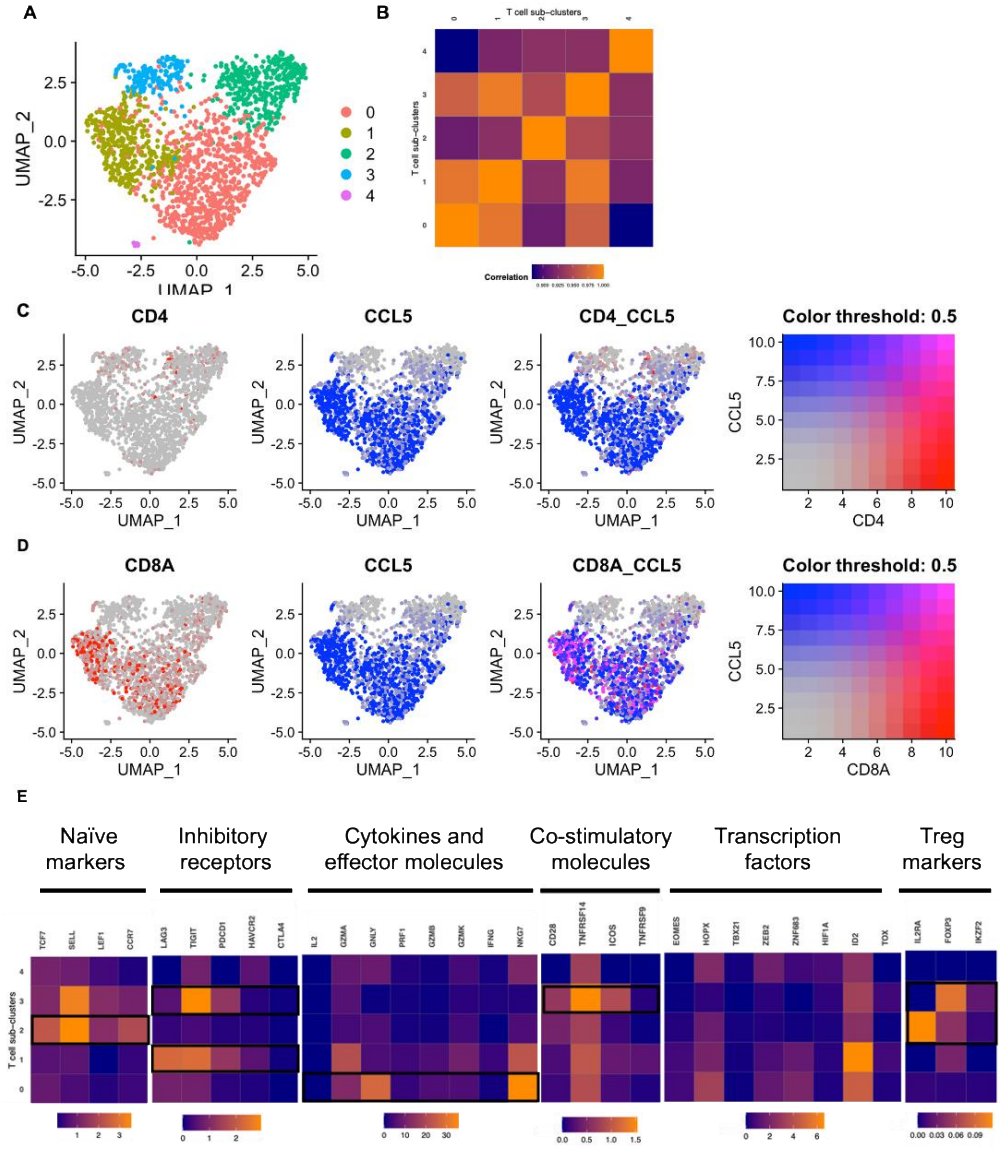
A
UMAP_2
UMAP_1
0
1
2
3
4
B
T cell sub−clusters
Correlation
C
CD4
CCL5
CD4_CCL5
Color threshold: 0.5
CCL5
CD4
D
CD8A
CCL5
CD8A_CCL5
Color threshold: 0.5
CCL5
CD8A
E
Naïve markers
Inhibitory receptors
Cytokines and effector molecules
Co-stimulatory molecules
Transcription factors
Treg markers
TCF7
SELL
LEF1
CCR7
LAG3
TIGIT
PDCD1
HAVCR2
CTLA4
IL2
GZMA
GNLY
PRF1
GZMB
GZMK
IFNG
NKG7
CD28
TNFRSF14
ICOS
TNFRSF9
EOMES
HOPX
TBX21
ZEB2
ZNF683
HIF1A
ID2
TOX
IL2RA
FOXP3
IKZF2
T cell sub−clusters

Figure 21. Clustering T cell subsets in ascites TME.

(A) The UMAP projection of T cell subclusters identified 5 clusters (colored by subclusters). (B) Expression profiles were examined by Pearson correlation coefficient between the mean profiles of T cell subclusters. (C-D) Co-expression of CCL5 with CD4 (C) and CD8A (D) in T cell subclusters visualized by Feature plots. (E) Heatmap showing mean expression of T cell function associated genes in each T cell subclusters. Black boxes highlight the prominent patterns used to define T cell subsets.

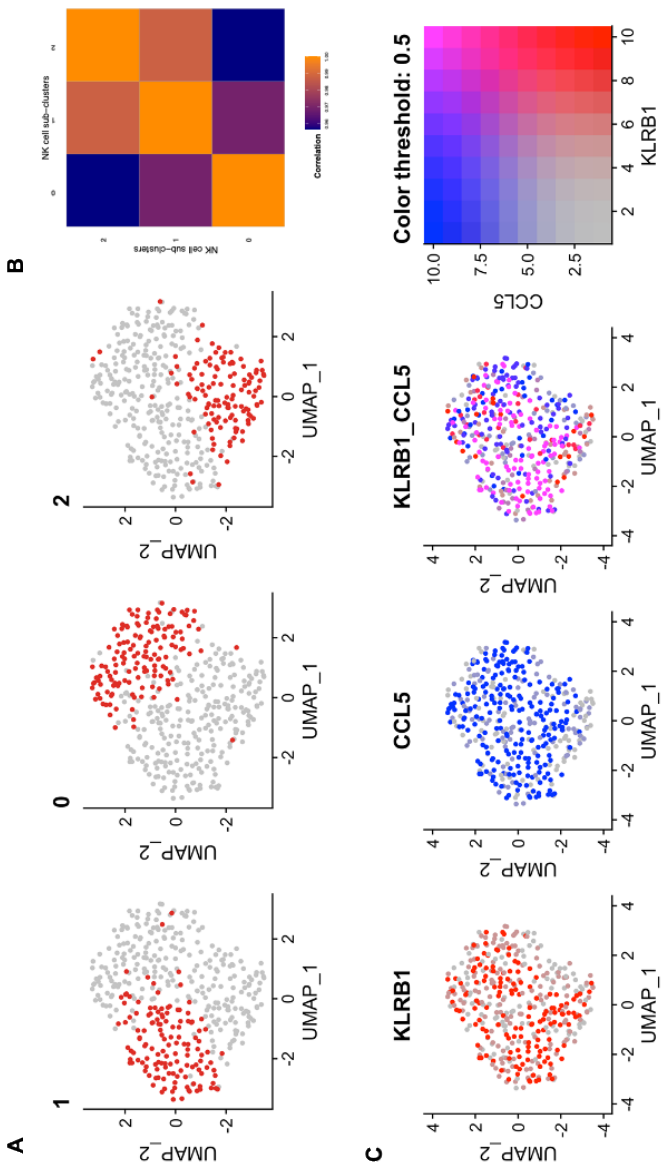

Fig. S11 NK cell subtype analysis.

(a) The UMAP projection of NK cell subclusters identified 3 sub clusters. (b) Expression profiles were examined by Pearson correlation coefficient between the mean profiles of NK cell subclusters. (c) KLRB1 and CCL5 expression in the NK cell subset.

4.3.6 SDC4 expression correlates with poor prognosis in ovarian cancer patients

We next assessed the prognostic value of SDC4 in ovarian cancer patients. Using datasets from TCGA, the patients were divided into two groups according to SDC4 (also known as SYDN4) expression. High expression levels of SDC4 was associated with significantly poor overall survival (OS) in ovarian cancer patients (Figure 22A). For further validation, we additionally analyzed GEO datasets (GSE9891, GSE3149, GSE26193 and GSE63885). Kaplan-Meier and log rank test analysis with GEO datasets also suggested that the SDC4 expression level was negatively correlated with OS in ovarian cancer patients (Figure 22B-E. In addition, we compared expressions of SDC4 at the transcript level in cancer and normal tissues, and we found significantly elevated transcript levels of SDC4 in ovarian cancer tissues (Figure 22F). Moreover, the SDC4 expression increased across the tumor stage (Figure 22G).

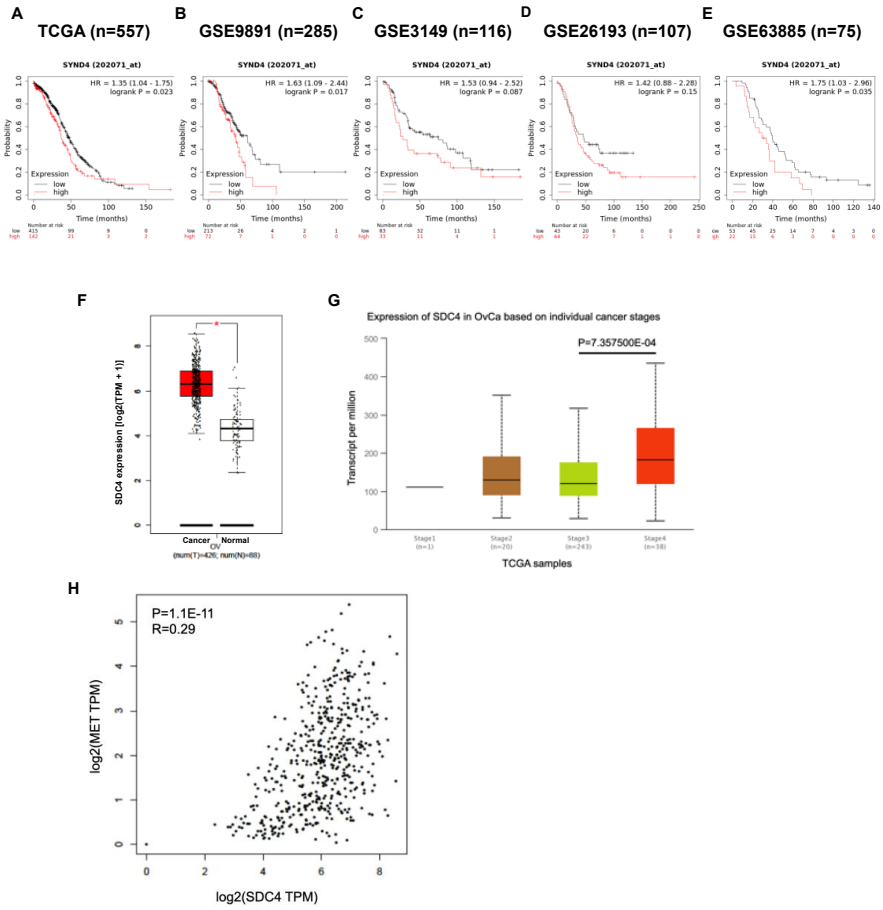
A
TCGA (n=557)
B
GSE9891 (n=285)
C
GSE3149 (n=116)
D
GSE26193 (n=107)
E
GSE63885 (n=75)
SYND4 (202071_at)
HR = 1.35 (1.04 - 1.75)
logrank P = 0.023
HR = 1.63 (1.09 - 2.44)
logrank P = 0.017
HR = 1.53 (0.94 - 2.52)
logrank P = 0.087
HR = 1.42 (0.88 - 2.28)
logrank P = 0.15
HR = 1.75 (1.03 - 2.96)
logrank P = 0.035
Probability
Expression
low
high
Time (months)
Number at risk
F
SDC4 expression [log2(TPM + 1)]
Cancer
Normal
OV
(num(T)=426; num(N)=88)
G
Expression of SDC4 in OvCa based on individual cancer stages
P=7.357500E-04
Transcript per million
Stage1
(n=1)
Stage2
(n=20)
Stage3
(n=243)
Stage4
(n=38)
TCGA samples
H
P=1.1E-11
R=0.29
log2(MET TPM)
log2(SDC4 TPM)

Figure 22. SDC4 expression is associated with survival of ovarian cancer patient.

(A-E) Higher expression of SDC4 was associated with poor overall survival of ovarian cancer patients. Ovarian cancer public datasets from (A) TCGA and (B-E) GEO database were used to examine the association between SDC4 expression level and overall survival of the patients. Kaplan-Meier survival curves were plotted by splitting patients into two groups (SDC4 high and SDC4 low). Groups were divided by 'split patients by' option set at 'auto select best cutoff'. The Kaplan-Meier plotter (KM plotter) tool was used. (F) The expression of SDC4 was elevated in ovarian cancer tissues compared to the normal tissues. TCGA and GTEx expression data were analyzed using GEPIA. (G) The SDC4 expression is significantly upregulated in the cancer tissues from stage IV patients. UALCAN was used to analyze the association of stage with SDC4 expression. (H) A Significant positive correlation was found between MET and SDC4. The correlation between mRNA expression levels of MET and SDC4 was analyzed with GEPIA using data from TCGA and GTEx database.

To examine the involvement of SDC4 in the anoikis resistance of ovarian cancer cells in the malignant ascites, we investigated a correlation between the average SDC4 expression and the proportion of cancer cells in each sample. Intriguingly, the proportion of cancer cells in the ascites TME positively correlates with average SDC4 expression (Figure S12A). This may imply that SDC4 expression could be vital for cancer cell survival in the ascites. cMet has often been cited in the literature as a key regulator of anoikis resistance in ovarian cancer (260). We observed that SDC4 is positively correlated with MET expression both in the tissue samples from TCGA and GTEx and in the malignant ascites-derived cancer cells (Figure 22H and Figure S12B), further supporting our hypothesis that the expression of SDC4 in ovarian cancer cells may promote cancer progression.

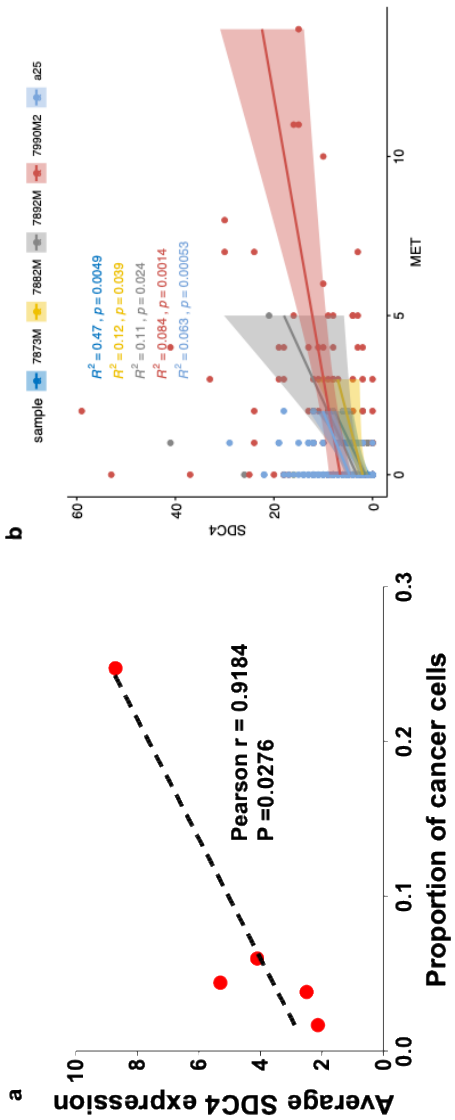

Fig. S12 SDC4 may be associated with cancer cell survival of ovarian cancer cells in the malignant ascites.

(**a**) Pearson correlation coefficient between the average SDC4 expression in ovarian cancer cells versus proportion of cancer cells within the ascites TME. (**b**) Pearson correlation coefficient between MET and SDC4 expression across patient samples at single cell level.

4.4 Discussion

The current study uncovered inter- and intra-patient heterogeneity of ovarian cancer and captured the landscape of both immune and non-immune cells enriched in ascites TME, using scRNA-seq combined with a computational approach. We determined a ligand-receptor intercellular communication model by analysis of a putative ligand-receptor interactions between receptors enriched in ovarian cancer cells and ligands expressed by immune cells in ascites TME. Although our computational model does not consider the spatial proximity between the cells of interest, ascites from ovarian cancer patients creates a unique TME as a reservoir of pro-tumorigenic soluble factors including CCL5 and other cytokines reported in our previous work (233). In this study, we found that CCL5-SDC4 axis may play a crucial role in ovarian cancer cell survival and poor patient prognosis. To validate our model, we analyzed the recently published scRNA-seq study of malignant ascites from patients with advanced-stage ovarian cancer (261). Also this analysis highlighted the putative role of intercellular communication through CCL5-SDC4 axis in immune cells and ovarian cancer cells (Figure 4). Moreover, TCGA and GEO analysis further supports the role of SDC4 in ovarian cancer progression (Figure 6).

Among immune cell-related clusters, we observed a highly heterogeneous macrophage population at the transcriptomic level, but we found that only subtle differences in macrophage subtype proportions exist across the five malignant ascites samples analyzed. Previous studies report the differential role of M1 and M2 macrophage subtypes in ovarian cancer progression. M2 subtypes has received the most attention in cancer biology due to their pro-tumorigenic role including stemness maintenance, promoting the chemoresistance and invasiveness in a number of cancer models, including ovarian cancer (250). The prognostic role of M1 subtypes in ovarian cancer show conflicting results. Our group reported a pro-tumorigenic role of in vitro polarized M1 macrophages in ovarian cancer (262). Similar results were also reported in in vitro studies of hepatocellular and bladder cancer (263). In

contrast, a plentiful number of reports suggest an anti-tumorigenic role of M1 macrophages in ovarian cancer (264, 265).

A recent study observed the prevalence of both M1 and M2 macrophages in ovarian cancer patient-derived ascites TME. The authors noted that the ratio of these subtypes are important, where a higher M1/M2 macrophage ratio was correlated with a higher overall survival and progression-free survival (260). An earlier study reported that platinum-based chemotherapy increases ovarian cancer cell potency to induce M2 macrophage polarization, resulting in an imbalance in macrophage subtypes in the TME (266). In a murine model, the re-balancing of macrophage subtypes toward M1 in the TME decreased tumor burden and prolonged survival (265). These results suggest that macrophage subtypes may have a stage-specific role and the balance of macrophage subtypes may play a crucial role in cancer progression. Future longitudinal studies of single-cell profiling of macrophage subtypes will give us a more definitive understanding of their role in ovarian cancer progression.

We showed molecular heterogeneity of T cell and NK cell population (Figure 5 and Figure S7A-C). As presented in figure 2D, the proportion of T cells was higher in the a25 sample than that in the other four patient samples. However, there is a possibility that difference may be due to the sample preparation method or clinical parameters of patients (e.g., treatment status, histology, etc.). Further investigation on the association between clinical parameters and the cellular constituents is warranted to understand the complex cellular interactions taking place in the malignant ascites niche.

Anoikis resistance is a primary feature of ovarian cancer cells to survive in ascites TME. We hypothesize that niche signals from ascites TME regulate or induce anoikis resistance in ovarian cancer cells. Though macrophages have received the most attention in cancer progression due to their abundance, our prediction model highlights the potential role of T cells and NK cells in anoikis resistance in ascites TME. Since we have only focused on this single process, the various roles of macrophages may have been underrepresented in our analysis. We observed the global overexpression of SDC4, a known receptor of CCL5, in ovarian cancer cells from all samples analyzed at the single cell level

(Figure 4C). SDC4 is a heparan sulfate proteoglycan that modulates focal adhesion and has been implicated in cancer progression and metastasis (267). Elevated SDC4 expression has been reported in hepatocellular cancer and mesotheliomas (268, 269). Previous ovarian cancer study observed that SDC4 is expressed in normal ovary and in both benign and malignant ovarian tumors (270). CCL5 is elevated in various types of cancers, including ovarian cancer(271). It has been shown that binding of CCL5 to SDC4 induces activation of PKCα (272, 273), which is involved in multiple pathways including cell cycle progression, tumorigenesis and metastatic dissemination (274), but the mechanistic role of SDC4-CCL5 in ovarian cancer progression remains poorly understood.

Given that CCL5 is enriched in T cells and NK cells in ascites TME and that SDC4 expression is restricted to ovarian cancer cells in our scRNA-seq data (Figure 4C), the aberrant levels of CCL5 in ascites TME is the critical determinant of ovarian cancer progression and poor prognosis. The expression of SDC4 in ovarian cancer cells was strongly correlated with the proportion of cancer cells found in ascites TME as well as with MET expression at single-cell level (Figure S8). Furthermore, TCGA and GEO data suggest that SDC4 is expressed in ovarian cancer cells and correlates with poor overall survival in ovarian cancer patients (Figure 6).

scRNA-seq has revolutionized our approach to understanding cancer progression. We have utilized this powerful technique, modeling the pathological mechanisms underlying ovarian cancer progression. Despite these findings, a number of challenges and limitations still remain in our model. We had limited access to patient information (e.g., survival status, stage, prognosis, treatment, histology, etc.), small sample size and sample processing bias (filtered tumor spheroids/clusters, our procedure enriched cancer cells and lymphocytes, and scRNA-seq targeted low total cell reads). Profiling a larger number of cancer cells with multiple samples in parallel would be required to validate the presence of inter-tumoral heterogeneity and to identify rare cancer stem cell populations. In addition, longitudinal sampling of the cancer cells over the course of treatment could facilitate our understanding of tumor

evolution and chemoresistance.

In summary, our study showed heterogeneous molecular programming of the various cells isolated from malignant ascites. Through the ligand-receptor interaction analysis between immune and cancer cells, we revealed that CCL5-SDC4 interaction is enriched. Survival analysis suggests that higher SDC4 expression is associated with poor prognosis in ovarian cancer patients. We also observed a strong positive correlation between SDC4 expression and the percentage of cancer cells in the malignant ascites. Thus we suggest CCL5-SDC4 interaction could be the vital signaling for cancer cell survival in the ovarian cancer TME.

5. References

1. W. X. Zong, J. D. Rabinowitz, E. White, Mitochondria and Cancer. *Molecular cell* **61**, 667-676 (2016).
2. S. L. Archer Mitochondrial Dynamics — Mitochondrial Fission and Fusion in Human Diseases. *New England Journal of Medicine* **369**, 2236-2251 (2013).
3. G. F. Bahr, E. Zeitler, Study of mitochondria in rat liver. Quantitative electron microscopy. *The Journal of cell biology* **15**, 489-501 (1962).
4. D. Hanahan, R. A. Weinberg, Hallmarks of cancer: the next generation. *Cell* **144**, 646-674 (2011).
5. S. Gururaja Rao, Mitochondrial Changes in Cancer. *Handbook of experimental pharmacology* **240**, 211-227 (2017).
6. R. J. DeBerardinis, N. S. Chandel, Fundamentals of cancer metabolism. *Science Advances* **2** (2016).
7. E. Q. Toyama *et al.*, Metabolism. AMP-activated protein kinase mediates mitochondrial fission in response to energy stress. *Science (New York, N.Y.)* **351**, 275-281 (2016).
8. S. H. Ko *et al.*, Succinate promotes stem cell migration through the GPR91-dependent regulation of DRP1-mediated mitochondrial fission. *Scientific reports* **7**, 12582 (2017).
9. D. Anastasiou, Tumour microenvironment factors shaping the cancer metabolism landscape. *British Journal Of Cancer* **116**, 277 (2016).
10. M. Liesa, M. Palacin, A. Zorzano, Mitochondrial dynamics in mammalian health and disease. *Physiological reviews* **89**, 799-845 (2009).
11. C. A. Mannella, W. J. Lederer, M. S. Jafri, The connection between inner membrane topology and mitochondrial function. *Journal of molecular and cellular cardiology* **62**, 51-57 (2013).
12. H. F. Jheng *et al.*, Mitochondrial fission contributes to mitochondrial dysfunction and insulin resistance in skeletal muscle. *Molecular and cellular biology* **32**, 309-319 (2012).
13. S. Cogliati *et al.*, Mitochondrial cristae shape determines respiratory chain supercomplexes assembly and respiratory efficiency. *Cell* **155**, 160-171 (2013).
14. L. L. Lackner, Shaping the dynamic mitochondrial network. *BMC Biology* **12**, 35 (2014).
15. J. Prudent, Heidi M. McBride, Mitochondrial Dynamics: ER Actin Tightens the Drp1 Noose. *Current Biology* **26**, R207-R209.
16. F. Korobova, V. Ramabhadran, H. N. Higgs, An actin-dependent step in mitochondrial fission mediated by the ER-associated formin INF2. *Science (New York, N.Y.)* **339**, 464-467 (2013).
17. U. Manor *et al.*, A mitochondria-anchored isoform of the actin-nucleating spire protein regulates mitochondrial division. *eLife* **4**

(2015).
18. K. Rehklau *et al.*, Cofilin1-dependent actin dynamics control DRP1-mediated mitochondrial fission. *Cell death & disease* **8**, e3063 (2017).
19. K. Arasaki *et al.*, A role for the ancient SNARE syntaxin 17 in regulating mitochondrial division. *Developmental cell* **32**, 304-317 (2015).
20. K. Onoue *et al.*, Fis1 acts as a mitochondrial recruitment factor for TBC1D15 that is involved in regulation of mitochondrial morphology. *Journal of cell science* **126**, 176 (2013).
21. H. Otera *et al.*, Mff is an essential factor for mitochondrial recruitment of Drp1 during mitochondrial fission in mammalian cells. *The Journal of cell biology* **191**, 1141 (2010).
22. H. Otera, N. Miyata, O. Kuge, K. Mihara, Drp1-dependent mitochondrial fission via MiD49/51 is essential for apoptotic cristae remodeling. *The Journal of cell biology* (2016).
23. R. Yu *et al.*, MIEF1/2 function as adaptors to recruit Drp1 to mitochondria and regulate the association of Drp1 with Mff. *Scientific reports* **7**, 880 (2017).
24. S. Fan *et al.*, Mitochondrial fission determines cisplatin sensitivity in tongue squamous cell carcinoma through the BRCA1-miR-593-5p-MFF axis. *Oncotarget* **6**, 14885-14904 (2015).
25. J. Zhao *et al.*, Human MIEF1 recruits Drp1 to mitochondrial outer membranes and promotes mitochondrial fusion rather than fission. *Embo j* **30**, 2762-2778 (2011).
26. R. Liu, D. C. Chan, The mitochondrial fission receptor Mff selectively recruits oligomerized Drp1. *Mol Biol Cell* **26**, 4466-4477 (2015).
27. R. Ramachandran, Mitochondrial dynamics: The dynamin superfamily and execution by collusion. *Seminars in cell & developmental biology* 10.1016/j.semcdb.2017.07.039 (2017).
28. C. A. Francy, R. W. Clinton, C. Fröhlich, C. Murphy, J. A. Mears, Cryo-EM Studies of Drp1 Reveal Cardiolipin Interactions that Activate the Helical Oligomer. *Scientific reports* **7**, 10744 (2017).
29. P. J. Macdonald *et al.*, A dimeric equilibrium intermediate nucleates Drp1 reassembly on mitochondrial membranes for fission. *Mol Biol Cell* **25**, 1905-1915 (2014).
30. A. Pagliuso, P. Cossart, F. Stavru, The ever-growing complexity of the mitochondrial fission machinery. *Cellular and molecular life sciences : CMLS* 10.1007/s00018-017-2603-0 (2017).
31. K. Basu *et al.*, Molecular mechanism of DRP1 assembly studied in vitro by cryo-electron microscopy. *PloS one* **12**, e0179397 (2017).
32. R. Okada *et al.*, Activation of the Small G Protein Arf6 by Dynamin2 through Guanine Nucleotide Exchange Factors in Endocytosis. *Scientific reports* **5**, 14919 (2015).

33. J. E. Lee, L. M. Westrate, H. Wu, C. Page, G. K. Voeltz, Multiple dynamin family members collaborate to drive mitochondrial division. *Nature* **540**, 139-143 (2016).
34. B. Cho, S. Y. Choi, H. M. Cho, H. J. Kim, W. Sun, Physiological and pathological significance of dynamin-related protein 1 (drp1)-dependent mitochondrial fission in the nervous system. *Experimental neurobiology* **22**, 149-157 (2013).
35. X. Qi, M. H. Disatnik, N. Shen, R. A. Sobel, D. Mochly-Rosen, Aberrant mitochondrial fission in neurons induced by protein kinase C{delta} under oxidative stress conditions in vivo. *Mol Biol Cell* **22**, 256-265 (2011).
36. N. Taguchi, N. Ishihara, A. Jofuku, T. Oka, K. Mihara, Mitotic phosphorylation of dynamin-related GTPase Drp1 participates in mitochondrial fission. *The Journal of biological chemistry* **282**, 11521-11529 (2007).
37. T. Bae *et al.*, Restoration of paclitaxel resistance by CDK1 intervention in drug-resistant ovarian cancer. *Carcinogenesis* **36**, 1561-1571 (2015).
38. J. Cai *et al.*, ERK/Drp1-dependent mitochondrial fission is involved in the MSC-induced drug resistance of T-cell acute lymphoblastic leukemia cells. *Cell death & disease* **7**, e2459 (2016).
39. L. Y. Chung *et al.*, Galectin-1 promotes lung cancer progression and chemoresistance by upregulating p38 MAPK, ERK, and cyclooxygenase-2. *Clinical cancer research : an official journal of the American Association for Cancer Research* **18**, 4037-4047 (2012).
40. B. Cho *et al.*, CDK5-dependent inhibitory phosphorylation of Drp1 during neuronal maturation. *Experimental & molecular medicine* **46**, e105 (2014).
41. M. M. Mandl *et al.*, Inhibition of Cdk5 induces cell death of tumor-initiating cells. *Br J Cancer* **116**, 912-922 (2017).
42. C. H. Chou *et al.*, GSK3beta-mediated Drp1 phosphorylation induced elongated mitochondrial morphology against oxidative stress. *PloS one* **7**, e49112 (2012).
43. X. J. Han *et al.*, CaM kinase I alpha-induced phosphorylation of Drp1 regulates mitochondrial morphology. *The Journal of cell biology* **182**, 573-585 (2008).
44. W. Wang *et al.*, Mitochondrial fission triggered by hyperglycemia is mediated by ROCK1 activation in podocytes and endothelial cells. *Cell metabolism* **15**, 186-200 (2012).
45. J. D. Wikstrom *et al.*, AMPK regulates ER morphology and function in stressed pancreatic beta-cells via phosphorylation of DRP1. *Molecular endocrinology (Baltimore, Md.)* **27**, 1706-1723 (2013).
46. S. Din *et al.*, Pim-1 preserves mitochondrial morphology by

inhibiting dynamin-related protein 1 translocation. *Proceedings of the National Academy of Sciences* **110**, 5969-5974 (2013).
47. C. R. Chang, C. Blackstone, Dynamic regulation of mitochondrial fission through modification of the dynamin-related protein Drp1. *Annals of the New York Academy of Sciences* **1201**, 34-39 (2010).
48. G. M. Cereghetti *et al.*, Dephosphorylation by calcineurin regulates translocation of Drp1 to mitochondria. *Proceedings of the National Academy of Sciences of the United States of America* **105**, 15803-15808 (2008).
49. C. Guo, K. A. Wilkinson, A. J. Evans, P. P. Rubin, J. M. Henley, SENP3-mediated deSUMOylation of Drp1 facilitates interaction with Mff to promote cell death. *Scientific reports* **7**, 43811 (2017).
50. Z. Zhou *et al.*, SUMOylation and SENP3 regulate STAT3 activation in head and neck cancer. *Oncogene* **35**, 5826-5838 (2016).
51. J. Prudent *et al.*, MAPL SUMOylation of Drp1 Stabilizes an ER/Mitochondrial Platform Required for Cell Death. *Molecular cell* **59**, 941-955.
52. D.-H. Cho *et al.*, S-Nitrosylation of Drp1 Mediates β-Amyloid-Related Mitochondrial Fission and Neuronal Injury. *Science (New York, N.Y.)* **324**, 102 (2009).
53. T. Gawlowski *et al.*, Modulation of dynamin-related protein 1 (DRP1) function by increased O-linked-beta-N-acetylglucosamine modification (O-GlcNAc) in cardiac myocytes. *The Journal of biological chemistry* **287**, 30024-30034 (2012).
54. A. Franco *et al.*, Correcting mitochondrial fusion by manipulating mitofusin conformations. *Nature* **540**, 74-79 (2016).
55. Y. L. Cao *et al.*, MFN1 structures reveal nucleotide-triggered dimerization critical for mitochondrial fusion. *Nature* **542**, 372-376 (2017).
56. J. Chiche *et al.*, Hypoxic enlarged mitochondria protect cancer cells from apoptotic stimuli. *Journal of cellular physiology* **222**, 648-657 (2010).
57. M. Roy, P. H. Reddy, M. Iijima, H. Sesaki, Mitochondrial division and fusion in metabolism. *Current opinion in cell biology* **33**, 111-118 (2015).
58. A. R. van Vliet, T. Verfaillie, P. Agostinis, New functions of mitochondria associated membranes in cellular signaling. *Biochimica et biophysica acta* **1843**, 2253-2262 (2014).
59. W. Wang *et al.*, Mitochondrial dysfunction-related genes in hepatocellular carcinoma. *Frontiers in bioscience (Landmark edition)* **18**, 1141-1149 (2013).
60. A. Sugiura *et al.*, MITOL regulates endoplasmic reticulum-mitochondria contacts via Mitofusin2. *Molecular cell* **51**, 20-34 (2013).

61. J. Li *et al.*, Mitofusin 1 is negatively regulated by microRNA 140 in cardiomyocyte apoptosis. *Molecular and cellular biology* **34**, 1788-1799 (2014).
62. X. Li *et al.*, MicroRNA-19b targets Mfn1 to inhibit Mfn1-induced apoptosis in osteosarcoma cells. *Neoplasma* **61**, 265-273 (2014).
63. P. Belenguer, L. Pellegrini, The dynamin GTPase OPA1: more than mitochondria? *Biochimica et biophysica acta* **1833**, 176-183 (2013).
64. R. Anand *et al.*, The i-AAA protease YME1L and OMA1 cleave OPA1 to balance mitochondrial fusion and fission. *The Journal of cell biology* **204**, 919-929 (2014).
65. T. Varanita *et al.*, The OPA1-dependent mitochondrial cristae remodeling pathway controls atrophic, apoptotic, and ischemic tissue damage. *Cell metabolism* **21**, 834-844 (2015).
66. S. Y. Choi *et al.*, A common lipid links Mfn-mediated mitochondrial fusion and SNARE-regulated exocytosis. *Nat Cell Biol* **8**, 1255-1262 (2006).
67. T. Wai, T. Langer, Mitochondrial Dynamics and Metabolic Regulation. *Trends in endocrinology and metabolism: TEM* **27**, 105-117 (2016).
68. J. Förtsch, E. Hummel, M. Krist, B. Westermann, The myosin-related motor protein Myo2 is an essential mediator of bud-directed mitochondrial movement in yeast. *The Journal of cell biology* **194**, 473 (2011).
69. M. C. Caino *et al.*, PI3K therapy reprograms mitochondrial trafficking to fuel tumor cell invasion. *Proceedings of the National Academy of Sciences* **112**, 8638 (2015).
70. M. C. Caino *et al.*, Syntaphilin controls a mitochondrial rheostat for proliferation-motility decisions in cancer. *The Journal of Clinical Investigation* **127**, 3755-3769 (2017).
71. S. Abounit, C. Zurzolo, Wiring through tunneling nanotubes – from electrical signals to organelle transfer. *Journal of cell science* **125**, 1089 (2012).
72. M. L. Vignais, A. Caicedo, J. M. Brondello, C. Jorgensen, Cell Connections by Tunneling Nanotubes: Effects of Mitochondrial Trafficking on Target Cell Metabolism, Homeostasis, and Response to Therapy. *Stem Cells Int* **2017**, 6917941 (2017).
73. M. W. Austefjord, H. H. Gerdes, X. Wang, Tunneling nanotubes: Diversity in morphology and structure. *Communicative & integrative biology* **7**, e27934 (2014).
74. E. Y. Plotnikov *et al.*, Intercellular transfer of mitochondria. *Biochemistry (Moscow)* **80**, 542-548 (2015).
75. J. Lu *et al.*, Tunneling nanotubes promote intercellular mitochondria transfer followed by increased invasiveness in bladder cancer cells. *Oncotarget* **8**, 15539-15552 (2017).
76. J. Pasquier *et al.*, Preferential transfer of mitochondria from

endothelial to cancer cells through tunneling nanotubes modulates chemoresistance. *Journal of translational medicine* **11**, 94 (2013).
77. M. Jang, S. S. Kim, J. Lee, Cancer cell metabolism: implications for therapeutic targets. *Experimental &Amp; Molecular Medicine* **45**, e45 (2013).
78. F. Dupuy *et al.*, PDK1-Dependent Metabolic Reprogramming Dictates Metastatic Potential in Breast Cancer. *Cell metabolism* **22**, 577-589 (2015).
79. K. M. Holmström, T. Finkel, Cellular mechanisms and physiological consequences of redox-dependent signalling. *Nature Reviews Molecular Cell Biology* **15**, 411 (2014).
80. G.-Y. Liou, P. Storz, Reactive oxygen species in cancer. *Free radical research* **44**, 10.3109/10715761003667554 (2010).
81. X. Li *et al.*, Targeting mitochondrial reactive oxygen species as novel therapy for inflammatory diseases and cancers. *Journal of Hematology & Oncology* **6**, 19 (2013).
82. H. Mei *et al.*, Reduced mtDNA copy number increases the sensitivity of tumor cells to chemotherapeutic drugs. *Cell death & disease* **6**, e1710 (2015).
83. N. Chen *et al.*, Elevated Mitochondrial DNA Copy Number in Peripheral Blood and Tissue Predict the Opposite Outcome of Cancer: A Meta-Analysis. *Scientific reports* **6**, 37404 (2016).
84. N. Guaragnella, S. Giannattasio, L. Moro, Mitochondrial dysfunction in cancer chemoresistance. *Biochemical pharmacology* **92**, 62-72 (2014).
85. A. Hori, M. Yoshida, T. Shibata, F. Ling, Reactive oxygen species regulate DNA copy number in isolated yeast mitochondria by triggering recombination-mediated replication. *Nucleic acids research* **37**, 749-761 (2009).
86. A. Prakash, S. Doublie, Base Excision Repair in the Mitochondria. *Journal of cellular biochemistry* **116**, 1490-1499 (2015).
87. J. Ballista-Hernandez *et al.*, Mitochondrial DNA Integrity Is Maintained by APE1 in Carcinogen-Induced Colorectal Cancer. *Molecular cancer research : MCR* **15**, 831-841 (2017).
88. Y. Gao *et al.*, DNA ligase III is critical for mtDNA integrity but not Xrcc1-mediated nuclear DNA repair. *Nature* **471**, 240-244 (2011).
89. C. Douarre *et al.*, Mitochondrial Topoisomerase I is Critical for Mitochondrial Integrity and Cellular Energy Metabolism. *PloS one* **7**, e41094 (2012).
90. E. Panieri, M. M. Santoro, ROS homeostasis and metabolism: a dangerous liason in cancer cells. *Cell Death &Amp; Disease* **7**, e2253 (2016).
91. M. Idelchik, U. Begley, T. J. Begley, J. A. Melendez, Mitochondrial ROS control of cancer. *Seminars in cancer biology* **47**, 57-66

(2017).
92. F. Weinberg *et al.*, Mitochondrial metabolism and ROS generation are essential for Kras-mediated tumorigenicity. *Proceedings of the National Academy of Sciences of the United States of America* **107**, 8788-8793 (2010).
93. B. Kim *et al.*, PGC1alpha induced by reactive oxygen species contributes to chemoresistance of ovarian cancer cells. *Oncotarget* **8**, 60299-60311 (2017).
94. G. Zhao *et al.*, Crosstalk between Mitochondrial Fission and Oxidative Stress in Paraquat-Induced Apoptosis in Mouse Alveolar Type II Cells. *International journal of biological sciences* **13**, 888-900 (2017).
95. S. Wu, F. Zhou, Z. Zhang, D. Xing, Mitochondrial oxidative stress causes mitochondrial fragmentation via differential modulation of mitochondrial fission-fusion proteins. *The FEBS journal* **278**, 941-954 (2011).
96. U. Cho, B. Kim, S. Kim, Y. Han, Y. S. Song, Pro-inflammatory M1 macrophage enhances metastatic potential of ovarian cancer cells through NF-kappaB activation. *Mol Carcinog* **57**, 235-242 (2018).
97. H. A. Alshaker, K. Z. Matalka, IFN-ɣ, IL-17 and TGF-β involvement in shaping the tumor microenvironment: The significance of modulating such cytokines in treating malignant solid tumors. *Cancer Cell International* **11**, 33 (2011).
98. J. Zhang *et al.*, Guanylate-binding protein 2 regulates Drp1-mediated mitochondrial fission to suppress breast cancer cell invasion. *Cell death & disease* **8**, e3151 (2017).
99. J. P. White *et al.*, IL-6 regulation on skeletal muscle mitochondrial remodeling during cancer cachexia in the ApcMin/+ mouse. *Skeletal muscle* **2**, 14 (2012).
100. Y. Zhang *et al.*, MicroRNA-106b induces mitochondrial dysfunction and insulin resistance in C2C12 myotubes by targeting mitofusin-2. *Molecular and cellular endocrinology* **381**, 230-240 (2013).
101. V. Romanello *et al.*, Mitochondrial fission and remodelling contributes to muscle atrophy. *Embo j* **29**, 1774-1785 (2010).
102. A. A. Ayantunde, S. L. Parsons, Pattern and prognostic factors in patients with malignant ascites: a retrospective study. *Annals of oncology : official journal of the European Society for Medical Oncology* **18**, 945-949 (2007).
103. S. Kim, B. Kim, Y. S. Song, Ascites modulates cancer cell behavior, contributing to tumor heterogeneity in ovarian cancer. *Cancer science* **107**, 1173-1178 (2016).
104. S. Kim *et al.*, Malignant ascites enhances migratory and invasive properties of ovarian cancer cells with membrane bound IL-6R in vitro. *Oncotarget* **7**, 83148-83159 (2016).

105. K. Izuishi, K. Kato, T. Ogura, T. Kinoshita, H. Esumi, Remarkable tolerance of tumor cells to nutrient deprivation: possible new biochemical target for cancer therapy. *Cancer research* **60**, 6201-6207 (2000).
106. P. Li *et al.*, Redox homeostasis protects mitochondria through accelerating ROS conversion to enhance hypoxia resistance in cancer cells. *Scientific reports* **6**, 22831 (2016).
107. K. L. Eales, K. E. Hollinshead, D. A. Tennant, Hypoxia and metabolic adaptation of cancer cells. *Oncogenesis* **5**, e190 (2016).
108. H. Wang *et al.*, The Effect of Propofol on Mitochondrial Fission during Oxygen-Glucose Deprivation and Reperfusion Injury in Rat Hippocampal Neurons. *PloS one* **11**, e0165052 (2016).
109. A. Casazza *et al.*, Tumor stroma: a complexity dictated by the hypoxic tumor microenvironment. *Oncogene* **33**, 1743-1754 (2014).
110. R. Bos *et al.*, Hypoxia-inducible factor-1alpha is associated with angiogenesis, and expression of bFGF, PDGF-BB, and EGFR in invasive breast cancer. *Histopathology* **46**, 31-36 (2005).
111. J. K. Salabei, B. G. Hill, Mitochondrial fission induced by platelet-derived growth factor regulates vascular smooth muscle cell bioenergetics and cell proliferation. *Redox Biol* **1**, 542-551 (2013).
112. W. Wu *et al.*, FUNDC1 regulates mitochondrial dynamics at the ER-mitochondrial contact site under hypoxic conditions. *The EMBO Journal* **35**, 1368-1384 (2016).
113. X. J. Han *et al.*, Mitochondrial dynamics regulates hypoxia-induced migration and antineoplastic activity of cisplatin in breast cancer cells. *International journal of oncology* **46**, 691-700 (2015).
114. I. Diebold *et al.*, BMPR2 preserves mitochondrial function and DNA during reoxygenation to promote endothelial cell survival and reverse pulmonary hypertension. *Cell metabolism* **21**, 596-608 (2015).
115. R. Rossignol *et al.*, Energy substrate modulates mitochondrial structure and oxidative capacity in cancer cells. *Cancer research* **64**, 985-993 (2004).
116. A. S. Rambold, B. Kostelecky, N. Elia, J. Lippincott-Schwartz, Tubular network formation protects mitochondria from autophagosomal degradation during nutrient starvation. *Proceedings of the National Academy of Sciences of the United States of America* **108**, 10190-10195 (2011).
117. Y. Kitaoka, K. Nakazato, R. Ogasawara, Combined effects of resistance training and calorie restriction on mitochondrial fusion and fission proteins in rat skeletal muscle. *Journal of applied physiology (Bethesda, Md. : 1985)* **121**, 806-810 (2016).
118. J. Y. Lee *et al.*, MFN1 deacetylation activates adaptive

mitochondrial fusion and protects metabolically challenged mitochondria. *Journal of cell science* **127**, 4954-4963 (2014).
119. J. Li *et al.*, Mitochondrial elongation-mediated glucose metabolism reprogramming is essential for tumour cell survival during energy stress. *Oncogene* **36**, 4901-4912 (2017).
120. C.-T. Cheng *et al.*, Metabolic Stress-Induced Phosphorylation of KAP1 Ser473 Blocks Mitochondrial Fusion in Breast Cancer Cells. *Cancer research* **76**, 5006 (2016).
121. G. Bonuccelli *et al.*, Ketones and lactate "fuel" tumor growth and metastasis: Evidence that epithelial cancer cells use oxidative mitochondrial metabolism. *Cell cycle (Georgetown, Tex.)* **9**, 3506-3514 (2010).
122. C. Guido *et al.*, Mitochondrial fission induces glycolytic reprogramming in cancer-associated myofibroblasts, driving stromal lactate production, and early tumor growth. *Oncotarget* **3**, 798-810 (2012).
123. J. Cui *et al.*, Melatonin alleviates inflammation-induced apoptosis in human umbilical vein endothelial cells via suppression of Ca2+ -XO-ROS-Drp1-mitochondrial fission axis by activation of AMPK/SERCA2a pathway. *Cell stress & chaperones* 10.1007/s12192-017-0841-6 (2017).
124. A. Rojas *et al.*, Diabetes and cancer: Looking at the multiligand/RAGE axis. *World J Diabetes* **2**, 108-113 (2011).
125. R. Kang *et al.*, The HMGB1/RAGE inflammatory pathway promotes pancreatic tumor growth by regulating mitochondrial bioenergetics. *Oncogene* **33**, 567-577 (2014).
126. Y. Cui, G. Guo, Immunomodulatory Function of the Tumor Suppressor p53 in Host Immune Response and the Tumor Microenvironment. *Int J Mol Sci* **17** (2016).
127. N. E. Scharping *et al.*, The Tumor Microenvironment Represses T Cell Mitochondrial Biogenesis to Drive Intratumoral T Cell Metabolic Insufficiency and Dysfunction. *Immunity* **45**, 374-388 (2016).
128. Michael D. Buck *et al.*, Mitochondrial Dynamics Controls T Cell Fate through Metabolic Programming. *Cell* **166**, 63-76.
129. D.-F. Suen, K. L. Norris, R. J. Youle, Mitochondrial dynamics and apoptosis. *Genes & development* **22**, 1577-1590 (2008).
130. R. Horbay, R. Bilyy, Mitochondrial dynamics during cell cycling. *Apoptosis : an international journal on programmed cell death* **21**, 1327-1335 (2016).
131. D. C. Altieri, Mitochondria on the move: emerging paradigms of organelle trafficking in tumour plasticity and metastasis. *British Journal Of Cancer* **117**, 301 (2017).
132. J. Rehman *et al.*, Inhibition of mitochondrial fission prevents cell cycle progression in lung cancer. *FASEB journal : official publication of the Federation of American Societies for*

Experimental Biology **26**, 2175-2186 (2012).
133. B. J. Belin, T. Lee, R. D. Mullins, DNA damage induces nuclear actin filament assembly by Formin -2 and Spire-(1/2) that promotes efficient DNA repair. [corrected]. *eLife* **4**, e07735 (2015).
134. Y. Huo *et al.*, Downregulation of vimentin expression increased drug resistance in ovarian cancer cells. *Oncotarget* **7**, 45876-45888 (2016).
135. L. Farrand *et al.*, An improved quantitative approach for the assessment of mitochondrial fragmentation in chemoresistant ovarian cancer cells. *PloS one* **8**, e74008 (2013).
136. L. Wei, M. Surma, S. Shi, N. Lambert-Cheatham, J. Shi, Novel Insights into the Roles of Rho Kinase in Cancer. *Archivum immunologiae et therapiae experimentalis* **64**, 259-278 (2016).
137. H. P. Joshi *et al.*, Dynamin 2 along with microRNA-199a reciprocally regulate hypoxia-inducible factors and ovarian cancer metastasis. *Proceedings of the National Academy of Sciences of the United States of America* **111**, 5331-5336 (2014).
138. B. Kong, Q. Wang, E. Fung, K. Xue, B. K. Tsang, p53 is required for cisplatin-induced processing of the mitochondrial fusion protein L-Opa1 that is mediated by the mitochondrial metallopeptidase Oma1 in gynecologic cancers. *The Journal of biological chemistry* **289**, 27134-27145 (2014).
139. C. Fiorini *et al.*, Mutant p53 stimulates chemoresistance of pancreatic adenocarcinoma cells to gemcitabine. *Biochimica et biophysica acta* **1853**, 89-100 (2015).
140. J. Prieto *et al.*, Early ERK1/2 activation promotes DRP1-dependent mitochondrial fission necessary for cell reprogramming. *Nature communications* **7**, 11124 (2016).
141. H. Tsuyoshi *et al.*, Saikosaponin-d, a calcium mobilizing agent, sensitizes chemoresistant ovarian cancer cells to cisplatin-induced apoptosis by facilitating mitochondrial fission and G2/M arrest. *Oncotarget* **8**, 99825-99840 (2017).
142. M. Shirane, K. I. Nakayama, Inherent calcineurin inhibitor FKBP38 targets Bcl-2 to mitochondria and inhibits apoptosis. *Nat Cell Biol* **5**, 28-37 (2003).
143. I. Zaja *et al.*, Cdk1, PKCdelta and calcineurin-mediated Drp1 pathway contributes to mitochondrial fission-induced cardiomyocyte death. *Biochem Biophys Res Commun* **453**, 710-721 (2014).
144. T. H. Hung *et al.*, FZD1 activates protein kinase C delta-mediated drug-resistance in multidrug-resistant MES-SA/Dx5 cancer cells. *The international journal of biochemistry & cell biology* **53**, 55-65 (2014).
145. C. M. Ferrer *et al.*, O-GlcNAcylation regulates cancer metabolism and survival stress signaling via regulation of the HIF-1 pathway.

Molecular cell **54**, 820-831 (2014).
146. M. Satoh, T. Hamamoto, N. Seo, Y. Kagawa, H. Endo, Differential sublocalization of the dynamin-related protein OPA1 isoforms in mitochondria. *Biochem Biophys Res Commun* **300**, 482-493 (2003).
147. L. Stiburek *et al.*, YME1L controls the accumulation of respiratory chain subunits and is required for apoptotic resistance, cristae morphogenesis, and cell proliferation. *Mol Biol Cell* **23**, 1010-1023 (2012).
148. M. Li, J. Yin, N. Mao, L. Pan, Upregulation of phosphorylated cofilin 1 correlates with taxol resistance in human ovarian cancer in vitro and in vivo. *Oncology reports* **29**, 58-66 (2013).
149. J. Chen *et al.*, Pim-1 plays a pivotal role in hypoxia-induced chemoresistance. *Oncogene* **28**, 2581-2592 (2009).
150. T. H. Hung *et al.*, Wnt5A regulates ABCB1 expression in multidrug-resistant cancer cells through activation of the non-canonical PKA/beta-catenin pathway. *Oncotarget* **5**, 12273-12290 (2014).
151. H. C. Pal, R. Prasad, S. K. Katiyar, Cryptolepine inhibits melanoma cell growth through coordinated changes in mitochondrial biogenesis, dynamics and metabolic tumor suppressor AMPKalpha1/2-LKB1. *Scientific reports* **7**, 1498 (2017).
152. L. Farrand *et al.*, Piceatannol enhances cisplatin sensitivity in ovarian cancer via modulation of p53, X-linked inhibitor of apoptosis protein (XIAP), and mitochondrial fission. *The Journal of biological chemistry* **288**, 23740-23750 (2013).
153. S. R. Chowdhury, U. Ray, B. P. Chatterjee, S. S. Roy, Targeted apoptosis in ovarian cancer cells through mitochondrial dysfunction in response to Sambucus nigra agglutinin. *Cell death & disease* **8**, e2762 (2017).
154. X. Zhou *et al.*, Ginkgolide K attenuates neuronal injury after ischemic stroke by inhibiting mitochondrial fission and GSK-3beta-dependent increases in mitochondrial membrane permeability. *Oncotarget* **8**, 44682-44693 (2017).
155. Z. Fan *et al.*, ABT737 enhances cholangiocarcinoma sensitivity to cisplatin through regulation of mitochondrial dynamics. *Experimental cell research* **335**, 68-81 (2015).
156. R. A. Anvekar *et al.*, Sensitization to the mitochondrial pathway of apoptosis augments melanoma tumor cell responses to conventional chemotherapeutic regimens. *Cell death & disease* **3**, e420 (2012).
157. R. C. Gregory-Bass *et al.*, Prohibitin silencing reverses stabilization of mitochondrial integrity and chemoresistance in ovarian cancer cells by increasing their sensitivity to apoptosis. *International Journal of Cancer. Journal International du Cancer*

122, 1923-1930 (2008).
158. L. Zhang, B. Fang, Mechanisms of resistance to TRAIL-induced apoptosis in cancer. *Cancer gene therapy* **12**, 228-237 (2005).
159. S. Ke *et al.*, Gold nanoparticles enhance TRAIL sensitivity through Drp1-mediated apoptotic and autophagic mitochondrial fission in NSCLC cells. *International journal of nanomedicine* **12**, 2531-2551 (2017).
160. G. Zhang *et al.*, Targeting mitochondrial biogenesis to overcome drug resistance to MAPK inhibitors. *J Clin Invest* **126**, 1834-1856 (2016).
161. B. Kong *et al.*, Mitochondrial dynamics regulating chemoresistance in gynecological cancers. *Annals of the New York Academy of Sciences* **1350**, 1-16 (2015).
162. Q. Huang *et al.*, Increased mitochondrial fission promotes autophagy and hepatocellular carcinoma cell survival through the ROS-modulated coordinated regulation of the NFKB and TP53 pathways. *Autophagy* **12**, 999-1014 (2016).
163. Z. Yang *et al.*, microRNA-488 inhibits chemoresistance of ovarian cancer cells by targeting Six1 and mitochondrial function. *Oncotarget* **8**, 80981-80993 (2017).
164. X. Wang, H. H. Gerdes, Transfer of mitochondria via tunneling nanotubes rescues apoptotic PC12 cells. *Cell death and differentiation* **22**, 1181-1191 (2015).
165. H. Han *et al.*, Bone marrow-derived mesenchymal stem cells rescue injured H9c2 cells via transferring intact mitochondria through tunneling nanotubes in an in vitro simulated ischemia/reperfusion model. *Molecular medicine reports* **13**, 1517-1524 (2016).
166. S. Desir *et al.*, Tunneling nanotube formation is stimulated by hypoxia in ovarian cancer cells. *Oncotarget* **7**, 43150-43161 (2016).
167. S. B. Coburn, F. Bray, M. E. Sherman, B. Trabert, International patterns and trends in ovarian cancer incidence, overall and by histologic subtype. *International journal of cancer* **140**, 2451-2460 (2017).
168. M. Matz *et al.*, Worldwide comparison of ovarian cancer survival: Histological group and stage at diagnosis (CONCORD-2). *Gynecologic oncology* **144**, 396-404 (2017).
169. H. K. Park, J. J. Ruterbusch, M. L. Cote, Recent Trends in Ovarian Cancer Incidence and Relative Survival in the United States by Race/Ethnicity and Histologic Subtypes. *Cancer epidemiology, biomarkers & prevention : a publication of the American Association for Cancer Research, cosponsored by the American Society of Preventive Oncology* **26**, 1511-1518 (2017).
170. S. Capriglione *et al.*, Ovarian cancer recurrence and early detection: may HE4 play a key role in this open challenge? A

systematic review of literature. *Medical oncology (Northwood, London, England)* **34**, 164 (2017).
171. A. Carreau, B. El Hafny-Rahbi, A. Matejuk, C. Grillon, C. Kieda, Why is the partial oxygen pressure of human tissues a crucial parameter? Small molecules and hypoxia. *Journal of cellular and molecular medicine* **15**, 1239-1253 (2011).
172. K. L. Eales, K. E. R. Hollinshead, D. A. Tennant, Hypoxia and metabolic adaptation of cancer cells. *Oncogenesis* **5**, e190 (2016).
173. F. Casciello *et al.*, G9a drives hypoxia-mediated gene repression for breast cancer cell survival and tumorigenesis. *Proceedings of the National Academy of Sciences of the United States of America* **114**, 7077-7082 (2017).
174. J. Kang *et al.*, FIH Is an Oxygen Sensor in Ovarian Cancer for G9a/GLP-Driven Epigenetic Regulation of Metastasis-Related Genes. *Cancer research* **78**, 1184-1199 (2018).
175. Y. Chen, L. Zhang, Y. Pan, X. Ren, Q. Hao, Over-expression of semaphorin4D, hypoxia-inducible factor-1alpha and vascular endothelial growth factor is related to poor prognosis in ovarian epithelial cancer. *International journal of molecular sciences* **13**, 13264-13274 (2012).
176. E. I. Braicu *et al.*, HIF1alpha is an independent prognostic factor for overall survival in advanced primary epithelial ovarian cancer - a study of the OVCAD Consortium. *OncoTargets and therapy* **7**, 1563-1569 (2014).
177. D. C. Altieri, Mitochondria on the move: emerging paradigms of organelle trafficking in tumour plasticity and metastasis. *British journal of cancer* **117**, 301-305 (2017).
178. A. Ferree, O. Shirihai, Mitochondrial dynamics: the intersection of form and function. *Advances in experimental medicine and biology* **748**, 13-40 (2012).
179. Y. Han *et al.*, Tumour microenvironment on mitochondrial dynamics and chemoresistance in cancer. *Free radical research* 10.1080/10715762.2018.1459594, 1-17 (2018).
180. S. L. Archer, Mitochondrial dynamics--mitochondrial fission and fusion in human diseases. *The New England journal of medicine* **369**, 2236-2251 (2013).
181. K. Itoh, K. Nakamura, M. Iijima, H. Sesaki, Mitochondrial dynamics in neurodegeneration. *Trends in cell biology* **23**, 64-71 (2013).
182. Y. H. Hong *et al.*, ROS Accumulation by PEITC Selectively Kills Ovarian Cancer Cells via UPR-Mediated Apoptosis. *Frontiers in oncology* **5**, 167 (2015).
183. B. Kim *et al.*, Adipose Stromal Cells from Visceral and Subcutaneous Fat Facilitate Migration of Ovarian Cancer Cells via IL-6/JAK2/STAT3 Pathway. *Cancer Res Treat* **49**, 338-349 (2017).

184. N. Gjorevski *et al.*, Designer matrices for intestinal stem cell and organoid culture. *Nature* **539**, 560-564 (2016).
185. M. Y. Turco *et al.*, Long-term, hormone-responsive organoid cultures of human endometrium in a chemically defined medium. *Nature cell biology* **19**, 568-577 (2017).
186. J. Jabs *et al.*, Screening drug effects in patient-derived cancer cells links organoid responses to genome alterations. *Molecular systems biology* **13**, 955 (2017).
187. C. Cocola *et al.*, FGF2 and EGF Are Required for Self-Renewal and Organoid Formation of Canine Normal and Tumor Breast Stem Cells. *Journal of cellular biochemistry* **118**, 570-584 (2017).
188. Y. A. Ren *et al.*, Mutant p53 Promotes Epithelial Ovarian Cancer by Regulating Tumor Differentiation, Metastasis, and Responsiveness to Steroid Hormones. *Cancer research* **76**, 2206-2218 (2016).
189. T. J. Humpton, K. H. Vousden, Regulation of Cellular Metabolism and Hypoxia by p53. *Cold Spring Harbor perspectives in medicine* **6** (2016).
190. J. H. Lee *et al.*, Hypoxia activates tumor suppressor p53 by inducing ATR-Chk1 kinase cascade-mediated phosphorylation and consequent 14-3-3gamma inactivation of MDMX protein. *The Journal of biological chemistry* **287**, 20898-20903 (2012).
191. E. Panieri, M. M. Santoro, ROS homeostasis and metabolism: a dangerous liason in cancer cells. *Cell death & disease* **7**, e2253 (2016).
192. B. Kim *et al.*, Inhibition of Drp1-dependent mitochondrial division impairs myogenic differentiation. *American journal of physiology. Regulatory, integrative and comparative physiology* **305**, R927-938 (2013).
193. G. V. Chaitanya, A. J. Steven, P. P. Babu, PARP-1 cleavage fragments: signatures of cell-death proteases in neurodegeneration. *Cell communication and signaling : CCS* **8**, 31 (2010).
194. J. A. Seo, B. Kim, D. N. Dhanasekaran, B. K. Tsang, Y. S. Song, Curcumin induces apoptosis by inhibiting sarco/endoplasmic reticulum Ca2+ ATPase activity in ovarian cancer cells. *Cancer letters* **371**, 30-37 (2016).
195. A. Soragni *et al.*, A Designed Inhibitor of p53 Aggregation Rescues p53 Tumor Suppression in Ovarian Carcinomas. *Cancer cell* **29**, 90-103 (2016).
196. O. Y. Pletjushkina *et al.*, Effect of oxidative stress on dynamics of mitochondrial reticulum. *Biochimica et biophysica acta* **1757**, 518-524 (2006).
197. P. A. Parone *et al.*, Preventing mitochondrial fission impairs mitochondrial function and leads to loss of mitochondrial DNA. *PloS one* **3**, e3257 (2008).

198. H. Otera, N. Miyata, O. Kuge, K. Mihara, Drp1-dependent mitochondrial fission via MiD49/51 is essential for apoptotic cristae remodeling. *The Journal of cell biology* **212**, 531-544 (2016).
199. B. Oettinghaus *et al.*, DRP1-dependent apoptotic mitochondrial fission occurs independently of BAX, BAK and APAF1 to amplify cell death by BID and oxidative stress. *Biochimica et biophysica acta* **1857**, 1267-1276 (2016).
200. D. Zhang *et al.*, Increased mitochondrial fission is critical for hypoxia-induced pancreatic beta cell death. *PloS one* **13**, e0197266 (2018).
201. Y. L. Shen *et al.*, TNF-alpha induces Drp1-mediated mitochondrial fragmentation during inflammatory cardiomyocyte injury. *International journal of molecular medicine* **41**, 2317-2327 (2018).
202. M. Akbarzadeh *et al.*, The potential therapeutic effect of melatonin on human ovarian cancer by inhibition of invasion and migration of cancer stem cells. *Scientific reports* **7**, 17062 (2017).
203. S. Xu *et al.*, Melatonin prevents abnormal mitochondrial dynamics resulting from the neurotoxicity of cadmium by blocking calcium-dependent translocation of Drp1 to the mitochondria. *Journal of pineal research* **60**, 291-302 (2016).
204. Y. Y. Wan *et al.*, Involvement of Drp1 in hypoxia-induced migration of human glioblastoma U251 cells. *Oncology reports* **32**, 619-626 (2014).
205. A. Ferreira-da-Silva *et al.*, Mitochondrial dynamics protein Drp1 is overexpressed in oncocytic thyroid tumors and regulates cancer cell migration. *PloS one* **10**, e0122308 (2015).
206. M. C. Caino *et al.*, PI3K therapy reprograms mitochondrial trafficking to fuel tumor cell invasion. *Proceedings of the National Academy of Sciences* **112**, 8638-8643 (2015).
207. C. T. Cheng *et al.*, Metabolic Stress-Induced Phosphorylation of KAP1 Ser473 Blocks Mitochondrial Fusion in Breast Cancer Cells. *Cancer research* **76**, 5006-5018 (2016).
208. Q. Xie *et al.*, Mitochondrial control by DRP1 in brain tumor initiating cells. *Nature neuroscience* **18**, 501-510 (2015).
209. S. Kim *et al.*, Tumor evolution and chemoresistance in ovarian cancer. *NPJ precision oncology* **2**, 20 (2018).
210. S. Kim *et al.*, Evaluating Tumor Evolution via Genomic Profiling of Individual Tumor Spheroids in a Malignant Ascites. *Scientific reports* **8**, 12724 (2018).
211. J. Y. Lee *et al.*, Tumor evolution and intratumor heterogeneity of an epithelial ovarian cancer investigated using next-generation sequencing. *BMC cancer* **15**, 85 (2015).
212. E. Girda, E. C. Huang, G. S. Leiserowitz, L. H. Smith, The Use of Endometrial Cancer Patient-Derived Organoid Culture for Drug

Sensitivity Testing Is Feasible. *International journal of gynecological cancer : official journal of the International Gynecological Cancer Society* **27**, 1701-1707 (2017).
213. X. Ma, The omentum, a niche for premetastatic ovarian cancer. *Journal of Experimental Medicine* **217** (2020).
214. R. L. Siegel, K. D. Miller, A. Jemal, Cancer statistics, 2020. *CA: A Cancer Journal for Clinicians* **70**, 7-30 (2020).
215. S. Al Habyan, C. Kalos, J. Szymborski, L. McCaffrey, Multicellular detachment generates metastatic spheroids during intra-abdominal dissemination in epithelial ovarian cancer. *Oncogene* **37**, 5127-5135 (2018).
216. S.-C. Sun, The noncanonical NF-κB pathway. *Immunological Reviews* **246**, 125-140 (2012).
217. U. Cho, B. Kim, S. Kim, Y. Han, Y. S. Song, Pro-inflammatory M1 macrophage enhances metastatic potential of ovarian cancer cells through NF-κB activation. *Molecular Carcinogenesis* **57**, 235-242 (2018).
218. J. Wang, S. Yi, J. Zhou, Y. Zhang, F. Guo, The NF-κB subunit RelB regulates the migration and invasion abilities and the radio-sensitivity of prostate cancer cells. *Int J Oncol* **49**, 381-392 (2016).
219. X. Zhou *et al.*, RelB plays an oncogenic role and conveys chemo-resistance to DLD-1 colon cancer cells. *Cancer Cell International* **18**, 181 (2018).
220. A. L. Rinkenbaugh, A. S. Baldwin, The NF-κB Pathway and Cancer Stem Cells. *Cells* **5**, 16 (2016).
221. W. Yang *et al.*, TRIM52 plays an oncogenic role in ovarian cancer associated with NF-kB pathway. *Cell Death & Disease* **9**, 908 (2018).
222. N. A. Espinoza-Sánchez, B. Győrffy, E. M. Fuentes-Pananá, M. Götte, Differential impact of classical and non-canonical NF-κB pathway-related gene expression on the survival of breast cancer patients. *Journal of Cancer* **10**, 5191-5211 (2019).
223. M. Wang *et al.*, RelB sustains endocrine resistant malignancy: an insight of noncanonical NF-κB pathway into breast Cancer progression. *Cell Communication and Signaling* **18**, 128 (2020).
224. C. Ai *et al.*, FOXM1 functions collaboratively with PLAU to promote gastric cancer progression. *Journal of Cancer* **11**, 788-794 (2020).
225. K. Yang *et al.*, Identification of SERPINE1, PLAU and ACTA1 as biomarkers of head and neck squamous cell carcinoma based on integrated bioinformatics analysis. *International Journal of Clinical Oncology* **24**, 1030-1041 (2019).
226. K. S. Kim, Y.-A. Lee, H. M. Choi, M. C. Yoo, H.-I. Yang, Implication of MMP-9 and urokinase plasminogen activator (uPA) in the activation of pro-matrix metalloproteinase (MMP)-13.

Rheumatology International **32**, 3069-3075 (2012).
227. C. M. Novak, E. N. Horst, C. C. Taylor, C. Z. Liu, G. Mehta, Fluid shear stress stimulates breast cancer cells to display invasive and chemoresistant phenotypes while upregulating PLAU in a 3D bioreactor. *Biotechnology and Bioengineering* **116**, 3084-3097 (2019).
228. L. A. Torre *et al.*, Ovarian cancer statistics, 2018. *CA: A Cancer Journal for Clinicians* **68**, 284-296 (2018).
229. S. Kim *et al.*, Tumor evolution and chemoresistance in ovarian cancer. *npj Precision Oncology* **2**, 1-9 (2018).
230. T. D.S, A. R, K. S.B, Mechanisms of transcoelomic metastasis in ovarian cancer. *Lancet Oncology* **7**, 925-934 (2006).
231. S. Kim, B. Kim, Y. S. Song, Ascites modulates cancer cell behavior, contributing to tumor heterogeneity in ovarian cancer. *Cancer Science* **107** (2016).
232. C. E. Ford, B. Werner, N. F. Hacker, K. Warton, The untapped potential of ascites in ovarian cancer research and treatment. *British Journal of Cancer* 10.1038/s41416-020-0875-x (2020).
233. S. Kim *et al.*, Malignant ascites enhances migratory and invasive properties of ovarian cancer cells with membrane bound IL-6R in vitro. *Oncotarget* **7**, 83148-83159 (2016).
234. S. Kim, M. Lee, D. N. Dhanasekaran, Y. S. Song, Activation of LXRα/β by cholesterol in malignant ascites promotes chemoresistance in ovarian cancer. *BMC Cancer* **18** (2018).
235. M. Schelker *et al.*, Estimation of immune cell content in tumour tissue using single-cell RNA-seq data. *Nature Communications* **8**, 1-12 (2017).
236. Y. Han *et al.*, Mitochondrial fission causes cisplatin resistance under hypoxic conditions via ROS in ovarian cancer cells. *Oncogene* **38**, 7089-7105 (2019).
237. A. Butler, P. Hoffman, P. Smibert, E. Papalexi, R. Satija, Integrating single-cell transcriptomic data across different conditions, technologies, and species. *Nature Biotechnology* **36**, 411-420 (2018).
238. T. Stuart *et al.*, Comprehensive Integration of Single-Cell Data. *Cell* **177**, 1888-1902.e1821 (2019).
239. G. Finak *et al.*, MAST: A flexible statistical framework for assessing transcriptional changes and characterizing heterogeneity in single-cell RNA sequencing data. *Genome Biology* **16**, 1-13 (2015).
240. C. Li *et al.*, Single-cell transcriptomics-based MacSpectrum reveals macrophage activation signatures in diseases. *JCI Insight* **4**, 1-21 (2019).
241. A. Subramanian *et al.*, Gene set enrichment analysis: A knowledge-based approach for interpreting genome-wide expression profiles. *Proceedings of the National Academy of*

Sciences of the United States of America **102**, 15545-15550 (2005).
242. A. Liberzon *et al.*, Molecular signatures database (MSigDB) 3.0. *Bioinformatics* **27**, 1739-1740 (2011).
243. G. Korotkevich, V. Sukhov, A. Sergushichev, Fast gene set enrichment analysis. *bioRxiv* 10.1101/060012, 60012-60012 (2019).
244. J. Bonnardel *et al.*, Supplemental Information Stellate Cells , Hepatocytes , and Endothelial Cells Imprint the Kupffer Cell Identity on Monocytes Colonizing the Liver Macrophage Niche PBS control 16h DT Top view Top view Clec4F Parenchyma CCR2-GFP Clec4F KI-67 Merged 7 days D. **51**.
245. R. Browaeys, W. Saelens, Y. Saeys, NicheNet: modeling intercellular communication by linking ligands to target genes. *Nature Methods* **17**, 159-162 (2020).
246. B. Gyorffy, P. Surowiak, J. Budczies, A. Lánczky, Online survival analysis software to assess the prognostic value of biomarkers using transcriptomic data in non-small-cell lung cancer. *PLoS ONE* **8** (2013).
247. Z. Tang *et al.*, GEPIA: a web server for cancer and normal gene expression profiling and interactive analyses. *Nucleic Acids Research* **45**, W98-W102 (2017).
248. D. S. Chandrashekar *et al.*, UALCAN: A Portal for Facilitating Tumor Subgroup Gene Expression and Survival Analyses. *Neoplasia (United States)* **19**, 649-658 (2017).
249. Y. Yang *et al.*, Crosstalk between hepatic tumor cells and macrophages via Wnt/β-catenin signaling promotes M2-like macrophage polarization and reinforces tumor malignant behaviors. *Cell Death and Disease* **9** (2018).
250. S. Raghavan, P. Mehta, Y. Xie, Y. L. Lei, G. Mehta, Ovarian cancer stem cells and macrophages reciprocally interact through the WNT pathway to promote pro-tumoral and malignant phenotypes in 3D engineered microenvironments. *Journal for ImmunoTherapy of Cancer* **7**, 1-15 (2019).
251. E. Vergadi, E. Ieronymaki, K. Lyroni, K. Vaporidi, C. Tsatsanis, Akt Signaling Pathway in Macrophage Activation and M1/M2 Polarization. *The Journal of Immunology* **198**, 1006-1014 (2017).
252. L. Roy, K. D. C. Dahl, Can stemness and chemoresistance be therapeutically targeted via signaling pathways in ovarian cancer? *Cancers* **10**, 1-23 (2018).
253. V. M. Peterson *et al.*, Ascites analysis by a microfluidic chip allows tumor-cell profiling. *Proceedings of the National Academy of Sciences of the United States of America* **110** (2013).
254. N. Scholler, N. Urban, C. a. Gene, CA125 in Ovarian Cancer Nathalie. *Biomarkers in medicine* **1**, 513-523 (2010).
255. S. C. Parte, S. K. Batra, S. S. Kakar, Characterization of stem cell

and cancer stem cell populations in ovary and ovarian tumors. *Journal of Ovarian Research* **11**, 1-16 (2018).
256. A. E. Powell *et al.*, Fusion between intestinal epithelial cells and macrophages in a cancer context results in nuclear reprogramming. *Cancer Research* **71**, 1497-1505 (2011).
257. M. Ramakrishnan, S. R. Mathur, A. Mukhopadhyay, Fusion-derived epithelial cancer cells express hematopoietic markers and contribute to stem cell and migratory phenotype in ovarian carcinoma. *Cancer Research* **73**, 5360-5370 (2013).
258. Q. Cai, L. Yan, Y. Xu, Anoikis resistance is a critical feature of highly aggressive ovarian cancer cells. 10.1038/onc.2014.264, 3315-3324 (2015).
259. X. Guo *et al.*, Global characterization of T cells in non-small-cell lung cancer by single-cell sequencing. *Nature Medicine* **24**, 978-985 (2018).
260. M. K. S. Tang, H. Y. Zhou, J. W. P. Yam, A. S. T. Wong, c-Met overexpression contributes to the acquired apoptotic resistance of nonadherent ovarian cancer cells through a cross talk mediated by phosphatidylinositol 3-kinase and extracellular signal-regulated kinase 1/2. *Neoplasia* **12**, 128-138 (2010).
261. B. Izar *et al.*, A single-cell landscape of high-grade serous ovarian cancer. *Nature Medicine* 10.1038/s41591-020-0926-0 (2020).
262. U. Cho, B. Kim, S. Kim, Y. Han, Y. S. Song, Pro-inflammatory M1 macrophage enhances metastatic potential of ovarian cancer cells through NF-κB activation. *Molecular Carcinogenesis* **57** (2018).
263. M. Dufresne *et al.*, Pro-inflammatory type-1 and anti-inflammatory type-2 macrophages differentially modulate cell survival and invasion of human bladder carcinoma T24 cells. *Molecular Immunology* **48**, 1556-1567 (2011).
264. C. W. Wanderley *et al.*, Paclitaxel reduces tumor growth by reprogramming tumor-associated macrophages to an M1 profile in a TLR4-dependent manner. *Cancer Research* **78**, 5891-5900 (2018).
265. M. Travers *et al.*, DFMO and 5-azacytidine increase M1 macrophages in the tumor microenvironment of murine ovarian cancer. *Cancer Research* **79**, 3445-3454 (2019).
266. E. M. Dijkgraaf *et al.*, Chemotherapy alters monocyte differentiation to favor generation of cancer-supporting m2 macrophages in the tumor microenvironment. *Cancer Research* **73**, 2480-2492 (2013).
267. A. Woods, J. R. Couchman, Syndecan-4 and focal adhesion function. *Current Opinion in Cell Biology* **13**, 578-583 (2001).
268. M. Gulyás, A. Hjerpe, Proteoglycans and WTI as markers for distinguishing adenocarcinoma, epithelioid mesothelioma, and

benign mesothelium. *Journal of Pathology* **199**, 479-487 (2003).
269. T. Roskams, R. De Vos, G. David, B. Van Damme, V. Desmet, Heparan sulphate proteoglycan expression in human primary liver tumours. *The Journal of Pathology* **185**, 290-297 (1998).
270. E. J. Davies *et al.* (2004) Distribution and Clinical Significance of Heparan Sulfate Proteoglycans in Ovarian Cancer.
271. D. Aldinucci, A. Colombatti (2014) The inflammatory chemokine CCL5 and cancer progression.
272. N. Charnaux *et al.*, RANTES (CCL5) induces a CCR5-dependent accelerated shedding of syndecan-1 (CD138) and syndecan-4 from HeLa cells and forms complexes with the shed ectodomains of these proteoglycans as well as with those of CD44. *Glycobiology* **15**, 119-130 (2005).
273. L. Maillard *et al.*, RANTES/CCL5 mediated-biological effects depend on the syndecan-4/PKC signaling pathway. *Biology Open* **3**, 995-1004 (2014).
274. R. Garg *et al.*, Protein kinase C and cancer: What we know and what we do not. *Oncogene* **33**, 5225-5237 (2014).

Appendix

Appendix – List of publications related to this thesis

Chapter I

1. Han Y, Cho U, Kim S, Park IS, Cho JH, Dhanasekaran DN, Song YS. Tumour microenvironment on mitochondrial dynamics and chemoresistance in cancer. Free Radic Res. 2018 Dec;52(11-12):1271-1287. doi: 10.1080/10715762.2018.1459594. Epub 2018 Apr 19. PMID: 29607684.

Chapter II

2. Han Y, Kim B, Cho U, Park IS, Kim SI, Dhanasekaran DN, Tsang BK, Song YS. Mitochondrial fission causes cisplatin resistance under hypoxic conditions via ROS in ovarian cancer cells. Oncogene. 2019 Nov;38(45):7089-7105. doi: 10.1038/s41388-019-0949-5. Epub 2019 Aug 13. PMID: 31409904.

Acknowledgements

I would like to express my sincere appreciation to a number of individuals who have supported my research in many ways. Without them, I would not have been able to complete my PhD study.

First of all, from the bottom of my heart I would like to thank my supervisor Professor Yong Sang Song for his consistent guidance and mentorship provided during my PhD study. I was lucky that I met him as a mentor that with his guidance and overall insight, I could grow both academically and personally.

I also would like to thank all the faculty members of Biomodulation who have taught and guided me into a wide-range of subjects in biomedical researches so that I could broaden my scopes of academic researches. I also would like to express my big thanks to all the collaborators who helped me throughout my study.

Also, I am extremely to thankful to my colleagues, both current and past lab members at the lab of gynecologic oncology. Especially Dr. Boyun Kim who led me to study hypoxia and mitochondrial dynamics, Dr. Soochi Kim for her help with data analysis for the single-cell study, all other senior members including Jae Young Jung, Untack Cho, Yanlin Luo, Hyeran Gwak and In Sil Park for numerous discussions and junior members including HyunA Jo, Wenyu Wang, Juwon Lee, Jihyun Lee, Hyunjae Lee and Heeyeon Kim who kept me going on and this work would not have been possible without their support and input. I also would like to show my gratitude to clinical research fellows at the Seoul National University, Dr. Se Ik Kim, Dr. Jae Hyun Cho and Dr. Aeran Seol, for providing clinical perspectives of researches and facilitating translational medical research.

Finally, I wish to express my deepest gratitude to my family and friends who were always supportive spiritually and putting up with me during the compilation of this dissertation and my life in general.

국문 초록

암 미세환경에 의해 조절되는 난소암세포의 항암제 저항성과 전이능 연구

한 영 진

서울대학교

농업생명과학대학 농생명공학부

바이오모듈레이션 전공

난소암은 사망률이 높은 가장 치명적인 유형의 부인과 악성 종양이다. 암 진단을받은 환자의 약 70%는 종양 감축 수술과 백금 기반 화학 요법에도 불구하고 암의 재발을 보인다. 이것은 주로 난소 암의 고도로 전이되는 능력과 종양 미세 환경으로 알려진 외인성 요인에 의해 발휘되는 화학 내성의 외인성 메커니즘 때문이다. 난소암 종양 미세 환경에 대한 일련의 연구에서, 종양 미세 환경 요인 (저산소증, 염증 및 악성 복수)이 화학 요법과 전이 가능성에 미치는 영향을 조사했다.

미토콘드리아는 종종 세포의 발전소라고 불린다. 미토콘드리아는 진핵 세포 내에서 중요한 소기관이며, 주변 환경의 외부 자극에 반응하여 분열과 융합 과정을 반복한다. 미토콘드리아의 형태적 변화는 퇴행성 신경병, 심혈관 질환 및 암을 포함한 여러 심각한 질병의 발병 및 진행과 관련이 있는 것으로 나타났다. 저산소증은 암 특징(cancer hallmark)의 조절을 통해 암 진행에 영향을 미치는 종양 미세환경의 중요한 특징이다. 저산소증은 미토콘드리아의 기능, 대사 및 구조의 변화를 유도하여 활성 산소 종(ROS)의 생성을 자극한다. 본 연구에서 저산소환경의 난소암 세포에서 미토콘드리아 역학을 조사하였다. 또한 저산소 조건(<1% O_2)에서 미토콘드리아 네트워크

가 암세포에서 약물 반응에 미치는 영향을 확인하였다. 저산소환경에서의 활성 산소 종은 미토콘드리아 분열을 증가시켰고, 이러한 현상은 항산화제인 N-아세틸 시스테인(NAC) 및 트롤록스(Trolox) 처리 시 완화되었다. 또한, 과산화수소(H_2O_2) 처리 시 pDrp1(Ser637)의 발현의 감소와 미토콘드리아의 분열이 증가하는 것을 확인하였다. 미토콘드리아 분열 저해 시, 저산소성 난소암 세포의 시스플라틴 감수성을 증가시켰다. 마지막으로, 진행성 난소암 환자의 악성 복수 또는 조직으로부터 분리 한 일차 종양 스페로이드(Speroids)에 Drp1 억제제인 Mdivi-1 전처리시, 시스플라틴 감수성이 증가되었다. 따라서, 난소암세포는 저산소 환경에서 항암제 시스플라틴의 저항성을 일으키고, 이것은 저산소 환경에서 증가한 활성산소를 통한 미토콘드리아 분열 때문이라는 것을 확인했다.

다음으로, 염증이 난소 암의 발생 및 진행과 밀접한 관련이 있다는 증거가 늘어나고 있습니다. 여기에서, 우리는 대체 NFκB 경로의 TNF 매개 활성화가 TNF에 의해 유도 된 세포 사멸에 대한 침입성과 저항성을 촉진한다고 가설을 세웠다. 염증 관련 사이토 카인 중 TNF는 다른 유형의 고형 종양에 비해 난소 암 조직에서 고도로 발현된다는 것을 발견했습니다. 48 시간 동안 TNF에 노출 된 난소암 세포는 증가 된 콜로니 형성 능력과 세포주기 진행을 보여 주었다. 또한 TNF 및 수용체(TNFRSF1A 및 TNFRSF1B)의 유전자 발현 수준은 전이성 난소 암 조직에서 동일한 환자의 1 차 조직보다 높게 나타났다. 또한 Matrigel 코팅 된 transwell inserts 분석 결과는 TNF가 난소 암 세포의 침습성을 촉진하는 것으로 나타났다. 이 과정에 관련된 메커니즘을 조사하기 위해 우리는 고전적 (p50 : p65) 및 대안적 (RELB : P52) NFκB 경로 조절제의 단백질 발현을 조사했습니다. 대체 NFKB 경로의 전사 인자 인 RELB의 더 높은 발현은 낮은 생존율과 관련이 있었다. The Cancer Genome Atlas (TCGA)의 307 개의 난소 종양 샘플을 사용하여 대체 NFKB 경로

유전자 (RELB 및 P52)와 암 침습 관련 프로테아제 (MMP9, PLAU) 간에 유의 한 양의 상관 관계를 발견했다. 프로테아제 어레이는 PLAU가 TNF에 의해 상향 조절되는 것으로 밝혀졌지만이 반응은 RELB 녹다운 난소 암 세포에는 없었다. 종합적으로, 이러한 발견은 난소 암 세포의 전이 과정에서 RelB 발현에 의해 매개되는 대체 NFκB 경로의 관여를 시사한다.

마지막으로, 난소 암 종양 미세환경인 악성 복수에 존재하는 세포 상호 작용을 이해하기 위해 난소 암 환자 5 명의 단일 세포 RNA 시퀀싱 데이터를 활용했다. 우리는 세포 유형별 시그니처의 발현 패턴을 기반으로 7 개의 별개의 세포 유형을 식별했다. 대식세포는 복수 종양 미세 환경에서 11 개의 하위 클러스터를 가진 가장 이질적인 세포 유형이었다. 대식세포 부분 집단의 해석은 MacSpectrum을 사용하여 수행되었다. 또한 복수에서 OC 세포의 종양 내 및 종양 간 이질성을 평가했다. NicheNet을 통한 리간드-수용체 상호 작용 분석을 통해 면역 세포와 OC 세포 간의 상호작용을 예측했다. 우리는 CCL5가 T 세포와 NK 세포에서 발현하여 아마도 SDC4를 통해 복수에서 OC 세포 생존을 조절한다는 것을 발견했다. 평균 SDC4 발현은 각 샘플에서 OC 세포 비율과 양의 상관 관계가 있었다. 증가 된 SDC4 발현은 OC 환자의 전체 생존율이 낮음을 예측했다. 전체적으로, 우리의 연구는 장기 생존 결과에서 T 세포와 NK 세포의 잠재적인 종양 촉진 역할을 강조하여 SDC4가 OC 세포 생존을위한 필수 분자이자 OC 환자의 예후 마커임을 시사한다.

주요어: 난소암, 약물 저항성, 종양 미세환경, 저산소증, 미토콘드리아 역학, 악성복수, 전이능, RelB

학 번 : 2015-22697